CALCULATION OF TEMPERATURE - OXYGEN FUGACITY TABLES FOR H_2-CO_2 GAS MIXTURES AT ONE ATMOSPHERE TOTAL PRESSURE, and AN INVESTIGATION OF THE ZOISITE-CLINOZOISITE TRANSITION

by

Arthur R. Prunier Jr.

Thesis submitted to the Graduate Faculty of the
Virginia Polytechnic Institute and State University
in partial fulfillment of the requirements for the degree of

MASTER OF SCIENCE

in

Geological Sciences

APPROVED:

D. A. Hewitt, Chairman

P. H. Ribbe

C. D. Williams

D. R. Wones

April, 1978

Blacksburg, Virginia

ACKNOWLEDGEMENTS

I gratefully acknowledge the support, widsom, and financial supply given to me by my Lord Jesus Christ, without which I would have been unable to complete this work. I also thank His servant

for spiritual and scientific advice over the past years. My advisory committee chairman deserves special recognition for his guidance and encouragement during the course of the research. and patiently reviewed earlier drafts of this thesis. Finally, I thank the National Science Foundation for financial assistance in the form of a Graduate Fellowship.

TABLE OF CONTENTS

LIST OF TABLES

LIST OF FIGURES

PART I

CALCULATION OF TEMPERATURE - OXYGEN FUGACITY TABLES FOR H_2 - CO_2 GAS MIXTURES AT ONE ATMOSPHERE TOTAL PRESSURE

INTRODUCTION

The ability to control oxidation conditions accurately when investigating phase equilibria in systems containing elements of variable oxidation state (e.g. the transition metals) is crucial to many disciplines. For example, the sensitivity of both liquidus temperatures and crystallization sequences in the system $FeO-Fe_2O_3-SiO_2$ to changes in oxygen fugacity (Osborn and Muan, 1963) is of great importance to both igneous petrology and the refractories industry. For such studies at one atmosphere pressure, a gas mixing furnace is one of the most versatile methods for controlling oxidation state by means of buffering the oxygen fugacity over a wide, continuous range of $T-f_{O_2}$ conditions.

Although there are many gas combinations suitable for buffering oxygen fugacity (Nafziger *et al.*, 1971), H_2-CO_2 mixtures in the C-H-O system are among the most useful because of the wide range of f_{O_2} values available over experimentally reasonable temperatures. In order to buffer a three component - one phase gas mixture it is necessary to fix four variables. This can be accomplished for H_2-CO_2 mixtures by fixing temperature, pressure and the initial H_2/CO_2 ratio, noticing that the latter ratio completely determines the gas composition and hence fixes the two independent compositional variables.

Tables yielding the volume percent CO_2 necessary to achieve desired oxygen fugacities at selected temperatures in H_2-CO_2 gas mixtures have recently been published by Deines, Nafziger, Ulmer and Woermann (1974). Unfortunately, most of the values reported at the more reducing conditions

are incorrect because the authors did not consider methane as an integral species in all equilibrium mixtures. Instead, they tried to approximate its effect post facto by stating that the presence of methane would affect the equilibrium oxygen fugacity only if

$$f_{CH_4} > \frac{f_{CO_2} f_{H_2O}^2}{f_{O_2}^2 K_6}$$

where K_6 is the equilibrium constant for the reaction $CH_4 + 2O_2 = CO_2 + 2H_2O$, and f_{CO_2}, f_{H_2O} and f_{O_2} are the equilibrium fugacities calculated when methane is disregarded (Dienes et al., 1974, p. 20). The fugacity of methane used in this comparison was estimated from the equilibrium constant relations for the reactions $CO + 3H_2 = CH_4 + H_2O$ and $2CO + 2H_2 = CH_4 + CO_2$, again using the equilibrium fugacities for CO, H_2, H_2O and CO_2 calculated when methane was disregarded. There are two reasons why such a comparison is not rigorously correct:

(1) If a $f_{CH_4} > f_{CO_2} f_{H_2O}^2/(f_{O_2}^2 K_6)$ affects the oxygen fugacity, then so should one less than it, since in either case all fugacities involved will change as reactions bring the gas system to equilibrium with methane.

(2) Even if the estimated $f_{CH_4} = f_{CO_2} f_{H_2O}^2/(f_{O_2}^2 K_6)$ (as it should at equilibrium), the methane can form only at the expense of the other gas species, thereby changing their partial pressures, and hence fugacities, from the values used in the calculations.

Because of their testing procedure, volume percentages of CO_2 in the starting mixture given by Dienes et al. (1974) are in error at the more

reducing conditions; the error reaches as high as 10% CO_2, absolute (41.5% CO_2 versus 31.74% CO_2, true; R_m = 1.410 versus 2.151 at 630°C, log f_{O_2} = -23.5).

Because of the usefulness of H_2-CO_2 gas mixing techniques, the convenience of having tabulated starting mixtures and the necessity of having uniformly correct values, the recalculation of H_2-CO_2 tables was initiated.

DEVELOPMENT

The initial H_2-CO_2 mixture, upon equilibration at P = 1 atm and some temperature T, will contain the gaseous species H_2, H_2O, CO_2, CO, O_2 and CH_4. (See Table I for explanation of symbols used in this development). The exact process by which the initial H_2 and CO_2 react and dissociate to form the final gaseous assemblage is of no interest, since at equilibrium the partial pressures of the various species are fixed regardless of the reaction path. However, it is advantageous to choose an arbitrary reaction path from the point of view of mathematical convenience. Hence, all CO and O_2 are considered to have formed by the dissociation reaction

$$(1) \quad CO_2 = CO + 1/2\ O_2.$$

H_2O is considered to have originated partly from the reaction

$$(2) \quad H_2O = H_2 + 1/2\ O_2$$

and partly from the reaction

$$(3) \quad CO + 3H_2 = CH_4 + H_2O,$$

while all methane is considered to have originated through reaction (3).

Letting the starting mixture contain n_1 moles of CO_2 and n_2 moles of H_2, n_2/n_1 can be defined as R_m, the initial mixing ratio. We can also let 'a' be the mole fraction of CO_2 which dissociates by reaction (1), let 'b' be the mole fraction of H_2 which reacts to form H_2O by reaction (2), and let 'c' be the mole fraction of H_2 which reacts to form CH_4 by reaction (3). Then at equilibrium the gases will be present in the following amounts (in moles):

TABLE I

Explanation of Symbols

R	gas constant, 1.98726×10^{-3} Kcal deg^{-1} $mole^{-1}$
T	temperature
P	pressure, total
P_i	partial pressure of i
f_i	fugacity of i
K_i	equilibrium constant for the i'th reaction
$\Delta G^\circ_{reac,i}$	free energy of reaction at T, 1 atm, for the i'th reaction
ΔG°_f	free energy of formation at T, 1 atm pressure
R_m	mixing ratio, H_2/CO_2 initial

$$n_{CO_2} = n_1(1-a) \qquad n_{H_2} = n_2(1-b-c)$$

$$n_{CO} = n_1 a - 1/3\ n_2 c \qquad n_{O_2} = 1/2\ n_1 a - 1/2\ n_2 b$$

$$n_{H_2O} = n_2(b + 1/3\ c) \qquad n_{CH_4} = 1/3\ n_2 c$$

The total number of moles of gas present at equilibrium equals $n_1\ (1 + a/2) + n_2\ (1 - b/2 - 2c/3)$, and at P = 1 atm, partial pressures of the gases at equilibrium are:

(4) $P_{CO_2} = 2(1-a)/(2+a+R_m[2-b-4c/3])$

(5) $P_{CO} = (2a-2R_m c/3)/(2+a+R_m[2-b-4c/3])$

(6) $P_{H_2} = 2R_m(1-b-c)/(2+a+R_m[2-b-4c/3])$

(7) $P_{H_2O} = 2R_m(b+c/3)/(2+a+R_m[2-b-4c/3])$

(8) $P_{O_2} = (a-bR_m)/(2+a+R_m[2-b-4c/3])$

(9) $P_{CH_4} = 2R_m c/3(2+a+R_m[2-b-4c/3])$

This set of equations reduces to equations 19 through 23 of Dienes et al. (1974, p. 18) when 'c' is zero, i.e. when methane is not taken to be an active participant in the equilibrium process.

The six independent equations (4) through (9) contain nine variables: P_{CO_2}, P_{CO}, P_{H_2}, P_{H_2O}, P_{CH_4}, a, b, c, and R_m[1]. Three more independent equations can be obtained from the equilibrium constant relations for reactions (1), (2), and (3),

$$(10)\quad K_1 = \frac{f_{CO}\ f_{O_2}^{1/2}}{f_{CO_2}}$$

---

[1] P_{O_2} is not considered as a variable in this treatment, but is held constant along with T and P when solving for the initial H_2/CO_2 ratio.

$$(11)\quad K_2 = \frac{f_{H_2}\, f_{O_2}^{1/2}}{f_{H_2O}}$$

$$(12)\quad K_3 = \frac{f_{CH_4}\, f_{H_2O}}{f_{CO}\, f_{H_2}^{3}}$$

Values for the equilibrium constants can be determined from free energy of formation data using the equation

$$(13)\quad K_i = \exp[-\Delta G^\circ_{reac,i}/RT]$$

(see Denbigh, 1971, p. 140 ff.).

By assuming ideal gas behavior (i.e. at the high temperatures involved for experiments at 1 atm pressure, $P_i = f_i$), equations (4) through (12) become a single set of simultaneous equations that can be solved at any P_{O_2} and T for the appropriate $H_2 - CO_2$ starting mixture. However, since the equations are non-linear and fairly complex, they are not to be solved by simple algebraic manipulations. The method finally arrived at for their solution involves a combination of algebraic manipulation and successive approximations.

In the solution to the equations P_{CO_2} was eliminated from the set of equations, and the eight remaining equations were rearranged so that each of the variables occurred once, by itself, to the left of the equality (Table II). Next, each variable was expressed in terms of 'c', either explicitly or implicitly. The variable 'b', as shown in equation (15), is already an explicit function of 'c'. The variable R_m in equation (16) can be converted into an explicit function of 'c' by substituting equations (14) and (15), yielding:

TABLE II

Rearranged Simultaneous Equations plus Derivational Source

	Equations	Source Equations
(14)	$a = \frac{K_1 + (cR_m f_{O_2}^{1/2})/3}{K_1 + f_{O_2}^{1/2}}$	(4), (5), (10)
(15)	$b = \frac{f_{O_2}^{1/2} - c(f_{O_2}^{1/2} + K_3/3)}{f_{O_2}^{1/2} + K_3}$	(6), (7), (11)
(16)	$R_m = \frac{a(1 - f_{O_2}) - 2f_{O_2}}{b(1 - f_{O_2}) + (2 - 4c/3)f_{O_2}}$	(8)
(17)	$P_{H_2O} = \frac{2R_m(b + c/3)}{2 + a + R_m(2 - b - 4c/3)}$	(7)
(18)	$P_{CO} = \frac{2(a - R_m c/3)}{2 + a + R_m(2 - b - 4c/3)}$	(5)
(19)	$P_{H_2} = \frac{2R_m(1 - b - c)}{2 + a + R_m(2 - b - 4c/3)}$	(6)
(20)	$P_{CH_4} = \frac{K_3 P_{H_2}^3 P_{CO}}{P_{H_2O}}$	(12)
(21)	$c = \frac{(6 + 3a + R_m[6 - 3b])P_{CH_4}}{R_m(2 + 4P_{CH_4})}$	(9)

$$(22)\quad R_m = \frac{C - 2f_{O_2}}{(A + 2f_{O_2}) - c(D + B + 4f_{O_2}/3)}$$

where

$$A = \frac{f_{O_2}^{1/2}(1-f_{O_2})}{f_{O_2}^{1/2} + K_3} \qquad B = \frac{(f_{O_2}^{1/2} + K_3/3)(1-f_{O_2})}{f_{O_2}^{1/2} + K_3}$$

$$C = \frac{K_1(1-f_{O_2})}{K_1 + f_{O_2}^{1/2}} \qquad D = \frac{f_{O_2}^{1/2}(1-f_{O_2})/3}{K_1 + f_{O_2}^{1/2}}$$

Equation (14) is an implicit function of only 'c' since R_m is a function of 'c' alone. Therefore, with 'a', 'b', and R_m expressed as functions of 'c' only, examination of Table II shows that all eight of the variables must, either explicitly or implicitly, also be functions of 'c'. In equation (21) it can be shown that 'c' is an implicit function of itself (i.e. c = Z(c)). This equality will not be true in general, but only for certain values of 'c', one of which will yield the correct $H_2 - CO_2$ mixing ratio for the selected T-f_{O_2} pair[2].

It is useful to define the function F(c) as

$$(23)\quad F(c) = Z(c) - c$$

---

[2]That more than one value of 'c' may satisfy equation (21) results because the set of simultaneous equations is not first order in 'c'.

The problem of solving for the gas starting mixture reduces to that of obtaining the physically sensible root of F(c). This is done by successive iterations using the Newton Raphson formula (Weeg and Reed, 1966),

$$(24)\quad c_{n+1} = c_n - \frac{F(c_n)}{F'(c_n)}$$

where $F'(c_n)$ is approximated by the formula,

$$F'(c_n) \sim \frac{F(c_n) - F(c_{n-1})}{c_n - c_{n-1}}$$

When sufficient convergence is achieved, the value of 'c' is used to evaluate R_m in equation (22). The volume percentage of CO_2 in the starting mixture may then be obtained using the formula

$$(25)\quad \%CO_2 = \frac{100\%}{(1 + R_m)} \cdot$$

A sufficient test for physical sensibility of the solution is that none of the corresponding gas partial pressures be negative or greater than 1 atm.

At very low oxygen fugacities the possibility of graphite precipitation exists, which can be represented by the reaction

$$(26)\quad CO_2 = C + O_2$$

At one atmosphere the limiting P_{O_2} below which graphite precipitates at some temperature can be found using the equilibrium constant relation for reaction (26),

$$K_{26} = \exp[-\Delta G^\circ_{reac,26}/RT] = \frac{f_{O_2}}{f_{CO_2}} = \frac{P_{O_2}}{P_{CO_2}}$$

or

$$(27)\quad P_{O_2\,limiting} = P_{CO_2} \cdot \exp[-\Delta G^\circ_{reac,26}/RT].$$

METHOD

The equations derived in the previous section were programmed in FORTRAN and solved using an IBM-370 computer (see Appendix for source listing).The equilibrium constants for reactions (1), (2), (3) and (26) were obtained, as indicated by equation (13), from the free energy changes, ΔG°_{reac}, for the reactions. The free energy of reaction data were derived from the JANAF (1971) tables for temperatures from 700 K to 2300 K and were then fitted to polynomials in T by Dienes et al (1974). Their 4th order polynomials were checked against the original JANAF data and were all satisfactory except for $\Delta G^{\circ}_{reac,3}$ where a new 5th order polynomial gave a statistically better fit to the data. The four polynomials in T used in the present program are given in Table III, accuracy being limited to three decimal places by the original data.

The choice of starting values for computer iteration using equation (24) presents a minor difficulty. For most higher f_{O_2} values (e.g. log $f_{O_2} > -22.0$), using an initial c = 0.0 works well, convergence being achieved within 20 cycles. In order to get convergence at low oxygen fugacities F(c) was computed for successively higher values of 'c' starting at zero until the first crossover (i.e. F(c) changes sign) occurred. The value of 'c' preceding the crossover was then used as the starting value for further iterations.

As implied by equation (24), the results of each cycle through the set of simultaneous equations was used to compute the starting value for

TABLE III

ΔG°_{reac} Polynomials

(temperature in celsius degrees)

$$*\Delta G^\circ_{reac,1} = 62.11033 - 2.144446 \times 10^{-2} T + 4.720325 \times 10^{-7} T^2 - 4.557429 \times 10^{-12} T^3 - 7.343018 \times 10^{-15} T^4$$

$$*\Delta G^\circ_{reac,2} = 55.02525 - 1.121221 \times 10^{-2} T - 2.080041 \times 10^{-6} T^2 + 7.648489 \times 10^{-10} T^3 - 1.123283 \times 10^{-13} T^4$$

$$\Delta G^\circ_{reac,3} = -35.67445 + 5.344917 \times 10^{-2} T + 9.900155 \times 10^{-6} T^2 - 6.474264 \times 10^{-9} T^3 + 2.077475 \times 10^{-12} T^4 - 2.697849 \times 10^{-16} T^5$$

$$*\Delta G^\circ_{reac,26} = 94.25770 + 7.321946 \times 10^{-4} T - 3.416474 \times 10^{-7} T^2 + 4.785862 \times 10^{-11} T^3$$

*From Dienes et al. (1974)

the next cycle. If the results for 'a', 'b', 'c' and R_m of any cycle all differed from the previous cycle by less than 0.01%, then convergence was considered to have been achieved, and the R_m value was converted to volume percent CO_2 in the H_2-CO_2 starting mixture using equation (25). If the test for graphite precipitation proved positive, stars (*****) were printed in the final tables instead of the calculated percentage CO_2.

RESULTS

Computer results show that for high f_{O_2} values $F(c) < 10^{-6}$ when c = 0, and therefore methane can be disregarded as a significant gas species in the equilibrium mixture. This is illustrated in Fig. 1 by the F(c) curve for log f_{O_2} = -18.0 at T = 650°C, which is a straight line whose only root is approximately at c = 0.0. However, as oxygen fugacity is reduced, F(c) no longer remains linear and develops multiple roots, as shown in Figure 1 by the F(c) curve for log f_{O_2} = -24.1 at 650°C. This curve has roots at c = 0.122 and 0.903, but the latter value yields negative equilibrium partial pressures for CH_4, CO and CO_2 and is therefore unacceptable. Because of the original definition of 'c', only roots of F(c) between 0.0 and 1.0 are physically meaningful and are therefore the only ones that need be considered.

The final results of the computer computations are presented as the volume percentage CO_2 in an initial H_2-CO_2 gas mixture for each T-f_{O_2} pair (see Table IV). Only values of volume percent CO_2 between 99.99 and 00.01 are listed, higher or lower values being replaced by blanks. As pointed out by Dienes et al (1974), calculations based on JANAF data tend to yield slightly more reduced f_{O_2} values for a given H_2- CO_2 gas mixture than do other data bases such as Wagman et al. (1945), Coughlin (1954), Wicks and Block (1968) and Elliot and Gleiser (1960). Huebner (1975) also observed that at high temperatures f_{O_2}'s calculated from JANAF data appear to be about 0.06 log atm units lower than values from electrochemical oxygen cells.

FIGURE 1

F(c) versus c at log (f_{O_2}) = -18.00 and -24.10, T = 650°C. The log (f_{O_2}) =-18.00 curve is illustrative of oxidizing conditions where methane is present below the 100 ppm level. The log (f_{O_2}) = -24.10 curve, illustrating more reducing conditions where methane becomes significant, shows two roots to the basic equation Z(c)-c = 0, but only the root at 0.122 has physical significance.

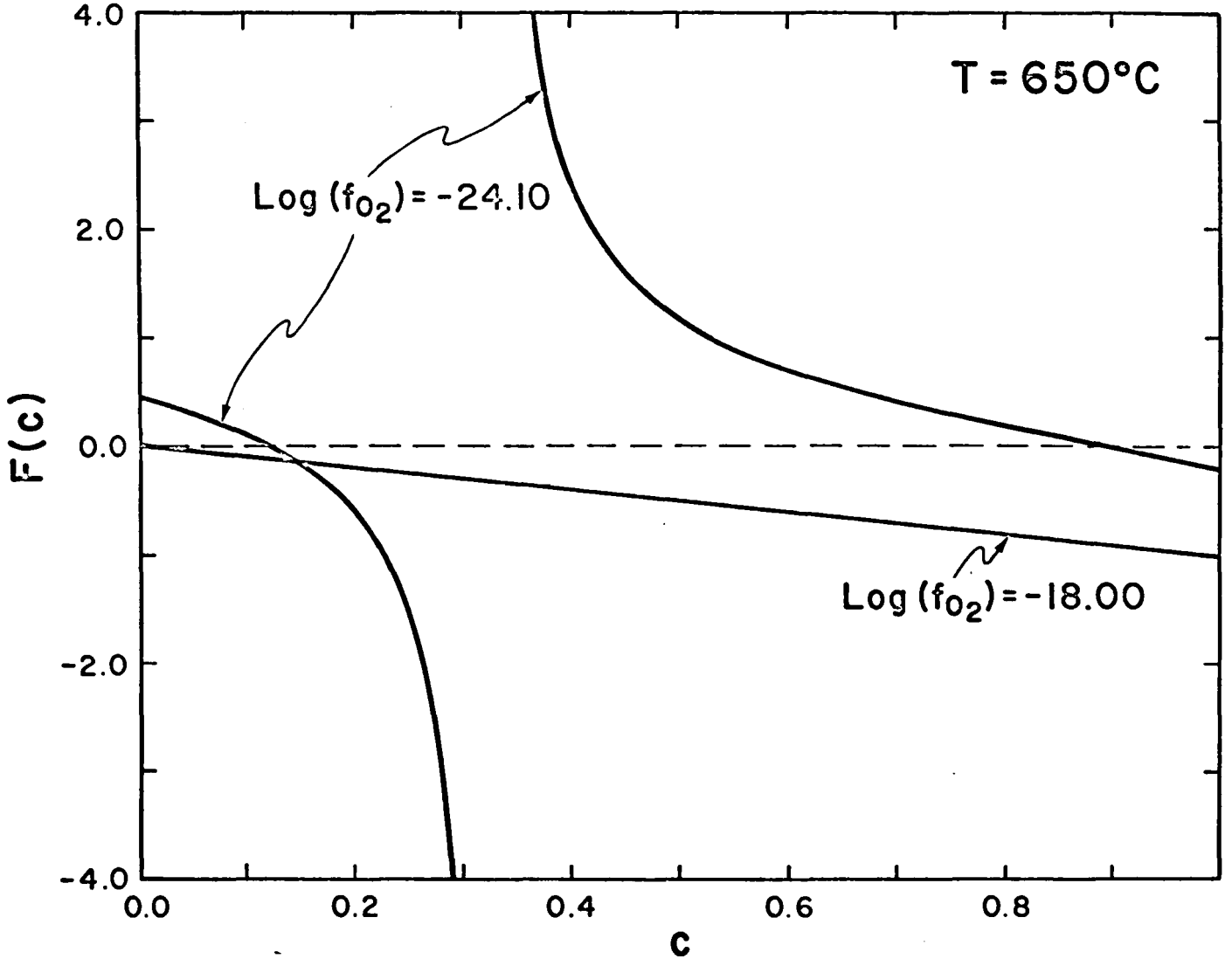
T = 650°C
Log (f_{O_2}) = -24.10
Log (f_{O_2}) = -18.00
F(c)
c
4.0
2.0
0.0
-2.0
-4.0
0.0
0.2
0.4
0.6
0.8

TABLE IV

Initial volume $\%CO_2$ yielding selected temperature - oxygen fugacity pairs.

TEMP C	LOG(OXYGEN FUGACITY)																			TEMP C
	-4.0	-4.2	-4.4	-4.6	-4.8	-5.0	-5.2	-5.4	-5.6	-5.8	-6.0	-6.2	-6.4	-6.6	-6.8	-7.0	-7.2	-7.4	-7.6	-7.8	
880																				880
890																			99.99	890
900																		99.99	99.99	900
910																	99.99	99.99	99.99	910
920																99.99	99.99	99.99	99.99	920
930															99.99	99.99	99.99	99.99	99.99	930
940														99.99	99.99	99.99	99.99	99.99	99.98	940
950													99.99	99.99	99.99	99.99	99.99	99.98	99.98	950
960												99.99	99.99	99.99	99.99	99.99	99.98	99.98	99.97	960
970											99.99	99.99	99.99	99.99	99.99	99.98	99.98	99.97	99.96	970
980										99.99	99.99	99.99	99.99	99.99	99.98	99.98	99.97	99.96	99.95	980
990									99.99	99.99	99.99	99.99	99.99	99.98	99.98	99.97	99.96	99.96	99.94	990
1000									99.99	99.99	99.99	99.99	99.98	99.98	99.97	99.97	99.96	99.94	99.93	1000
1010								99.99	99.99	99.99	99.99	99.98	99.98	99.97	99.97	99.96	99.95	99.93	99.91	1010
1020							99.99	99.99	99.99	99.99	99.98	99.98	99.97	99.97	99.96	99.95	99.93	99.92	99.90	1020
1030						99.99	99.99	99.99	99.99	99.98	99.98	99.97	99.97	99.96	99.95	99.94	99.92	99.90	99.87	1030
1040						99.99	99.99	99.99	99.98	99.98	99.98	99.97	99.96	99.95	99.94	99.92	99.90	99.88	99.84	1040
1050					99.99	99.99	99.99	99.99	99.98	99.98	99.97	99.96	99.95	99.94	99.92	99.91	99.88	99.85	99.81	1050
1060					99.99	99.99	99.99	99.98	99.98	99.97	99.96	99.95	99.94	99.93	99.91	99.89	99.86	99.82	99.77	1060
1070				99.99	99.99	99.99	99.98	99.98	99.97	99.97	99.96	99.94	99.93	99.91	99.89	99.86	99.83	99.78	99.72	1070
1080				99.99	99.99	99.98	99.98	99.97	99.97	99.96	99.95	99.93	99.92	99.89	99.87	99.83	99.79	99.74	99.67	1080
1090				99.99	99.99	99.98	99.98	99.97	99.96	99.95	99.94	99.92	99.90	99.87	99.84	99.80	99.75	99.68	99.60	1090
1100			99.99	99.99	99.98	99.98	99.97	99.96	99.95	99.94	99.92	99.90	99.88	99.85	99.81	99.76	99.70	99.62	99.52	1100
1110			99.99	99.99	99.98	99.97	99.96	99.96	99.94	99.93	99.91	99.89	99.86	99.82	99.77	99.71	99.64	99.55	99.43	1110
1120		99.99	99.99	99.98	99.97	99.97	99.96	99.95	99.93	99.91	99.89	99.86	99.83	99.78	99.73	99.66	99.57	99.46	99.32	1120
1130		99.99	99.98	99.98	99.97	99.96	99.95	99.94	99.92	99.90	99.87	99.84	99.80	99.74	99.68	99.60	99.49	99.36	99.20	1130
1140		99.99	99.98	99.97	99.96	99.95	99.94	99.92	99.90	99.88	99.85	99.81	99.76	99.70	99.62	99.52	99.40	99.24	99.05	1140
1150	99.99	99.99	99.98	99.97	99.96	99.94	99.93	99.91	99.89	99.86	99.82	99.77	99.72	99.64	99.55	99.43	99.29	99.11	98.88	1150
1160	99.99	99.98	99.97	99.96	99.95	99.93	99.92	99.89	99.87	99.83	99.79	99.73	99.66	99.58	99.47	99.33	99.16	98.95	98.68	1160
1170	99.99	99.98	99.97	99.95	99.94	99.92	99.90	99.88	99.84	99.80	99.75	99.69	99.61	99.50	99.38	99.22	99.02	98.77	98.46	1170
1180	99.98	99.97	99.96	99.94	99.93	99.91	99.88	99.85	99.82	99.77	99.71	99.63	99.54	99.42	99.27	99.08	98.85	98.56	98.19	1180
1190	99.99	99.98	99.96	99.95	99.93	99.92	99.89	99.86	99.83	99.78	99.73	99.66	99.57	99.46	99.32	99.14	98.93	98.65	98.32	97.89	1190
1200	99.99	99.97	99.96	99.94	99.92	99.90	99.87	99.84	99.80	99.75	99.68	99.60	99.50	99.37	99.20	99.00	98.75	98.43	98.04	97.55	1200
1210	99.98	99.97	99.95	99.93	99.91	99.88	99.85	99.81	99.77	99.70	99.63	99.53	99.41	99.26	99.07	98.84	98.54	98.18	97.72	97.16	1210
1220	99.98	99.96	99.94	99.92	99.89	99.86	99.83	99.78	99.73	99.66	99.57	99.46	99.32	99.14	98.92	98.65	98.31	97.89	97.37	96.72	1220
1230	99.97	99.95	99.93	99.90	99.88	99.84	99.80	99.75	99.68	99.60	99.50	99.37	99.21	99.01	98.75	98.44	98.05	97.56	96.96	96.22	1230
1240	99.96	99.94	99.91	99.89	99.86	99.82	99.77	99.71	99.63	99.54	99.42	99.27	99.08	98.85	98.56	98.20	97.75	97.19	96.50	95.66	1240
1250	99.95	99.93	99.90	99.87	99.83	99.79	99.73	99.66	99.57	99.46	99.33	99.16	98.94	98.67	98.34	97.92	97.41	96.77	95.99	95.03	1250
1260	99.94	99.91	99.88	99.85	99.81	99.75	99.69	99.61	99.51	99.38	99.22	99.03	98.78	98.47	98.09	97.61	97.02	96.30	95.41	94.33	1260
1270	99.93	99.90	99.86	99.82	99.78	99.72	99.64	99.55	99.43	99.29	99.11	98.88	98.60	98.24	97.81	97.26	96.59	95.77	94.77	93.55	1270
1280	99.92	99.88	99.84	99.80	99.74	99.67	99.59	99.48	99.35	99.18	98.97	98.71	98.39	97.99	97.49	96.87	96.11	95.18	94.06	92.70	1280
1290	99.90	99.86	99.82	99.77	99.70	99.63	99.53	99.41	99.25	99.06	98.83	98.53	98.16	97.70	97.13	96.43	95.57	94.53	93.27	91.76	1290
1300	99.88	99.84	99.79	99.73	99.66	99.57	99.46	99.32	99.15	98.93	98.66	98.32	97.90	97.38	96.73	95.94	94.98	93.81	92.40	90.73	1300
1310	99.86	99.82	99.76	99.69	99.61	99.51	99.38	99.22	99.02	98.78	98.47	98.08	97.61	97.02	96.29	95.40	94.32	93.02	91.46	89.62	1310
1320	99.84	99.79	99.72	99.65	99.55	99.44	99.29	99.11	98.89	98.61	98.25	97.82	97.28	96.61	95.80	94.80	93.60	92.15	90.43	88.42	1320
1330	99.82	99.76	99.68	99.60	99.49	99.36	99.20	98.99	98.73	98.41	98.02	97.52	96.92	96.17	95.25	94.14	92.80	91.21	89.32	87.13	1330
1340	99.79	99.72	99.64	99.54	99.42	99.27	99.09	98.85	98.56	98.20	97.75	97.20	96.51	95.67	94.65	93.42	91.94	90.18	88.13	85.75	1340
1350	99.76	99.68	99.59	99.48	99.34	99.17	98.96	98.70	98.37	97.96	97.46	96.83	96.07	95.13	93.99	92.62	91.00	89.08	86.85	84.30	1350
1360	99.72	99.64	99.53	99.41	99.25	99.06	98.82	98.53	98.16	97.70	97.13	96.43	95.57	94.53	93.27	91.76	89.98	87.90	85.49	82.77	1360
1370	99.68	99.59	99.47	99.33	99.16	98.94	98.67	98.33	97.92	97.40	96.77	95.98	95.03	93.87	92.49	90.83	88.89	86.64	84.06	81.17	1370
1380	99.64	99.53	99.40	99.24	99.05	98.80	98.50	98.12	97.65	97.08	96.37	95.50	94.44	93.16	91.63	89.83	87.72	85.30	82.56	79.51	1380
1390	99.59	99.47	99.32	99.14	98.92	98.65	98.31	97.89	97.36	96.72	95.93	94.96	93.79	92.38	90.72	88.75	86.48	83.89	80.99	77.79	1390
1400	99.53	99.40	99.24	99.04	98.79	98.48	98.10	97.63	97.04	96.32	95.44	94.37	93.09	91.55	89.73	87.61	85.17	82.42	79.36	76.03	1400

TABLE IV CONTINUED

TEMP C	LOG(OXYGEN FUGACITY)																			TEMP C
	-4.0	-4.2	-4.4	-4.6	-4.8	-5.0	-5.2	-5.4	-5.6	-5.8	-6.0	-6.2	-6.4	-6.6	-6.8	-7.0	-7.2	-7.4	-7.6	-7.8	
1410	99.47	99.32	99.14	98.92	98.64	98.29	97.87	97.34	96.69	95.89	94.92	93.74	92.32	90.64	88.67	86.39	83.80	80.89	77.69	74.23	1410
1420	99.40	99.24	99.03	98.78	98.47	98.09	97.61	97.02	96.30	95.42	94.34	93.05	91.50	89.68	87.55	85.11	82.36	79.30	75.97	72.40	1420
1430	99.33	99.14	98.91	98.63	98.29	97.86	97.33	96.68	95.87	94.90	93.72	92.30	90.62	88.64	86.36	83.77	80.86	77.66	74.21	70.56	1430
1440	99.24	99.04	98.78	98.47	98.09	97.61	97.02	96.30	95.41	94.34	93.04	91.49	89.67	87.55	85.11	82.36	79.31	75.99	72.44	68.71	1440
1450	99.15	98.92	98.64	98.29	97.86	97.33	96.68	95.88	94.91	93.73	92.31	90.63	88.66	86.39	83.80	80.90	77.72	74.29	70.65	66.85	1450
1460	99.05	98.79	98.48	98.10	97.62	97.03	96.31	95.43	94.36	93.07	91.53	89.71	87.60	85.17	82.43	79.40	76.09	72.56	68.85	65.00	1460
1470	98.93	98.65	98.31	97.88	97.35	96.70	95.91	94.94	93.77	92.36	90.69	88.73	86.47	83.90	81.02	77.85	74.44	70.82	67.05	63.17	1470
1480	98.81	98.50	98.12	97.64	97.06	96.34	95.47	94.41	93.13	91.60	89.80	87.70	85.29	82.57	79.55	76.27	72.76	69.07	65.25	61.35	1480
1490	98.68	98.33	97.91	97.38	96.74	95.95	94.99	93.83	92.44	90.79	88.85	86.61	84.05	81.19	78.05	74.66	71.07	67.32	63.47	59.56	1490
1500	98.53	98.15	97.68	97.10	96.39	95.53	94.48	93.22	91.71	89.92	87.85	85.46	82.77	79.78	76.52	73.03	69.37	65.58	61.70	57.79	1500
1510	98.37	97.95	97.43	96.80	96.02	95.07	93.93	92.56	90.92	89.01	86.79	84.27	81.43	78.32	74.96	71.39	67.67	63.85	59.96	56.04	1510
1520	98.19	97.73	97.16	96.46	95.61	94.58	93.33	91.85	90.09	88.04	85.68	83.02	80.06	76.83	73.38	69.74	65.98	62.13	58.24	54.33	1520
1530	98.00	97.49	96.86	96.10	95.17	94.05	92.70	91.09	89.21	87.02	84.53	81.73	78.65	75.32	71.78	68.09	64.29	60.43	56.54	52.64	1530
1540	97.79	97.23	96.54	95.71	94.70	93.48	92.02	90.29	88.28	85.96	83.33	80.40	77.21	73.79	70.18	66.45	62.63	58.76	54.88	50.98	1540
1550	97.56	96.95	96.20	95.29	94.19	92.87	91.29	89.44	87.30	84.84	82.08	79.04	75.75	72.24	68.58	64.81	60.98	57.11	53.24	49.36	1550
1560	97.31	96.64	95.83	94.84	93.64	92.22	90.53	88.55	86.27	83.69	80.80	77.65	74.26	70.69	66.98	63.19	59.35	55.49	51.62	47.76	1560
1570	97.04	96.31	95.43	94.35	93.06	91.52	89.71	87.61	85.20	82.49	79.49	76.23	72.76	69.13	65.39	61.59	57.75	53.89	50.04	46.18	1570
1580	96.75	95.96	94.99	93.83	92.44	90.79	88.86	86.62	84.09	81.25	78.14	74.80	71.26	67.58	63.82	60.00	56.17	52.32	48.48	44.64	1580
1590	96.44	95.58	94.53	93.28	91.78	90.01	87.96	85.60	82.94	79.98	76.77	73.34	69.75	66.04	62.26	58.44	54.61	50.78	46.95	43.12	1590
1600	96.10	95.17	94.04	92.69	91.08	89.20	87.01	84.53	81.75	78.69	75.38	71.89	68.24	64.50	60.71	56.90	53.08	49.27	45.45	41.63	1600
1610	95.74	94.73	93.51	92.06	90.34	88.34	86.03	83.42	80.53	77.37	73.98	70.42	66.74	62.99	59.19	55.39	51.58	47.77	43.97	40.16	1610
1620	95.36	94.26	92.95	91.39	89.56	87.44	85.01	82.28	79.28	76.02	72.57	68.96	65.25	61.48	57.69	53.90	50.10	46.31	42.51	38.72	1620
1630	94.94	93.76	92.36	90.69	88.74	86.50	83.95	81.11	78.00	74.67	71.15	67.50	63.77	60.00	56.22	52.43	48.65	44.87	41.08	37.31	1630
1640	94.50	93.23	91.73	89.95	87.89	85.52	82.86	79.91	76.71	73.30	69.73	66.05	62.31	58.54	54.77	50.99	47.22	43.45	39.67	35.92	1640
1650	94.03	92.67	91.06	89.17	86.99	84.51	81.74	78.69	75.40	71.92	68.31	64.61	60.86	57.10	53.34	49.58	45.81	42.05	38.29	34.55	1650
1660	93.53	92.08	90.36	88.36	86.06	83.47	80.58	77.44	74.08	70.55	66.90	63.18	59.44	55.68	51.93	48.18	44.43	40.68	36.93	33.21	1660
1670	93.00	91.45	89.63	87.51	85.10	82.39	79.41	76.17	72.75	69.17	65.50	61.78	58.03	54.29	50.55	46.81	43.07	39.32	35.59	31.90	1670
1680	92.44	90.79	88.86	86.63	84.10	81.29	78.21	74.90	71.41	67.80	64.11	60.39	56.65	52.92	49.19	45.46	41.72	37.99	34.28	30.62	1680
1690	91.85	90.09	88.05	85.71	83.08	80.16	76.99	73.61	70.08	66.44	62.74	59.01	55.29	51.57	47.85	44.13	40.40	36.68	32.99	29.36	1690
1700	91.23	89.37	87.21	84.76	82.02	79.01	75.76	72.32	68.74	65.08	61.38	57.66	53.95	50.24	46.53	42.82	39.10	35.40	31.73	28.14	1700
1710	90.58	88.61	86.34	83.79	80.94	77.84	74.52	71.02	67.42	63.74	60.04	56.33	52.63	48.93	45.23	41.53	37.82	34.13	30.49	26.94	1710
1720	89.89	87.82	85.44	82.78	79.84	76.65	73.27	69.73	66.10	62.42	58.72	55.02	51.33	47.65	43.95	40.25	36.56	32.89	29.28	25.78	1720
1730	89.18	86.99	84.51	81.75	78.72	75.45	72.01	68.44	64.79	61.11	57.42	53.73	50.06	46.38	42.69	39.00	35.32	31.67	28.10	24.65	1730
1740	88.43	86.14	83.56	80.69	77.58	74.25	70.76	67.16	63.50	59.82	56.14	52.47	48.80	45.13	41.45	37.77	34.10	30.47	26.94	23.55	1740
1750	87.65	85.26	82.58	79.62	76.42	73.04	69.51	65.89	62.22	58.55	54.88	51.22	47.56	43.89	40.22	36.55	32.90	29.30	25.82	22.49	1750
1760	86.85	84.35	81.57	78.53	75.26	71.82	68.26	64.63	60.96	57.30	53.64	49.99	46.34	42.68	39.01	35.35	31.72	28.16	24.72	21.46	1760
1770	86.02	83.42	80.54	77.42	74.09	70.61	67.02	63.38	59.72	56.06	52.42	48.78	45.13	41.48	37.82	34.17	30.56	27.04	23.65	20.46	1770
1780	85.16	82.46	79.50	76.30	72.92	69.39	65.79	62.14	58.49	54.85	51.21	47.58	43.95	40.30	36.65	33.01	29.43	25.95	22.62	19.50	1780
1790	84.27	81.48	78.44	75.17	71.74	68.19	64.57	60.93	57.28	53.65	50.03	46.41	42.77	39.13	35.49	31.87	28.32	24.89	21.62	18.57	1790
1800	83.37	80.49	77.36	74.04	70.56	66.99	63.36	59.73	56.09	52.47	48.86	45.25	41.62	37.98	34.35	30.75	27.24	23.85	20.65	17.68	1800
1810	82.44	79.47	76.28	72.90	69.39	65.80	62.17	58.54	54.92	51.32	47.71	44.10	40.48	36.85	33.23	29.65	26.18	22.84	19.71	16.83	1810
1820	81.49	78.45	75.19	71.76	68.22	64.62	61.00	57.38	53.77	50.17	46.58	42.97	39.35	35.73	32.12	28.58	25.14	21.87	18.81	16.00	1820
1830	80.52	77.40	74.09	70.62	67.06	63.46	59.84	56.23	52.63	49.05	45.46	41.85	38.24	34.62	31.04	27.52	24.13	20.92	17.94	15.22	1830
1840	79.54	76.35	72.99	69.49	65.91	62.30	58.69	55.10	51.51	47.94	44.35	40.75	37.14	33.54	29.97	26.49	23.15	20.01	17.10	14.46	1840
1850	78.54	75.30	71.88	68.36	64.77	61.17	57.57	53.98	50.41	46.84	43.26	39.66	36.06	32.47	28.93	25.49	22.20	19.12	16.29	13.74	1850
1860	77.54	74.23	70.78	67.24	63.65	60.05	56.46	52.89	49.32	45.76	42.18	38.59	34.99	31.41	27.90	24.50	21.28	18.27	15.52	13.05	1860
1870	76.52	73.17	69.68	66.12	62.53	58.94	55.36	51.80	48.25	44.69	41.12	37.53	33.94	30.38	26.90	23.55	20.38	17.44	14.77	12.39	1870
1880	75.50	72.10	68.59	65.02	61.43	57.85	54.29	50.74	47.19	43.64	40.06	36.48	32.90	29.36	25.91	22.61	19.51	16.65	14.06	11.77	1880
1890	74.47	71.03	67.50	63.93	60.35	56.78	53.23	49.69	46.15	42.60	39.02	35.44	31.88	28.36	24.96	21.71	18.67	15.89	13.38	11.17	1890
1900	73.44	69.97	66.43	62.85	59.28	55.72	52.18	48.65	45.12	41.57	38.00	34.42	30.87	27.38	24.02	20.83	17.86	15.15	12.73	10.60	1900
1910	72.41	68.91	65.36	61.79	58.22	54.68	51.15	47.63	44.10	40.55	36.98	33.41	29.88	26.43	23.11	19.97	17.08	14.45	12.11	10.06	1910
1920	71.38	67.86	64.30	60.74	57.18	53.65	50.14	46.62	43.09	39.54	35.98	32.42	28.91	25.49	22.22	19.15	16.32	13.77	11.51	9.55	1920
1930	70.35	66.82	63.26	59.70	56.16	52.64	49.13	45.62	42.09	38.54	34.98	31.44	27.95	24.57	21.35	18.35	15.60	13.13	10.95	9.06	1930

TABLE IV CONTINUED

TEMP C	LOG(OXYGEN FUGACITY)																				TEMP C
	-4.0	-4.2	-4.4	-4.6	-4.8	-5.0	-5.2	-5.4	-5.6	-5.8	-6.0	-6.2	-6.4	-6.6	-6.8	-7.0	-7.2	-7.4	-7.6	-7.8	
1940	69.32	65.78	62.23	58.68	55.15	51.64	48.14	44.64	41.11	37.56	34.01	30.48	27.01	23.67	20.51	17.57	14.90	12.51	10.41	8.59	1940
1950	68.30	64.76	61.21	57.67	54.16	50.66	47.17	43.66	40.13	36.59	33.04	29.53	26.10	22.80	19.70	16.83	14.23	11.91	9.89	8.15	1950
1960	67.29	63.75	60.20	56.68	53.18	49.69	46.20	42.70	39.17	35.63	32.09	28.60	25.20	21.95	18.91	16.11	13.58	11.35	9.40	7.74	1960
1970	66.29	62.75	59.21	55.70	52.21	48.73	45.25	41.74	38.22	34.68	31.15	27.68	24.32	21.12	18.14	15.41	12.96	10.81	8.94	7.34	1970
1980	65.30	61.76	58.23	54.73	51.26	47.78	44.30	40.80	37.27	33.74	30.22	26.78	23.46	20.32	17.40	14.74	12.37	10.29	8.50	6.97	1980
1990	64.32	60.78	57.27	53.78	50.32	46.85	43.37	39.86	36.34	32.81	29.31	25.90	22.62	19.54	16.68	14.10	11.81	9.80	8.07	6.61	1990
2000	63.34	59.82	56.32	52.85	49.39	45.93	42.45	38.94	35.42	31.90	28.42	25.04	21.81	18.78	15.99	13.48	11.26	9.33	7.68	6.27	2000

	-8.0	-8.2	-8.4	-8.6	-8.8	-9.0	-9.2	-9.4	-9.6	-9.8	-10.0	-10.2	-10.4	-10.6	-10.8	-11.0	-11.2	-11.4	-11.6	-11.8	
720																					720
730																				99.99	730
740																			99.99	99.99	740
750																		99.99	99.99	99.99	750
760																	99.99	99.99	99.99	99.99	760
770																99.99	99.99	99.99	99.99	99.98	770
780														99.99	99.99	99.99	99.99	99.98	99.98	99.97	780
790													99.99	99.99	99.99	99.99	99.98	99.98	99.97	99.96	790
800												99.99	99.99	99.99	99.98	99.98	99.98	99.97	99.96	99.95	800
810										99.99	99.99	99.99	99.99	99.98	99.98	99.97	99.97	99.96	99.95	99.94	810
820									99.99	99.99	99.99	99.99	99.98	99.98	99.97	99.97	99.96	99.95	99.93	99.91	820
830								99.99	99.99	99.99	99.99	99.98	99.98	99.98	99.97	99.96	99.95	99.94	99.93	99.91	830
840							99.99	99.99	99.99	99.99	99.98	99.98	99.98	99.97	99.96	99.95	99.94	99.92	99.90	99.88	840
850						99.99	99.99	99.99	99.99	99.98	99.98	99.98	99.97	99.96	99.95	99.94	99.92	99.90	99.88	99.84	850
860				99.99	99.99	99.99	99.99	99.99	99.98	99.98	99.97	99.97	99.96	99.95	99.94	99.92	99.90	99.87	99.84	99.80	860
870			99.99	99.99	99.99	99.99	99.99	99.98	99.98	99.97	99.97	99.96	99.95	99.93	99.92	99.89	99.87	99.83	99.79	99.73	870
880	99.99	99.99	99.99	99.99	99.99	99.98	99.98	99.97	99.97	99.96	99.95	99.93	99.91	99.89	99.86	99.83	99.78	99.73	99.66	99.57	880
890	99.99	99.99	99.99	99.99	99.98	99.98	99.97	99.96	99.96	99.94	99.93	99.91	99.89	99.86	99.82	99.78	99.72	99.65	99.56	99.44	890
900	99.99	99.99	99.99	99.98	99.98	99.97	99.96	99.95	99.94	99.93	99.91	99.89	99.86	99.82	99.77	99.72	99.64	99.55	99.43	99.29	900
910	99.99	99.99	99.98	99.98	99.97	99.96	99.95	99.94	99.93	99.91	99.88	99.86	99.82	99.77	99.71	99.64	99.54	99.43	99.28	99.09	910
920	99.99	99.98	99.98	99.97	99.96	99.95	99.94	99.93	99.91	99.88	99.85	99.82	99.77	99.71	99.63	99.54	99.42	99.27	99.09	98.85	920
930	99.98	99.98	99.97	99.96	99.95	99.94	99.93	99.91	99.88	99.85	99.81	99.77	99.71	99.63	99.54	99.42	99.27	99.08	98.85	98.55	930
940	99.98	99.97	99.96	99.95	99.94	99.93	99.91	99.88	99.85	99.81	99.77	99.71	99.63	99.54	99.42	99.27	99.08	98.84	98.55	98.18	940
950	99.97	99.96	99.95	99.94	99.93	99.91	99.88	99.85	99.81	99.77	99.71	99.63	99.54	99.42	99.27	99.08	98.85	98.55	98.19	97.73	950
960	99.96	99.95	99.94	99.93	99.91	99.88	99.85	99.82	99.77	99.71	99.63	99.54	99.42	99.27	99.09	98.85	98.56	98.20	97.75	97.18	960
970	99.95	99.94	99.93	99.91	99.88	99.86	99.82	99.77	99.71	99.64	99.54	99.43	99.28	99.09	98.86	98.58	98.22	97.77	97.21	96.52	970
980	99.94	99.93	99.91	99.89	99.86	99.82	99.77	99.72	99.64	99.55	99.43	99.29	99.11	98.88	98.59	98.24	97.80	97.25	96.57	95.73	980
990	99.93	99.91	99.89	99.86	99.82	99.78	99.72	99.65	99.56	99.44	99.30	99.12	98.90	98.62	98.27	97.83	97.29	96.62	95.80	94.78	990
1000	99.91	99.89	99.86	99.83	99.78	99.73	99.65	99.57	99.45	99.31	99.14	98.92	98.64	98.30	97.87	97.34	96.69	95.88	94.88	93.67	1000
1010	99.89	99.87	99.83	99.79	99.73	99.66	99.58	99.47	99.33	99.16	98.94	98.67	98.34	97.92	97.40	96.76	95.97	95.00	93.81	92.37	1010
1020	99.87	99.83	99.79	99.74	99.67	99.59	99.48	99.35	99.18	98.97	98.71	98.38	97.97	97.47	96.84	96.07	95.12	93.96	92.56	90.88	1020
1030	99.84	99.80	99.75	99.68	99.60	99.49	99.37	99.20	99.00	98.74	98.43	98.03	97.54	96.93	96.18	95.25	94.13	92.76	91.12	89.16	1030
1040	99.80	99.75	99.69	99.61	99.51	99.39	99.23	99.03	98.78	98.48	98.09	97.62	97.03	96.30	95.40	94.30	92.98	91.38	89.47	87.23	1040
1050	99.76	99.70	99.62	99.53	99.41	99.25	99.06	98.83	98.53	98.16	97.70	97.13	96.42	95.55	94.49	93.20	91.65	89.80	87.62	85.07	1050
1060	99.71	99.64	99.55	99.43	99.28	99.10	98.87	98.58	98.23	97.78	97.23	96.55	95.71	94.69	93.44	91.94	90.14	88.02	85.55	82.70	1060
1070	99.65	99.56	99.45	99.31	99.14	98.92	98.64	98.30	97.87	97.34	96.68	95.88	94.89	93.69	92.24	90.50	88.44	86.04	83.27	80.12	1070
1080	99.58	99.48	99.34	99.17	98.96	98.70	98.37	97.96	97.45	96.82	96.05	95.10	93.94	92.54	90.87	88.88	86.55	83.86	80.80	77.37	1080
1090	99.50	99.37	99.21	99.01	98.76	98.44	98.05	97.56	96.96	96.22	95.31	94.20	92.85	91.24	89.32	87.07	84.46	81.49	78.14	74.45	1090
1100	99.40	99.25	99.06	98.82	98.52	98.14	97.68	97.10	96.39	95.52	94.46	93.17	91.62	89.77	87.60	85.08	82.19	78.94	75.33	71.41	1100

TABLE IV CONTINUED

TEMP C	LOG(OXYGEN FUGACITY)																				TEMP C
	-8.0	-8.2	-8.4	-8.6	-8.8	-9.0	-9.2	-9.4	-9.6	-9.8	-10.0	-10.2	-10.4	-10.6	-10.8	-11.0	-11.2	-11.4	-11.6	-11.8	
1110	99.29	99.10	98.88	98.59	98.24	97.79	97.25	96.57	95.74	94.72	93.49	92.00	90.23	88.14	85.70	82.91	79.75	76.24	72.40	68.28	1110
1120	99.15	98.93	98.66	98.33	97.91	97.39	96.75	95.95	94.99	93.81	92.39	90.69	88.68	86.33	83.63	80.57	77.15	73.40	69.37	65.09	1120
1130	98.99	98.74	98.42	98.02	97.53	96.92	96.17	95.25	94.13	92.77	91.15	89.22	86.97	84.36	81.40	78.08	74.43	70.48	66.28	61.88	1130
1140	98.81	98.51	98.13	97.67	97.09	96.38	95.51	94.44	93.15	91.60	89.76	87.60	85.09	82.23	79.01	75.46	71.60	67.48	63.15	58.67	1140
1150	98.60	98.24	97.80	97.26	96.59	95.76	94.75	93.53	92.05	90.30	88.23	85.82	83.06	79.95	76.50	72.73	68.70	64.44	60.02	55.49	1150
1160	98.35	97.94	97.43	96.79	96.01	95.06	93.90	92.50	90.83	88.85	86.55	83.89	80.89	77.54	73.87	69.93	65.75	61.39	56.91	52.36	1160
1170	98.07	97.59	96.99	96.26	95.36	94.26	92.94	91.35	89.47	87.27	84.72	81.83	78.59	75.02	71.17	67.07	62.78	58.36	53.84	49.29	1170
1180	97.74	97.18	96.49	95.65	94.62	93.37	91.86	90.08	87.98	85.54	82.76	79.63	76.17	72.41	68.40	64.19	59.82	55.35	50.83	46.31	1180
1190	97.37	96.73	95.93	94.96	93.78	92.36	90.67	88.67	86.35	83.68	80.66	77.32	73.66	69.74	65.60	61.30	56.88	52.40	47.89	43.40	1190
1200	96.95	96.20	95.29	94.19	92.85	91.25	89.35	87.14	84.59	81.69	78.46	74.91	71.08	67.02	62.79	58.42	53.98	49.50	45.03	40.60	1200
1210	96.47	95.62	94.58	93.32	91.81	90.02	87.92	85.48	82.70	79.59	76.15	72.42	68.45	64.29	59.98	55.58	51.13	46.68	42.25	37.89	1210
1220	95.92	94.95	93.77	92.36	90.67	88.67	86.36	83.70	80.70	77.38	73.76	69.88	65.80	61.55	57.20	52.79	48.35	43.93	39.56	35.28	1220
1230	95.31	94.21	92.88	91.29	89.41	87.21	84.68	81.80	78.60	75.09	71.31	67.31	63.13	58.83	54.46	50.05	45.64	41.26	36.96	32.78	1230
1240	94.63	93.39	91.89	90.12	88.04	85.63	82.88	79.80	76.41	72.73	68.82	64.71	60.47	56.14	51.76	47.37	43.00	38.68	34.46	30.39	1240
1250	93.87	92.47	90.81	88.84	86.56	83.94	80.99	77.71	74.14	70.32	66.30	62.12	57.84	53.50	49.12	44.76	40.43	36.19	32.07	28.12	1250
1260	93.03	91.46	89.62	87.46	84.97	82.15	79.00	75.54	71.82	67.89	63.78	59.55	55.24	50.90	46.55	42.22	37.96	33.79	29.78	25.96	1260
1270	92.10	90.36	88.33	85.97	83.28	80.26	76.93	73.31	69.47	65.43	61.26	57.00	52.69	48.36	44.03	39.76	35.56	31.49	27.59	23.92	1270
1280	91.08	89.16	86.94	84.38	81.49	78.29	74.79	71.04	67.09	62.98	58.77	54.49	50.18	45.87	41.59	37.37	33.26	29.29	25.52	22.00	1280
1290	89.97	87.87	85.45	82.69	79.62	76.24	72.60	68.73	64.70	60.54	56.30	52.02	47.73	43.45	39.22	35.07	31.04	27.19	23.56	20.20	1290
1300	88.76	86.48	83.86	80.92	77.67	74.14	70.37	66.41	62.31	58.12	53.88	49.61	45.34	41.10	36.92	32.85	28.92	25.19	21.71	18.51	1300
1310	87.47	84.99	82.19	79.07	75.66	71.99	68.12	64.09	59.95	55.74	51.49	47.24	43.00	38.81	34.70	30.71	26.89	23.30	19.97	16.94	1310
1320	86.08	83.42	80.44	77.15	73.60	69.82	65.86	61.78	57.61	53.39	49.16	44.93	40.73	36.59	32.55	28.66	24.96	21.51	18.34	15.48	1320
1330	84.61	81.77	78.62	75.18	71.50	67.62	63.60	59.48	55.30	51.09	46.88	42.68	38.52	34.45	30.49	26.70	23.13	19.83	16.82	14.14	1330
1340	83.06	80.04	76.73	73.16	69.38	65.43	61.36	57.22	53.04	48.84	44.65	40.48	36.38	32.37	28.51	24.83	21.40	18.25	15.41	12.89	1340
1350	81.43	78.25	74.80	71.11	67.24	63.24	59.14	54.99	50.81	46.63	42.47	38.35	34.30	30.37	26.61	23.06	19.77	16.78	14.10	11.75	1350
1360	79.73	76.41	72.83	69.04	65.11	61.06	56.95	52.80	48.63	44.48	40.35	36.27	32.29	28.45	24.80	21.38	18.24	15.40	12.89	10.70	1360
1370	77.98	74.52	70.83	66.97	62.98	58.91	54.79	50.64	46.50	42.37	38.28	34.26	30.35	26.61	23.07	19.79	16.80	14.13	11.78	9.74	1370
1380	76.17	72.59	68.81	64.89	60.87	56.78	52.66	48.53	44.41	40.31	36.27	32.31	28.49	24.84	21.43	18.30	15.46	12.95	10.75	8.86	1380
1390	74.33	70.64	66.80	62.83	58.78	54.69	50.58	46.47	42.37	38.31	34.32	30.43	26.69	23.16	19.89	16.90	14.22	11.86	9.81	8.06	1390
1400	72.45	68.69	64.78	60.78	56.72	52.64	48.54	44.45	40.38	36.36	32.42	28.61	24.98	21.57	18.43	15.58	13.06	10.85	8.95	7.33	1400
1410	70.56	66.72	62.77	58.76	54.70	50.62	46.54	42.47	38.44	34.46	30.59	26.87	23.34	20.05	17.05	14.36	11.98	9.92	8.16	6.67	1410
1420	68.65	64.76	60.79	56.76	52.70	48.64	44.58	40.54	36.54	32.62	28.82	25.19	21.78	18.62	15.77	13.22	10.99	9.07	7.44	6.06	1420
1430	66.74	62.82	58.83	54.80	50.75	46.70	42.66	38.65	34.70	30.84	27.12	23.59	20.29	17.28	14.56	12.16	10.08	8.29	6.78	5.51	1430
1440	64.84	60.89	56.89	52.87	48.83	44.80	40.79	36.81	32.91	29.11	25.48	22.06	18.89	16.01	13.44	11.19	9.24	7.58	6.18	5.02	1440
1450	62.95	58.99	54.99	50.97	46.95	42.94	38.96	35.02	31.17	27.45	23.91	20.60	17.56	14.82	12.39	10.28	8.46	6.93	5.64	4.57	1450
1460	61.08	57.11	53.11	49.11	45.11	41.12	37.17	33.27	29.48	25.84	22.41	19.22	16.31	13.71	11.42	9.44	7.75	6.33	5.14	4.16	1460
1470	59.23	55.26	51.27	47.28	43.30	39.34	35.42	31.58	27.85	24.30	20.97	17.91	15.14	12.67	10.52	8.67	7.10	5.79	4.69	3.79	1470
1480	57.41	53.44	49.47	45.49	41.53	37.60	33.72	29.93	26.28	22.83	19.61	16.67	14.03	11.71	9.69	7.97	6.51	5.29	4.28	3.45	1480
1490	55.61	51.66	47.70	43.74	39.80	35.90	32.06	28.33	24.77	21.42	18.32	15.51	13.00	10.81	8.92	7.31	5.96	4.84	3.91	3.15	1490
1500	53.85	49.90	45.96	42.02	38.10	34.23	30.45	26.79	23.32	20.07	17.09	14.41	12.04	9.98	8.21	6.72	5.46	4.42	3.57	2.87	1500
1510	52.11	48.18	44.25	40.33	36.44	32.61	28.88	25.30	21.92	18.79	15.94	13.39	11.15	9.21	7.56	6.17	5.01	4.05	3.26	2.62	1510
1520	50.41	46.49	42.58	38.68	34.82	31.04	27.37	23.87	20.59	17.57	14.85	12.43	10.31	8.50	6.96	5.66	4.59	3.71	2.98	2.39	1520
1530	48.74	44.83	40.93	37.06	33.24	29.50	25.91	22.50	19.32	16.42	13.82	11.53	9.54	7.84	6.40	5.20	4.21	3.39	2.73	2.19	1530
1540	47.09	43.20	39.32	35.48	31.69	28.02	24.49	21.18	18.11	15.33	12.86	10.69	8.82	7.23	5.89	4.78	3.86	3.11	2.50	2.00	1540
1550	45.48	41.60	37.74	33.93	30.19	26.57	23.13	19.92	16.97	14.31	11.96	9.91	8.16	6.67	5.43	4.39	3.55	2.85	2.29	1.83	1550
1560	43.89	40.03	36.20	32.42	28.73	25.18	21.83	18.72	15.88	13.34	11.11	9.19	7.54	6.15	5.00	4.04	3.26	2.62	2.10	1.68	1560
1570	42.33	38.49	34.68	30.94	27.31	23.84	20.58	17.57	14.85	12.44	10.33	8.51	6.97	5.68	4.60	3.72	2.99	2.40	1.92	1.54	1570
1580	40.80	36.98	33.20	29.50	25.93	22.54	19.38	16.48	13.88	11.59	9.59	7.89	6.44	5.24	4.24	3.42	2.75	2.21	1.77	1.41	1580
1590	39.30	35.50	31.76	28.11	24.60	21.30	18.24	15.45	12.97	10.79	8.91	7.31	5.96	4.84	3.91	3.15	2.53	2.03	1.62	1.30	1590
1600	37.82	34.05	30.34	26.75	23.32	20.11	17.15	14.48	12.11	10.05	8.27	6.77	5.51	4.47	3.60	2.90	2.33	1.86	1.49	1.19	1600
1610	36.38	32.63	28.97	25.43	22.08	18.96	16.11	13.56	11.31	9.35	7.68	6.27	5.10	4.12	3.33	2.67	2.14	1.72	1.37	1.10	1610
1620	34.95	31.24	27.63	24.16	20.89	17.87	15.13	12.69	10.55	8.70	7.13	5.81	4.72	3.81	3.07	2.47	1.98	1.58	1.26	1.01	1620
1630	33.56	29.89	26.33	22.93	19.75	16.83	14.20	11.87	9.84	8.10	6.62	5.39	4.37	3.52	2.83	2.27	1.82	1.46	1.16	0.93	1630

TABLE IV CONTINUED

TEMP C	LOG(OXYGEN FUGACITY)																				TEMP C
	-8.0	-8.2	-8.4	-8.6	-8.8	-9.0	-9.2	-9.4	-9.6	-9.8	-10.0	-10.2	-10.4	-10.6	-10.8	-11.0	-11.2	-11.4	-11.6	-11.8	
1640	32.20	28.57	25.06	21.75	18.66	15.84	13.32	11.10	9.18	7.54	6.15	5.00	4.04	3.26	2.62	2.10	1.68	1.34	1.07	0.85	1640
1650	30.87	27.28	23.84	20.61	17.62	14.90	12.49	10.38	8.56	7.01	5.71	4.63	3.74	3.01	2.42	1.94	1.55	1.24	0.99	0.79	1650
1660	29.56	26.03	22.66	19.51	16.62	14.01	11.71	9.70	7.98	6.53	5.31	4.30	3.47	2.79	2.24	1.79	1.43	1.14	0.91	0.73	1660
1670	28.29	24.82	21.52	18.46	15.67	13.17	10.97	9.07	7.44	6.07	4.93	3.99	3.22	2.58	2.07	1.66	1.33	1.06	0.84	0.67	1670
1680	27.05	23.64	20.42	17.46	14.76	12.37	10.28	8.47	6.94	5.65	4.58	3.70	2.98	2.39	1.92	1.53	1.23	0.98	0.78	0.62	1680
1690	25.85	22.50	19.37	16.49	13.91	11.62	9.63	7.92	6.47	5.26	4.26	3.44	2.77	2.22	1.78	1.42	1.13	0.90	0.72	0.57	1690
1700	24.68	21.40	18.36	15.58	13.09	10.91	9.01	7.40	6.04	4.90	3.96	3.20	2.57	2.06	1.65	1.32	1.05	0.84	0.67	0.53	1700
1710	23.54	20.34	17.39	14.71	12.32	10.24	8.44	6.91	5.63	4.57	3.69	2.97	2.38	1.91	1.53	1.22	0.97	0.78	0.62	0.49	1710
1720	22.44	19.32	16.46	13.88	11.59	9.61	7.90	6.46	5.25	4.26	3.43	2.76	2.22	1.77	1.42	1.13	0.90	0.72	0.57	0.46	1720
1730	21.38	18.34	15.57	13.09	10.90	9.01	7.40	6.04	4.90	3.97	3.20	2.57	2.06	1.65	1.32	1.05	0.84	0.67	0.53	0.42	1730
1740	20.36	17.40	14.73	12.34	10.25	8.46	6.93	5.65	4.58	3.70	2.98	2.39	1.92	1.53	1.22	0.98	0.78	0.62	0.49	0.39	1740
1750	19.37	16.50	13.92	11.63	9.64	7.93	6.49	5.28	4.27	3.45	2.77	2.23	1.78	1.43	1.14	0.91	0.72	0.58	0.46	0.37	1750
1760	18.42	15.64	13.15	10.96	9.07	7.44	6.08	4.94	3.99	3.22	2.59	2.07	1.66	1.33	1.06	0.84	0.67	0.54	0.43	0.34	1760
1770	17.50	14.82	12.43	10.33	8.52	6.98	5.69	4.62	3.73	3.00	2.41	1.93	1.55	1.24	0.99	0.79	0.63	0.50	0.40	0.32	1770
1780	16.63	14.03	11.73	9.73	8.01	6.55	5.33	4.32	3.49	2.80	2.25	1.80	1.44	1.15	0.92	0.73	0.58	0.46	0.37	0.29	1780
1790	15.79	13.29	11.08	9.17	7.53	6.15	5.00	4.04	3.26	2.62	2.10	1.68	1.34	1.07	0.86	0.68	0.54	0.43	0.34	0.27	1790
1800	14.98	12.57	10.46	8.63	7.08	5.77	4.68	3.78	3.05	2.45	1.96	1.57	1.25	1.00	0.80	0.64	0.51	0.40	0.32	0.25	1800
1810	14.21	11.90	9.87	8.13	6.66	5.42	4.39	3.54	2.85	2.29	1.83	1.47	1.17	0.93	0.74	0.59	0.47	0.38	0.30	0.24	1810
1820	13.48	11.25	9.32	7.66	6.26	5.09	4.12	3.32	2.67	2.14	1.71	1.37	1.09	0.87	0.70	0.55	0.44	0.35	0.28	0.22	1820
1830	12.78	10.64	8.79	7.21	5.88	4.78	3.86	3.11	2.50	2.00	1.60	1.28	1.02	0.82	0.65	0.52	0.41	0.33	0.26	0.21	1830
1840	12.12	10.06	8.30	6.79	5.53	4.49	3.62	2.92	2.34	1.88	1.50	1.20	0.96	0.76	0.61	0.48	0.38	0.31	0.24	0.19	1840
1850	11.48	9.51	7.83	6.40	5.21	4.22	3.40	2.74	2.20	1.76	1.41	1.12	0.90	0.71	0.57	0.45	0.36	0.29	0.23	0.18	1850
1860	10.88	9.00	7.39	6.03	4.90	3.96	3.19	2.57	2.06	1.65	1.32	1.05	0.84	0.67	0.53	0.42	0.34	0.27	0.21	0.17	1860
1870	10.31	8.50	6.97	5.68	4.61	3.72	3.00	2.41	1.93	1.55	1.23	0.98	0.79	0.63	0.50	0.40	0.32	0.25	0.20	0.16	1870
1880	9.76	8.04	6.58	5.36	4.34	3.50	2.82	2.26	1.81	1.45	1.16	0.92	0.74	0.59	0.47	0.37	0.30	0.23	0.19	0.15	1880
1890	9.25	7.60	6.21	5.05	4.09	3.30	2.65	2.13	1.70	1.36	1.09	0.87	0.69	0.55	0.44	0.35	0.28	0.22	0.17	0.14	1890
1900	8.76	7.19	5.86	4.76	3.85	3.10	2.49	2.00	1.60	1.28	1.02	0.81	0.65	0.52	0.41	0.33	0.26	0.21	0.16	0.13	1900
1910	8.29	6.80	5.54	4.49	3.63	2.92	2.34	1.88	1.50	1.20	0.96	0.76	0.61	0.48	0.39	0.31	0.24	0.19	0.15	0.12	1910
1920	7.86	6.43	5.23	4.23	3.42	2.75	2.21	1.77	1.41	1.13	0.90	0.72	0.57	0.45	0.36	0.29	0.23	0.18	0.14	0.11	1920
1930	7.44	6.08	4.94	3.99	3.22	2.59	2.08	1.66	1.33	1.06	0.85	0.67	0.54	0.43	0.34	0.27	0.21	0.17	0.14	0.11	1930
1940	7.05	5.75	4.66	3.77	3.04	2.44	1.96	1.56	1.25	1.00	0.80	0.63	0.50	0.40	0.32	0.25	0.20	0.16	0.13	0.10	1940
1950	6.68	5.44	4.41	3.56	2.86	2.30	1.84	1.47	1.18	0.94	0.75	0.60	0.47	0.38	0.30	0.24	0.19	0.15	0.12	0.10	1950
1960	6.33	5.14	4.17	3.36	2.70	2.17	1.74	1.39	1.11	0.88	0.70	0.56	0.45	0.36	0.28	0.22	0.18	0.14	0.11	0.09	1960
1970	5.99	4.87	3.94	3.17	2.55	2.05	1.64	1.31	1.04	0.83	0.66	0.53	0.42	0.33	0.27	0.21	0.17	0.13	0.11	0.08	1970
1980	5.68	4.61	3.72	3.00	2.41	1.93	1.54	1.23	0.98	0.79	0.63	0.50	0.40	0.32	0.25	0.20	0.16	0.13	0.10	0.08	1980
1990	5.38	4.36	3.52	2.83	2.28	1.82	1.46	1.16	0.93	0.74	0.59	0.47	0.37	0.30	0.24	0.19	0.15	0.12	0.09	0.07	1990
2000	5.10	4.13	3.33	2.68	2.15	1.72	1.38	1.10	0.88	0.70	0.56	0.44	0.35	0.28	0.22	0.18	0.14	0.11	0.09	0.07	2000

	-12.0	-12.2	-12.4	-12.6	-12.8	-13.0	-13.2	-13.4	-13.6	-13.8	-14.0	-14.2	-14.4	-14.6	-14.8	-15.0	-15.2	-15.4	-15.6	-15.8	
600																					600
610																				99.99	610
620																		99.99	99.99	99.99	620
630																	99.99	99.99	99.99	99.99	630
640															99.99	99.99	99.99	99.99	99.99	99.98	640
650													99.99	99.99	99.99	99.99	99.99	99.98	99.98	99.97	650
660											99.99	99.99	99.99	99.99	99.99	99.98	99.98	99.97	99.97	99.96	660
670										99.99	99.99	99.99	99.99	99.98	99.98	99.98	99.97	99.96	99.95	99.94	670
680								99.99	99.99	99.99	99.99	99.99	99.98	99.98	99.97	99.96	99.96	99.94	99.93	99.91	680

TABLE IV CONTINUED

TEMP C	LOG(OXYGEN FUGACITY)																				TEMP C
	-12.0	-12.2	-12.4	-12.6	-12.8	-13.0	-13.2	-13.4	-13.6	-13.8	-14.0	-14.2	-14.4	-14.6	-14.8	-15.0	-15.2	-15.4	-15.6	-15.8	
690						99.99	99.99	99.99	99.99	99.99	99.98	99.98	99.97	99.97	99.96	99.95	99.93	99.92	99.90	99.87	690
700					99.99	99.99	99.99	99.99	99.99	99.98	99.98	99.97	99.96	99.95	99.94	99.93	99.91	99.88	99.85	99.81	700
710			99.99	99.99	99.99	99.99	99.99	99.98	99.98	99.97	99.97	99.96	99.95	99.93	99.92	99.89	99.87	99.83	99.79	99.73	710
720		99.99	99.99	99.99	99.99	99.98	99.98	99.98	99.97	99.96	99.95	99.94	99.92	99.91	99.88	99.85	99.81	99.76	99.70	99.62	720
730	99.99	99.99	99.99	99.99	99.98	99.98	99.97	99.97	99.96	99.95	99.93	99.92	99.89	99.87	99.83	99.79	99.73	99.67	99.58	99.47	730
740	99.99	99.99	99.99	99.98	99.98	99.97	99.96	99.95	99.94	99.93	99.91	99.88	99.85	99.81	99.77	99.70	99.63	99.53	99.41	99.26	740
750	99.99	99.98	99.98	99.97	99.97	99.96	99.95	99.93	99.92	99.90	99.87	99.84	99.79	99.74	99.67	99.59	99.49	99.35	99.19	98.98	750
760	99.98	99.98	99.97	99.96	99.96	99.94	99.93	99.91	99.89	99.86	99.82	99.78	99.72	99.64	99.55	99.44	99.29	99.11	98.88	98.59	760
770	99.98	99.97	99.96	99.95	99.94	99.92	99.90	99.88	99.85	99.81	99.76	99.69	99.61	99.51	99.39	99.23	99.03	98.78	98.47	98.08	770
780	99.97	99.96	99.95	99.93	99.92	99.89	99.87	99.83	99.79	99.74	99.67	99.58	99.47	99.34	99.17	98.95	98.68	98.35	97.93	97.40	780
790	99.95	99.94	99.93	99.91	99.89	99.86	99.82	99.77	99.72	99.64	99.55	99.43	99.29	99.10	98.87	98.59	98.23	97.78	97.21	96.51	790
800	99.94	99.92	99.90	99.88	99.85	99.81	99.76	99.70	99.62	99.52	99.39	99.24	99.04	98.80	98.49	98.11	97.63	97.03	96.28	95.36	800
810	99.92	99.90	99.87	99.84	99.80	99.74	99.68	99.59	99.49	99.36	99.19	98.98	98.72	98.40	97.99	97.48	96.85	96.06	95.09	93.89	810
820	99.89	99.86	99.83	99.78	99.73	99.66	99.57	99.46	99.32	99.14	98.92	98.65	98.31	97.88	97.34	96.67	95.85	94.83	93.57	92.04	820
830	99.86	99.82	99.77	99.71	99.64	99.55	99.43	99.28	99.10	98.87	98.58	98.22	97.77	97.21	96.51	95.64	94.58	93.27	91.68	89.75	830
840	99.81	99.76	99.70	99.62	99.53	99.40	99.25	99.06	98.82	98.51	98.14	97.67	97.08	96.35	95.45	94.35	92.99	91.34	89.35	86.96	840
850	99.75	99.69	99.61	99.51	99.38	99.22	99.02	98.77	98.45	98.06	97.57	96.96	96.21	95.28	94.13	92.73	91.03	88.98	86.54	83.66	850
860	99.68	99.59	99.49	99.36	99.19	98.98	98.72	98.40	97.99	97.49	96.86	96.08	95.12	93.94	92.50	90.76	88.66	86.16	83.23	79.83	860
870	99.58	99.47	99.33	99.16	98.95	98.68	98.35	97.93	97.41	96.76	95.96	94.98	93.77	92.30	90.51	88.37	85.84	82.86	79.42	75.51	870
880	99.46	99.32	99.14	98.92	98.65	98.30	97.88	97.34	96.68	95.86	94.86	93.62	92.12	90.30	88.13	85.56	82.55	79.08	75.15	70.77	880
890	99.30	99.12	98.90	98.62	98.27	97.83	97.29	96.61	95.78	94.75	93.50	91.97	90.13	87.93	85.33	82.30	78.81	74.86	70.48	65.70	890
900	99.11	98.88	98.59	98.24	97.79	97.24	96.55	95.71	94.67	93.40	91.85	89.99	87.77	85.15	82.10	78.60	74.65	70.28	65.52	60.45	900
910	98.86	98.57	98.21	97.76	97.20	96.51	95.66	94.60	93.32	91.76	89.89	87.65	85.02	81.97	78.47	74.52	70.16	65.42	60.38	55.12	910
920	98.56	98.20	97.74	97.18	96.48	95.62	94.56	93.27	91.70	89.82	87.58	84.95	81.89	78.39	74.46	70.11	65.40	60.40	55.18	49.86	920
930	98.19	97.73	97.16	96.46	95.60	94.54	93.24	91.67	89.79	87.55	84.92	81.86	78.38	74.47	70.15	65.47	60.50	55.32	50.04	44.76	930
940	97.73	97.16	96.46	95.59	94.53	93.24	91.67	89.79	87.56	84.93	81.90	78.43	74.54	70.25	65.61	60.68	55.55	50.31	45.06	39.91	940
950	97.17	96.47	95.61	94.55	93.26	91.70	89.83	87.60	85.00	81.98	78.54	74.68	70.42	65.82	60.94	55.85	50.65	45.44	40.31	35.37	950
960	96.49	95.63	94.58	93.30	91.75	89.89	87.69	85.10	82.11	78.70	74.87	70.66	66.10	61.26	56.22	51.06	45.89	40.79	35.85	31.17	960
970	95.67	94.63	93.36	91.83	89.99	87.81	85.25	82.29	78.91	75.13	70.96	66.45	61.66	56.66	51.55	46.41	41.33	36.40	31.72	27.33	970
980	94.70	93.45	91.93	90.12	87.96	85.43	82.51	79.17	75.44	71.32	66.86	62.12	57.17	52.10	46.99	41.94	37.02	32.32	27.92	23.87	980
990	93.55	92.06	90.27	88.15	85.66	82.77	79.49	75.80	71.73	67.33	62.64	57.74	52.72	47.64	42.61	37.70	32.99	28.57	24.47	20.76	990
1000	92.21	90.45	88.36	85.91	83.08	79.84	76.21	72.20	67.85	63.22	58.37	53.39	48.35	43.34	38.44	33.72	29.27	25.14	21.37	17.99	1000
1010	90.65	88.61	86.20	83.41	80.23	76.66	72.71	68.42	63.85	59.06	54.12	49.12	44.13	39.24	34.51	30.04	25.86	22.04	18.60	15.56	1010
1020	88.87	86.52	83.79	80.66	77.15	73.27	69.04	64.53	59.80	54.91	49.94	44.98	40.09	35.36	30.86	26.64	22.76	19.26	16.14	13.42	1020
1030	86.86	84.19	81.13	77.68	73.87	69.71	65.26	60.58	55.75	50.82	45.88	41.01	36.27	31.74	27.48	23.54	19.97	16.78	13.98	11.56	1030
1040	84.62	81.63	78.25	74.50	70.42	66.03	61.42	56.63	51.75	46.84	41.97	37.23	32.67	28.37	24.38	20.74	17.47	14.59	12.08	9.94	1040
1050	82.15	78.85	75.17	71.16	66.85	62.29	57.56	52.72	47.84	42.99	38.25	33.67	29.32	25.27	21.56	18.21	15.24	12.66	10.43	8.54	1050
1060	79.47	75.88	71.94	67.70	63.21	58.54	53.74	48.89	44.06	39.31	34.71	30.33	26.22	22.44	19.01	15.95	13.28	10.96	9.00	7.34	1060
1070	76.61	72.75	68.58	64.16	59.55	54.80	49.99	45.18	40.43	35.82	31.40	27.23	23.37	19.86	16.71	13.94	11.54	9.49	7.75	6.30	1070
1080	73.59	69.50	65.15	60.60	55.90	51.13	46.34	41.60	36.97	32.51	28.30	24.37	20.77	17.53	14.67	12.17	10.02	8.21	6.68	5.42	1080
1090	70.44	66.17	61.68	57.03	52.30	47.54	42.81	38.17	33.69	29.42	25.42	21.74	18.41	15.44	12.85	10.61	8.70	7.09	5.76	4.65	1090
1100	67.21	62.79	58.20	53.51	48.78	44.06	39.42	34.91	30.59	26.53	22.77	19.34	16.27	13.58	11.24	9.24	7.55	6.13	4.96	4.00	1100
1110	63.93	59.40	54.76	50.06	45.36	40.71	36.18	31.83	27.70	23.86	20.34	17.17	14.36	11.92	9.82	8.04	6.54	5.30	4.28	3.45	1110
1120	60.63	56.03	51.37	46.69	42.05	37.50	33.11	28.93	25.00	21.39	18.12	15.20	12.65	10.45	8.57	6.99	5.68	4.59	3.70	2.97	1120
1130	57.34	52.72	48.06	43.43	38.87	34.45	30.21	26.21	22.51	19.13	16.11	13.44	11.13	9.15	7.48	6.08	4.92	3.97	3.19	2.56	1130
1140	54.09	49.46	44.85	40.28	35.83	31.55	27.48	23.69	20.21	17.08	14.30	11.87	9.78	8.01	6.53	5.29	4.27	3.44	2.76	2.21	1140
1150	50.90	46.30	41.74	37.27	32.94	28.81	24.94	21.36	18.11	15.21	12.67	10.47	8.59	7.01	5.70	4.61	3.71	2.98	2.39	1.92	1150
1160	47.78	43.23	38.74	34.38	30.20	26.24	22.57	19.21	16.19	13.53	11.21	9.23	7.55	6.14	4.97	4.01	3.23	2.59	2.08	1.66	1160
1170	44.75	40.26	35.87	31.64	27.61	23.84	20.37	17.24	14.45	12.01	9.91	8.13	6.62	5.37	4.34	3.50	2.81	2.25	1.80	1.44	1170
1180	41.81	37.40	33.13	29.03	25.18	21.61	18.35	15.44	12.88	10.66	8.76	7.16	5.82	4.71	3.80	3.05	2.45	1.96	1.57	1.25	1180
1190	38.98	34.67	30.52	26.58	22.91	19.54	16.50	13.81	11.47	9.45	7.74	6.30	5.11	4.12	3.32	2.67	2.14	1.71	1.36	1.09	1190
1200	36.26	32.06	28.05	24.28	20.80	17.64	14.81	12.34	10.20	8.37	6.83	5.55	4.49	3.62	2.91	2.33	1.87	1.49	1.19	0.95	1200
1210	33.64	29.57	25.71	22.12	18.84	15.89	13.26	11.01	9.06	7.41	6.03	4.89	3.94	3.17	2.55	2.04	1.63	1.30	1.04	0.83	1210

TABLE IV CONTINUED

TEMP C	LOG(OXYGEN FUGACITY)																				TEMP C
	-12.0	-12.2	-12.4	-12.6	-12.8	-13.0	-13.2	-13.4	-13.6	-13.8	-14.0	-14.2	-14.4	-14.6	-14.8	-15.0	-15.2	-15.4	-15.6	-15.8	
1220	31.15	27.21	23.52	20.12	17.04	14.29	11.89	9.82	8.05	6.57	5.33	4.31	3.47	2.79	2.23	1.79	1.43	1.14	0.91	0.72	1220
1230	28.77	24.99	21.47	18.26	15.38	12.84	10.64	8.75	7.15	5.81	4.71	3.80	3.05	2.45	1.96	1.57	1.25	1.00	0.80	0.63	1230
1240	26.52	22.90	19.56	16.55	13.87	11.53	9.51	7.79	6.35	5.15	4.16	3.35	2.69	2.16	1.73	1.38	1.10	0.88	0.70	0.56	1240
1250	24.39	20.94	17.79	14.97	12.49	10.33	8.49	6.94	5.64	4.56	3.68	2.96	2.37	1.90	1.52	1.21	0.97	0.77	0.61	0.49	1250
1260	22.39	19.11	16.15	13.53	11.23	9.26	7.59	6.18	5.01	4.05	3.26	2.62	2.10	1.68	1.34	1.07	0.85	0.68	0.54	0.43	1260
1270	20.52	17.42	14.65	12.21	10.10	8.30	6.77	5.50	4.45	3.59	2.89	2.32	1.85	1.48	1.18	0.94	0.75	0.60	0.48	0.38	1270
1280	18.77	15.85	13.27	11.01	9.07	7.43	6.05	4.90	3.96	3.19	2.56	2.05	1.64	1.31	1.05	0.83	0.66	0.53	0.42	0.33	1280
1290	17.14	14.41	12.00	9.92	8.15	6.65	5.40	4.37	3.52	2.83	2.27	1.82	1.45	1.16	0.93	0.74	0.59	0.47	0.37	0.30	1290
1300	15.63	13.08	10.85	8.94	7.32	5.96	4.83	3.90	3.14	2.52	2.02	1.61	1.29	1.03	0.82	0.65	0.52	0.41	0.33	0.26	1300
1310	14.24	11.86	9.80	8.05	6.57	5.34	4.32	3.48	2.80	2.24	1.79	1.43	1.14	0.91	0.73	0.58	0.46	0.37	0.29	0.23	1310
1320	12.95	10.75	8.85	7.25	5.90	4.78	3.86	3.11	2.49	2.00	1.60	1.28	1.02	0.81	0.65	0.51	0.41	0.33	0.26	0.21	1320
1330	11.78	9.73	7.99	6.52	5.30	4.28	3.45	2.78	2.23	1.78	1.42	1.14	0.91	0.72	0.58	0.46	0.36	0.29	0.23	0.18	1330
1340	10.70	8.81	7.21	5.87	4.76	3.84	3.09	2.48	1.99	1.59	1.27	1.01	0.81	0.64	0.51	0.41	0.32	0.26	0.20	0.16	1340
1350	9.71	7.98	6.51	5.29	4.28	3.45	2.77	2.22	1.78	1.42	1.13	0.90	0.72	0.57	0.46	0.36	0.29	0.23	0.18	0.15	1350
1360	8.82	7.22	5.88	4.76	3.85	3.10	2.49	1.99	1.59	1.27	1.01	0.81	0.64	0.51	0.41	0.32	0.26	0.21	0.16	0.13	1360
1370	8.00	6.53	5.31	4.29	3.46	2.78	2.23	1.79	1.43	1.14	0.91	0.72	0.58	0.46	0.37	0.29	0.23	0.18	0.15	0.12	1370
1380	7.26	5.91	4.79	3.87	3.11	2.50	2.00	1.60	1.28	1.02	0.81	0.65	0.52	0.41	0.33	0.26	0.21	0.16	0.13	0.10	1380
1390	6.58	5.35	4.33	3.49	2.81	2.25	1.80	1.44	1.15	0.92	0.73	0.58	0.46	0.37	0.29	0.23	0.19	0.15	0.12	0.09	1390
1400	5.97	4.84	3.91	3.15	2.53	2.03	1.62	1.30	1.03	0.82	0.66	0.52	0.42	0.33	0.26	0.21	0.17	0.13	0.11	0.08	1400
1410	5.42	4.39	3.54	2.84	2.28	1.83	1.46	1.17	0.93	0.74	0.59	0.47	0.37	0.30	0.24	0.19	0.15	0.12	0.09	0.07	1410
1420	4.92	3.97	3.20	2.57	2.06	1.65	1.32	1.05	0.84	0.67	0.53	0.42	0.34	0.27	0.21	0.17	0.13	0.11	0.08	0.07	1420
1430	4.47	3.60	2.90	2.33	1.86	1.49	1.19	0.95	0.76	0.60	0.48	0.38	0.30	0.24	0.19	0.15	0.12	0.10	0.08	0.06	1430
1440	4.06	3.27	2.63	2.11	1.68	1.35	1.07	0.86	0.68	0.54	0.43	0.34	0.27	0.22	0.17	0.14	0.11	0.09	0.07	0.05	1440
1450	3.69	2.97	2.38	1.91	1.53	1.22	0.97	0.77	0.62	0.49	0.39	0.31	0.25	0.20	0.16	0.12	0.10	0.08	0.06	0.05	1450
1460	3.35	2.69	2.16	1.73	1.38	1.10	0.88	0.70	0.56	0.44	0.35	0.28	0.22	0.18	0.14	0.11	0.09	0.07	0.06	0.04	1460
1470	3.05	2.45	1.96	1.57	1.25	1.00	0.80	0.63	0.51	0.40	0.32	0.25	0.20	0.16	0.13	0.10	0.08	0.06	0.05	0.04	1470
1480	2.78	2.23	1.78	1.42	1.14	0.91	0.72	0.58	0.46	0.36	0.29	0.23	0.18	0.15	0.12	0.09	0.07	0.06	0.05	0.04	1480
1490	2.53	2.03	1.62	1.30	1.03	0.82	0.66	0.52	0.42	0.33	0.26	0.21	0.17	0.13	0.11	0.08	0.07	0.05	0.04	0.03	1490
1500	2.30	1.85	1.48	1.18	0.94	0.75	0.60	0.47	0.38	0.30	0.24	0.19	0.15	0.12	0.10	0.08	0.06	0.05	0.04	0.03	1500
1510	2.10	1.68	1.34	1.07	0.86	0.68	0.54	0.43	0.34	0.27	0.22	0.17	0.14	0.11	0.09	0.07	0.05	0.04	0.03	0.03	1510
1520	1.92	1.53	1.23	0.98	0.78	0.62	0.49	0.39	0.31	0.25	0.20	0.16	0.12	0.10	0.08	0.06	0.05	0.04	0.03	0.02	1520
1530	1.75	1.40	1.12	0.89	0.71	0.57	0.45	0.36	0.29	0.23	0.18	0.14	0.11	0.09	0.07	0.06	0.05	0.04	0.03	0.02	1530
1540	1.60	1.28	1.02	0.81	0.65	0.52	0.41	0.33	0.26	0.21	0.16	0.13	0.10	0.08	0.07	0.05	0.04	0.03	0.03	0.02	1540
1550	1.47	1.17	0.93	0.74	0.59	0.47	0.38	0.30	0.24	0.19	0.15	0.12	0.09	0.08	0.06	0.05	0.04	0.03	0.02	0.02	1550
1560	1.34	1.07	0.85	0.68	0.54	0.43	0.34	0.27	0.22	0.17	0.14	0.11	0.09	0.07	0.05	0.04	0.03	0.03	0.02	0.02	1560
1570	1.23	0.98	0.78	0.62	0.50	0.39	0.31	0.25	0.20	0.16	0.13	0.10	0.08	0.06	0.05	0.04	0.03	0.03	0.02	0.02	1570
1580	1.13	0.90	0.72	0.57	0.45	0.36	0.29	0.23	0.18	0.14	0.11	0.09	0.07	0.06	0.05	0.04	0.03	0.02	0.02	0.01	1580
1590	1.03	0.82	0.66	0.52	0.42	0.33	0.26	0.21	0.17	0.13	0.11	0.08	0.07	0.05	0.04	0.03	0.03	0.02	0.02	0.01	1590
1600	0.95	0.76	0.60	0.48	0.38	0.30	0.24	0.19	0.15	0.12	0.10	0.08	0.06	0.05	0.04	0.03	0.02	0.02	0.02	0.01	1600
1610	0.87	0.70	0.55	0.44	0.35	0.28	0.22	0.18	0.14	0.11	0.09	0.07	0.06	0.04	0.04	0.03	0.02	0.02	0.01	0.01	1610
1620	0.80	0.64	0.51	0.41	0.32	0.26	0.20	0.16	0.13	0.10	0.08	0.06	0.05	0.04	0.03	0.03	0.02	0.02	0.01	0.01	1620
1630	0.74	0.59	0.47	0.37	0.30	0.24	0.19	0.15	0.12	0.09	0.07	0.06	0.05	0.04	0.03	0.02	0.02	0.01	0.01	0.01	1630
1640	0.68	0.54	0.43	0.34	0.27	0.22	0.17	0.14	0.11	0.09	0.07	0.05	0.04	0.03	0.03	0.02	0.02	0.01	0.01	0.01	1640
1650	0.63	0.50	0.40	0.32	0.25	0.20	0.16	0.13	0.10	0.08	0.06	0.05	0.04	0.03	0.03	0.02	0.02	0.01	0.01	0.01	1650
1660	0.58	0.46	0.37	0.29	0.23	0.18	0.15	0.12	0.09	0.07	0.06	0.05	0.04	0.03	0.02	0.02	0.01	0.01	0.01	0.01	1660
1670	0.54	0.43	0.34	0.27	0.21	0.17	0.14	0.11	0.09	0.07	0.05	0.04	0.03	0.03	0.02	0.02	0.01	0.01	0.01	0.01	1670
1680	0.49	0.39	0.31	0.25	0.20	0.16	0.13	0.10	0.08	0.06	0.05	0.04	0.03	0.02	0.02	0.02	0.01	0.01	0.01	0.01	1680
1690	0.46	0.36	0.29	0.23	0.18	0.15	0.12	0.09	0.07	0.06	0.05	0.04	0.03	0.02	0.02	0.01	0.01	0.01	0.01	0.01	1690
1700	0.42	0.34	0.27	0.21	0.17	0.13	0.11	0.08	0.07	0.05	0.04	0.03	0.03	0.02	0.02	0.01	0.01	0.01	0.01	0.01	1700
1710	0.39	0.31	0.25	0.20	0.16	0.12	0.10	0.08	0.06	0.05	0.04	0.03	0.02	0.02	0.02	0.01	0.01	0.01	0.01		1710
1720	0.36	0.29	0.23	0.18	0.15	0.12	0.09	0.07	0.06	0.05	0.04	0.03	0.02	0.02	0.01	0.01	0.01	0.01	0.01		1720
1730	0.34	0.27	0.21	0.17	0.13	0.11	0.08	0.07	0.05	0.04	0.03	0.03	0.02	0.02	0.01	0.01	0.01	0.01	0.01		1730
1740	0.31	0.25	0.20	0.16	0.12	0.10	0.08	0.06	0.05	0.04	0.03	0.02	0.02	0.02	0.01	0.01	0.01	0.01			1740

TABLE IV CONTINUED

TEMP C	LOG(OXYGEN FUGACITY)																			TEMP C
	-12.0	-12.2	-12.4	-12.6	-12.8	-13.0	-13.2	-13.4	-13.6	-13.8	-14.0	-14.2	-14.4	-14.6	-14.8	-15.0	-15.2	-15.4	-15.6	-15.8	
1750	0.29	0.23	0.18	0.15	0.12	0.09	0.07	0.06	0.05	0.04	0.03	0.02	0.02	0.01	0.01	0.01	0.01	0.01			1750
1760	0.27	0.21	0.17	0.14	0.11	0.09	0.07	0.05	0.04	0.03	0.03	0.02	0.02	0.01	0.01	0.01	0.01	0.01			1760
1770	0.25	0.20	0.16	0.13	0.10	0.08	0.06	0.05	0.04	0.03	0.03	0.02	0.02	0.01	0.01	0.01	0.01	0.01			1770
1780	0.23	0.19	0.15	0.12	0.09	0.07	0.06	0.05	0.04	0.03	0.02	0.02	0.01	0.01	0.01	0.01	0.01				1780
1790	0.22	0.17	0.14	0.11	0.09	0.07	0.05	0.04	0.03	0.03	0.02	0.02	0.01	0.01	0.01	0.01	0.01				1790
1800	0.20	0.16	0.13	0.10	0.08	0.06	0.05	0.04	0.03	0.03	0.02	0.02	0.01	0.01	0.01	0.01	0.01				1800
1810	0.19	0.15	0.12	0.09	0.08	0.06	0.05	0.04	0.03	0.02	0.02	0.02	0.01	0.01	0.01	0.01					1810
1820	0.18	0.14	0.11	0.09	0.07	0.06	0.04	0.04	0.03	0.02	0.02	0.01	0.01	0.01	0.01	0.01					1820
1830	0.16	0.13	0.10	0.08	0.07	0.05	0.04	0.03	0.03	0.02	0.02	0.01	0.01	0.01	0.01	0.01					1830
1840	0.15	0.12	0.10	0.08	0.06	0.05	0.04	0.03	0.02	0.02	0.02	0.01	0.01	0.01	0.01						1840
1850	0.14	0.11	0.09	0.07	0.06	0.05	0.04	0.03	0.02	0.02	0.01	0.01	0.01	0.01	0.01						1850
1860	0.13	0.11	0.08	0.07	0.05	0.04	0.03	0.03	0.02	0.02	0.01	0.01	0.01	0.01	0.01						1860
1870	0.13	0.10	0.08	0.06	0.05	0.04	0.03	0.03	0.02	0.02	0.01	0.01	0.01	0.01	0.01						1870
1880	0.12	0.09	0.07	0.06	0.05	0.04	0.03	0.02	0.02	0.01	0.01	0.01	0.01	0.01							1880
1890	0.11	0.09	0.07	0.06	0.04	0.04	0.03	0.02	0.02	0.01	0.01	0.01	0.01	0.01							1890
1900	0.10	0.08	0.07	0.05	0.04	0.03	0.03	0.02	0.02	0.01	0.01	0.01	0.01	0.01							1900
1910	0.10	0.08	0.06	0.05	0.04	0.03	0.02	0.02	0.02	0.01	0.01	0.01	0.01								1910
1920	0.09	0.07	0.06	0.05	0.04	0.03	0.02	0.02	0.01	0.01	0.01	0.01	0.01								1920
1930	0.09	0.07	0.05	0.04	0.03	0.03	0.02	0.02	0.01	0.01	0.01	0.01	0.01								1930
1940	0.08	0.06	0.05	0.04	0.03	0.03	0.02	0.02	0.01	0.01	0.01	0.01	0.01								1940
1950	0.08	0.06	0.05	0.04	0.03	0.02	0.02	0.02	0.01	0.01	0.01	0.01									1950
1960	0.07	0.06	0.05	0.04	0.03	0.02	0.02	0.01	0.01	0.01	0.01	0.01									1960
1970	0.07	0.05	0.04	0.03	0.03	0.02	0.02	0.01	0.01	0.01	0.01	0.01									1970
1980	0.06	0.05	0.04	0.03	0.03	0.02	0.02	0.01	0.01	0.01	0.01	0.01									1980
1990	0.06	0.05	0.04	0.03	0.02	0.02	0.01	0.01	0.01	0.01	0.01										1990
2000	0.06	0.04	0.04	0.03	0.02	0.02	0.01	0.01	0.01	0.01	0.01										2000

	-16.0	-16.2	-16.4	-16.6	-16.8	-17.0	-17.2	-17.4	-17.6	-17.8	-18.0	-18.2	-18.4	-18.6	-18.8	-19.0	-19.2	-19.4	-19.6	-19.8	
500																					500
510																					510
520																			99.99	99.99	520
530																	99.99	99.99	99.99	99.99	530
540															99.99	99.99	99.99	99.99	99.98	99.98	540
550												99.99	99.99	99.99	99.99	99.99	99.98	99.98	99.97	99.97	550
560										99.99	99.99	99.99	99.99	99.99	99.98	99.98	99.97	99.97	99.96	99.95	560
570								99.99	99.99	99.99	99.99	99.99	99.98	99.98	99.97	99.97	99.96	99.95	99.93	99.91	570
580						99.99	99.99	99.99	99.99	99.99	99.98	99.98	99.97	99.97	99.96	99.95	99.93	99.91	99.89	99.86	580
590				99.99	99.99	99.99	99.99	99.99	99.98	99.98	99.97	99.97	99.96	99.95	99.93	99.91	99.89	99.86	99.83	99.78	590
600		99.99	99.99	99.99	99.99	99.99	99.98	99.98	99.97	99.97	99.96	99.95	99.93	99.91	99.89	99.86	99.83	99.78	99.73	99.66	600
610	99.99	99.99	99.99	99.99	99.98	99.98	99.97	99.97	99.96	99.95	99.93	99.92	99.89	99.87	99.83	99.79	99.73	99.66	99.58	99.47	610
620	99.99	99.99	99.98	99.98	99.97	99.97	99.96	99.95	99.94	99.92	99.90	99.87	99.84	99.79	99.74	99.67	99.59	99.48	99.35	99.18	620
630	99.98	99.98	99.98	99.97	99.96	99.95	99.94	99.92	99.90	99.88	99.84	99.80	99.75	99.69	99.61	99.50	99.37	99.21	99.01	98.75	630
640	99.98	99.97	99.96	99.95	99.94	99.93	99.91	99.88	99.85	99.81	99.76	99.70	99.62	99.53	99.40	99.25	99.06	98.81	98.50	98.11	640
650	99.96	99.96	99.94	99.93	99.91	99.89	99.86	99.82	99.78	99.72	99.65	99.55	99.44	99.29	99.11	98.88	98.59	98.22	97.76	97.18	650
660	99.95	99.93	99.92	99.90	99.87	99.83	99.79	99.74	99.67	99.58	99.47	99.34	99.17	98.95	98.68	98.34	97.91	97.37	96.69	95.84	660
670	99.92	99.90	99.88	99.85	99.81	99.76	99.69	99.61	99.51	99.38	99.23	99.03	98.77	98.46	98.06	97.56	96.93	96.14	95.16	93.93	670
680	99.89	99.86	99.82	99.77	99.72	99.64	99.55	99.43	99.29	99.10	98.87	98.58	98.21	97.76	97.18	96.46	95.55	94.42	93.02	91.27	680
690	99.84	99.79	99.74	99.67	99.59	99.48	99.35	99.18	98.97	98.70	98.37	97.95	97.42	96.77	95.94	94.91	93.63	92.04	90.08	87.67	690

TABLE IV CONTINUED

TEMP C	LOG(OXYGEN FUGACITY)																			TEMP C
	-16.0	-16.2	-16.4	-16.6	-16.8	-17.0	-17.2	-17.4	-17.6	-17.8	-18.0	-18.2	-18.4	-18.6	-18.8	-19.0	-19.2	-19.4	-19.6	-19.8	
700	99.76	99.70	99.63	99.53	99.41	99.26	99.07	98.82	98.52	98.14	97.67	97.07	96.32	95.39	94.23	92.79	91.01	88.83	86.16	82.96	700
710	99.66	99.58	99.47	99.33	99.16	98.94	98.67	98.33	97.90	97.36	96.69	95.85	94.81	93.51	91.91	89.94	87.53	84.61	81.13	77.04	710
720	99.53	99.40	99.25	99.05	98.81	98.51	98.12	97.64	97.04	96.29	95.36	94.20	92.76	90.99	88.83	86.20	83.04	79.30	74.95	69.98	720
730	99.33	99.16	98.95	98.67	98.33	97.91	97.38	96.71	95.88	94.85	93.57	91.99	90.05	87.70	84.86	81.47	77.49	72.91	67.74	62.05	730
740	99.07	98.83	98.53	98.16	97.69	97.10	96.36	95.45	94.32	92.92	91.20	89.10	86.56	83.51	79.91	75.72	70.94	65.60	59.81	53.68	740
750	98.71	98.38	97.97	97.46	96.81	96.01	95.01	93.78	92.26	90.40	88.14	85.42	82.18	78.38	74.00	69.05	63.59	57.72	51.59	45.38	750
760	98.23	97.78	97.22	96.52	95.65	94.57	93.24	91.60	89.61	87.19	84.30	80.88	76.91	72.36	67.27	61.71	55.80	49.69	43.57	37.62	760
770	97.59	96.98	96.23	95.29	94.13	92.70	90.95	88.82	86.26	83.21	79.63	75.49	70.80	65.59	59.97	54.04	47.98	41.96	36.15	30.70	770
780	96.75	95.93	94.93	93.68	92.16	90.30	88.05	85.35	82.16	78.43	74.15	69.34	64.05	58.37	52.45	46.45	40.53	34.86	29.58	24.77	780
790	95.65	94.57	93.25	91.63	89.67	87.30	84.48	81.15	77.29	72.89	67.98	62.63	56.93	51.03	45.09	39.28	33.74	28.60	23.96	19.84	790
800	94.23	92.83	91.13	89.06	86.58	83.64	80.20	76.22	71.73	66.74	61.33	55.63	49.76	43.89	38.18	32.77	27.77	23.26	19.27	15.82	800
810	92.42	90.64	88.48	85.90	82.86	79.31	75.24	70.65	65.61	60.18	54.47	48.65	42.85	37.24	31.94	27.06	22.67	18.79	15.44	12.58	810
820	90.18	87.96	85.27	82.13	78.49	74.33	69.68	64.59	59.15	53.46	47.68	41.95	36.43	31.24	26.46	22.17	18.40	15.13	12.34	9.99	820
830	87.43	84.68	81.46	77.74	73.51	68.81	63.69	58.24	52.58	46.85	41.19	35.76	30.65	25.97	21.77	18.07	14.87	12.15	9.85	7.94	830
840	84.14	80.85	77.06	72.79	68.05	62.91	57.46	51.83	46.15	40.56	35.20	30.18	25.58	21.45	17.82	14.68	12.00	9.74	7.86	6.31	840
850	80.30	76.47	72.15	67.38	62.24	56.80	51.21	45.58	40.05	34.76	29.81	25.28	21.21	17.63	14.54	11.90	9.67	7.82	6.28	5.03	850
860	75.95	71.60	66.82	61.67	56.26	50.70	45.12	39.65	34.42	29.53	25.06	21.04	17.51	14.45	11.83	9.63	7.79	6.27	5.03	4.01	860
870	71.14	66.35	61.22	55.83	50.31	44.77	39.36	34.19	29.35	24.92	20.94	17.44	14.41	11.81	9.62	7.79	6.28	5.04	4.03	3.21	870
880	65.98	60.86	55.50	50.02	44.54	39.17	34.05	29.25	24.86	20.91	17.43	14.41	11.83	9.64	7.82	6.31	5.07	4.06	3.24	2.57	880
890	60.61	55.28	49.84	44.40	39.08	34.00	29.24	24.87	20.94	17.48	14.46	11.88	9.70	7.87	6.36	5.11	4.10	3.27	2.60	2.07	890
900	55.16	49.75	44.36	39.08	34.03	29.30	24.95	21.04	17.57	14.56	11.97	9.78	7.95	6.43	5.17	4.15	3.32	2.64	2.10	1.67	900
910	49.76	44.41	39.17	34.15	29.43	25.10	21.19	17.72	14.70	12.10	9.90	8.05	6.51	5.25	4.21	3.37	2.69	2.14	1.70	1.35	910
920	44.54	39.34	34.34	29.64	25.32	21.40	17.92	14.88	12.27	10.04	8.18	6.62	5.34	4.29	3.44	2.75	2.19	1.74	1.38	1.09	920
930	39.59	34.61	29.93	25.60	21.67	18.18	15.11	12.47	10.22	8.33	6.75	5.45	4.39	3.52	2.81	2.24	1.78	1.42	1.12	0.89	930
940	34.95	30.27	25.94	22.00	18.48	15.39	12.71	10.43	8.51	6.91	5.58	4.49	3.61	2.89	2.30	1.84	1.46	1.16	0.92	0.72	940
950	30.69	26.34	22.38	18.83	15.70	12.99	10.68	8.72	7.08	5.73	4.62	3.71	2.97	2.37	1.89	1.51	1.20	0.95	0.75	0.59	950
960	26.81	22.82	19.23	16.07	13.32	10.96	8.96	7.29	5.90	4.76	3.82	3.06	2.45	1.95	1.56	1.24	0.98	0.78	0.62	0.49	960
970	23.31	19.69	16.48	13.68	11.27	9.23	7.51	6.09	4.91	3.95	3.17	2.54	2.03	1.61	1.28	1.02	0.81	0.64	0.51	0.40	970
980	20.20	16.93	14.08	11.62	9.53	7.76	6.30	5.09	4.10	3.29	2.63	2.10	1.68	1.34	1.06	0.84	0.67	0.53	0.42	0.33	980
990	17.44	14.53	12.01	9.86	8.05	6.53	5.28	4.26	3.42	2.74	2.19	1.75	1.39	1.11	0.88	0.70	0.55	0.44	0.35	0.27	990
1000	15.02	12.44	10.23	8.36	6.80	5.50	4.44	3.57	2.86	2.29	1.83	1.46	1.16	0.92	0.73	0.58	0.46	0.36	0.29	0.23	1000
1010	12.91	10.63	8.70	7.08	5.74	4.63	3.73	2.99	2.39	1.91	1.53	1.22	0.97	0.77	0.61	0.48	0.38	0.30	0.24	0.19	1010
1020	11.07	9.08	7.40	6.00	4.85	3.91	3.14	2.51	2.01	1.60	1.28	1.02	0.81	0.64	0.51	0.40	0.32	0.25	0.20	0.16	1020
1030	9.49	7.75	6.29	5.09	4.10	3.30	2.64	2.11	1.69	1.35	1.07	0.85	0.68	0.54	0.43	0.34	0.27	0.21	0.17	0.13	1030
1040	8.13	6.61	5.35	4.32	3.47	2.79	2.23	1.78	1.42	1.13	0.90	0.72	0.57	0.45	0.36	0.28	0.22	0.18	0.14	0.11	1040
1050	6.96	5.64	4.56	3.67	2.94	2.36	1.89	1.51	1.20	0.96	0.76	0.60	0.48	0.38	0.30	0.24	0.19	0.15	0.12	0.09	1050
1060	5.96	4.82	3.88	3.12	2.50	2.00	1.60	1.27	1.01	0.81	0.64	0.51	0.41	0.32	0.25	0.20	0.16	0.13	0.10	0.08	1060
1070	5.10	4.12	3.31	2.65	2.12	1.70	1.36	1.08	0.86	0.68	0.54	0.43	0.34	0.27	0.22	0.17	0.13	0.11	0.08	0.07	1070
1080	4.37	3.52	2.83	2.26	1.81	1.44	1.15	0.92	0.73	0.58	0.46	0.37	0.29	0.23	0.18	0.14	0.11	0.09	0.07	0.06	1080
1090	3.75	3.01	2.41	1.93	1.54	1.23	0.98	0.78	0.62	0.49	0.39	0.31	0.25	0.20	0.16	0.12	0.10	0.08	0.06	0.05	1090
1100	3.22	2.58	2.07	1.65	1.32	1.05	0.84	0.67	0.53	0.42	0.33	0.27	0.21	0.17	0.13	0.10	0.08	0.07	0.05	0.04	1100
1110	2.77	2.22	1.77	1.42	1.13	0.90	0.72	0.57	0.45	0.36	0.29	0.23	0.18	0.14	0.11	0.09	0.07	0.06	0.04	0.03	1110
1120	2.38	1.91	1.52	1.21	0.97	0.77	0.61	0.49	0.39	0.31	0.24	0.19	0.15	0.12	0.10	0.08	0.06	0.05	0.04	0.03	1120
1130	2.05	1.64	1.31	1.04	0.83	0.66	0.53	0.42	0.33	0.26	0.21	0.17	0.13	0.10	0.08	0.07	0.05	0.04	0.03	0.03	1130
1140	1.77	1.41	1.13	0.90	0.72	0.57	0.45	0.36	0.29	0.23	0.18	0.14	0.11	0.09	0.07	0.06	0.04	0.04	0.03	0.02	1140
1150	1.53	1.22	0.97	0.78	0.62	0.49	0.39	0.31	0.25	0.20	0.16	0.12	0.10	0.08	0.06	0.05	0.04	0.03	0.02	0.02	1150
1160	1.32	1.06	0.84	0.67	0.53	0.42	0.34	0.27	0.21	0.17	0.13	0.11	0.08	0.07	0.05	0.04	0.03	0.03	0.02	0.02	1160
1170	1.15	0.92	0.73	0.58	0.46	0.37	0.29	0.23	0.18	0.15	0.12	0.09	0.07	0.06	0.05	0.04	0.03	0.02	0.02	0.01	1170
1180	1.00	0.79	0.63	0.50	0.40	0.32	0.25	0.20	0.16	0.13	0.10	0.08	0.06	0.05	0.04	0.03	0.02	0.02	0.02	0.01	1180
1190	0.87	0.69	0.55	0.44	0.35	0.28	0.22	0.17	0.14	0.11	0.09	0.07	0.05	0.04	0.03	0.03	0.02	0.02	0.01	0.01	1190
1200	0.76	0.60	0.48	0.38	0.30	0.24	0.19	0.15	0.12	0.10	0.08	0.06	0.05	0.04	0.03	0.02	0.02	0.01	0.01	0.01	1200
1210	0.66	0.52	0.42	0.33	0.26	0.21	0.17	0.13	0.11	0.08	0.07	0.05	0.04	0.03	0.03	0.02	0.02	0.01	0.01	0.01	1210
1220	0.58	0.46	0.36	0.29	0.23	0.18	0.15	0.12	0.09	0.07	0.06	0.05	0.04	0.03	0.02	0.02	0.01	0.01	0.01	0.01	1220

TABLE IV CONTINUED

TEMP C	LOG(OXYGEN FUGACITY)																				TEMP C
	-16.0	-16.2	-16.4	-16.6	-16.8	-17.0	-17.2	-17.4	-17.6	-17.8	-18.0	-18.2	-18.4	-18.6	-18.8	-19.0	-19.2	-19.4	-19.6	-19.8	
1230	0.50	0.40	0.32	0.25	0.20	0.16	0.13	0.10	0.08	0.06	0.05	0.04	0.03	0.03	0.02	0.02	0.01	0.01	0.01	0.01	1230
1240	0.44	0.35	0.28	0.22	0.18	0.14	0.11	0.09	0.07	0.06	0.04	0.04	0.03	0.02	0.02	0.01	0.01	0.01	0.01	0.01	1240
1250	0.39	0.31	0.25	0.20	0.16	0.12	0.10	0.08	0.06	0.05	0.04	0.03	0.02	0.02	0.02	0.01	0.01	0.01	0.01		1250
1260	0.34	0.27	0.22	0.17	0.14	0.11	0.09	0.07	0.05	0.04	0.03	0.03	0.02	0.02	0.01	0.01	0.01	0.01	0.01		1260
1270	0.30	0.24	0.19	0.15	0.12	0.10	0.08	0.06	0.05	0.04	0.03	0.02	0.02	0.02	0.01	0.01	0.01	0.01			1270
1280	0.27	0.21	0.17	0.13	0.11	0.08	0.07	0.05	0.04	0.03	0.03	0.02	0.02	0.01	0.01	0.01	0.01	0.01			1280
1290	0.24	0.19	0.15	0.12	0.09	0.07	0.06	0.05	0.04	0.03	0.02	0.02	0.01	0.01	0.01	0.01	0.01				1290
1300	0.21	0.17	0.13	0.10	0.08	0.07	0.05	0.04	0.03	0.03	0.02	0.02	0.01	0.01	0.01	0.01	0.01				1300
1310	0.18	0.15	0.12	0.09	0.07	0.06	0.05	0.04	0.03	0.02	0.02	0.01	0.01	0.01	0.01	0.01					1310
1320	0.16	0.13	0.10	0.08	0.07	0.05	0.04	0.03	0.03	0.02	0.02	0.01	0.01	0.01	0.01	0.01					1320
1330	0.15	0.12	0.09	0.07	0.06	0.05	0.04	0.03	0.02	0.02	0.01	0.01	0.01	0.01	0.01						1330
1340	0.13	0.10	0.08	0.06	0.05	0.04	0.03	0.03	0.02	0.02	0.01	0.01	0.01	0.01	0.01						1340
1350	0.12	0.09	0.07	0.06	0.05	0.04	0.03	0.02	0.02	0.01	0.01	0.01	0.01	0.01							1350
1360	0.10	0.08	0.07	0.05	0.04	0.03	0.03	0.02	0.02	0.01	0.01	0.01	0.01	0.01							1360
1370	0.09	0.07	0.06	0.05	0.04	0.03	0.02	0.02	0.01	0.01	0.01	0.01	0.01								1370
1380	0.08	0.07	0.05	0.04	0.03	0.03	0.02	0.02	0.01	0.01	0.01	0.01	0.01								1380
1390	0.07	0.06	0.05	0.04	0.03	0.02	0.02	0.01	0.01	0.01	0.01	0.01									1390
1400	0.07	0.05	0.04	0.03	0.03	0.02	0.02	0.01	0.01	0.01	0.01	0.01									1400
1410	0.06	0.05	0.04	0.03	0.02	0.02	0.01	0.01	0.01	0.01	0.01										1410
1420	0.05	0.04	0.03	0.03	0.02	0.02	0.01	0.01	0.01	0.01	0.01										1420
1430	0.05	0.04	0.03	0.02	0.02	0.02	0.01	0.01	0.01	0.01											1430
1440	0.04	0.03	0.03	0.02	0.02	0.01	0.01	0.01	0.01	0.01											1440
1450	0.04	0.03	0.02	0.02	0.02	0.01	0.01	0.01	0.01												1450
1460	0.04	0.03	0.02	0.02	0.01	0.01	0.01	0.01	0.01												1460
1470	0.03	0.03	0.02	0.02	0.01	0.01	0.01	0.01	0.01												1470
1480	0.03	0.02	0.02	0.01	0.01	0.01	0.01	0.01													1480
1490	0.03	0.02	0.02	0.01	0.01	0.01	0.01	0.01													1490
1500	0.02	0.02	0.02	0.01	0.01	0.01	0.01														1500
1510	0.02	0.02	0.01	0.01	0.01	0.01	0.01														1510
1520	0.02	0.02	0.01	0.01	0.01	0.01															1520
1530	0.02	0.01	0.01	0.01	0.01	0.01															1530
1540	0.02	0.01	0.01	0.01	0.01	0.01															1540
1550	0.02	0.01	0.01	0.01	0.01																1550
1560	0.01	0.01	0.01	0.01	0.01																1560
1570	0.01	0.01	0.01	0.01	0.01																1570
1580	0.01	0.01	0.01	0.01																	1580
1590	0.01	0.01	0.01	0.01																	1590
1600	0.01	0.01	0.01																		1600
1610	0.01	0.01	0.01																		1610
1620	0.01	0.01	0.01																		1620
1630	0.01	0.01																			1630
1640	0.01	0.01																			1640
1650	0.01	0.01																			1650
1660	0.01																				1660
1670	0.01																				1670
1680																					1680

TABLE IV CONTINUED

TEMP C	LOG(OXYGEN FUGACITY)																			TEMP C
	-20.0	-20.2	-20.4	-20.6	-20.8	-21.0	-21.2	-21.4	-21.6	-21.8	-22.0	-22.2	-22.4	-22.6	-22.8	-23.0	-23.2	-23.4	-23.6	-23.8	
500				99.99	99.99	99.99	99.99	99.99	99.98	99.98	99.97	99.97	99.96	99.94	99.93	99.91	99.89	99.86	99.82	99.78	500
510		99.99	99.99	99.99	99.99	99.98	99.98	99.98	99.97	99.96	99.95	99.94	99.92	99.90	99.88	99.85	99.81	99.75	99.69	99.61	510
520	99.99	99.99	99.99	99.98	99.98	99.97	99.97	99.96	99.95	99.93	99.92	99.89	99.87	99.83	99.79	99.73	99.66	99.57	99.46	99.32	520
530	99.99	99.98	99.98	99.97	99.96	99.95	99.94	99.93	99.91	99.89	99.86	99.82	99.77	99.71	99.64	99.54	99.42	99.27	99.08	98.83	530
540	99.98	99.97	99.96	99.95	99.94	99.92	99.90	99.88	99.85	99.81	99.76	99.69	99.61	99.51	99.39	99.22	99.02	98.76	98.43	98.02	540
550	99.96	99.95	99.94	99.92	99.90	99.87	99.84	99.80	99.75	99.68	99.60	99.49	99.36	99.19	98.97	98.70	98.36	97.92	97.37	96.66	550
560	99.93	99.92	99.90	99.87	99.83	99.79	99.74	99.67	99.58	99.47	99.33	99.16	98.94	98.66	98.30	97.85	97.28	96.55	95.63	94.44	560
570	99.89	99.86	99.83	99.79	99.73	99.66	99.57	99.46	99.32	99.14	98.91	98.63	98.27	97.81	97.23	96.49	95.55	94.35	92.83	90.89	570
580	99.83	99.78	99.73	99.66	99.57	99.45	99.31	99.13	98.90	98.61	98.25	97.79	97.20	96.46	95.52	94.32	92.81	90.88	88.44	85.34	580
590	99.73	99.65	99.56	99.45	99.31	99.13	98.90	98.61	98.25	97.79	97.21	96.47	95.54	94.36	92.86	90.97	88.58	85.58	81.77	76.90	590
600	99.57	99.46	99.32	99.14	98.91	98.63	98.27	97.82	97.25	96.52	95.61	94.45	92.99	91.14	88.82	85.92	82.30	77.76	71.97	64.33	600
610	99.33	99.16	98.94	98.66	98.31	97.87	97.31	96.60	95.71	94.59	93.17	91.39	89.16	86.38	82.92	78.65	73.36	66.71	58.17	47.23	610
620	98.97	98.70	98.36	97.93	97.39	96.71	95.86	94.78	93.42	91.71	89.58	86.92	83.64	79.62	74.71	68.72	61.36	52.25	41.42	30.34	620
630	98.43	98.02	97.50	96.85	96.03	95.00	93.71	92.09	90.06	87.54	84.44	80.65	76.06	70.56	63.98	56.12	46.85	36.60	26.88	19.26	630
640	97.62	97.01	96.23	95.26	94.04	92.51	90.60	88.23	85.31	81.75	77.46	72.34	66.33	59.30	51.19	42.10	32.66	24.15	17.54	12.87	640
650	96.45	95.54	94.39	92.96	91.17	88.96	86.23	82.90	78.89	74.12	68.54	62.12	54.82	46.69	38.01	29.45	21.95	16.13	11.94	8.99	650
660	94.77	93.44	91.78	89.72	87.18	84.08	80.35	75.90	70.71	64.75	58.04	50.63	42.68	34.53	26.80	20.16	14.97	11.15	8.41	6.43	660
670	92.39	90.49	88.15	85.28	81.82	77.69	72.86	67.30	61.05	54.17	46.79	39.14	31.58	24.59	18.66	13.98	10.48	7.92	6.04	4.66	670
680	89.12	86.49	83.29	79.48	74.99	69.80	63.95	57.50	50.57	43.34	36.06	29.06	22.74	17.39	13.14	9.91	7.50	5.72	4.39	3.40	680
690	84.75	81.24	77.09	72.27	66.79	60.71	54.15	47.26	40.25	33.37	26.91	21.16	16.31	12.42	9.41	7.14	5.44	4.17	3.21	2.49	690
700	79.14	74.68	69.58	63.87	57.64	51.05	44.27	37.52	31.04	25.07	19.80	15.37	11.78	8.98	6.83	5.21	3.98	3.06	2.36	1.83	700
710	72.31	66.96	61.07	54.76	48.19	41.57	35.11	29.01	23.47	18.63	14.55	11.23	8.60	6.57	5.01	3.83	2.94	2.26	1.75	1.35	710
720	64.44	58.43	52.09	45.60	39.16	32.99	27.24	22.08	17.60	13.82	10.73	8.27	6.34	4.85	3.70	2.84	2.18	1.67	1.29	1.00	720
730	55.96	49.63	43.25	37.02	31.12	25.70	20.88	16.70	13.18	10.30	7.97	6.14	4.70	3.60	2.75	2.11	1.62	1.25	0.96	0.75	730
740	47.40	41.15	35.13	29.49	24.36	19.82	15.91	12.62	9.90	7.71	5.96	4.58	3.51	2.69	2.06	1.58	1.21	0.93	0.72	0.56	740
750	39.28	33.45	28.05	23.18	18.90	15.22	12.12	9.55	7.47	5.80	4.48	3.44	2.64	2.02	1.55	1.18	0.91	0.70	0.54	0.42	750
760	31.98	26.80	22.16	18.09	14.61	11.67	9.24	7.26	5.66	4.39	3.38	2.60	1.99	1.52	1.17	0.89	0.69	0.53	0.41	0.32	760
770	25.71	21.27	17.39	14.07	11.28	8.97	7.07	5.54	4.31	3.33	2.57	1.97	1.51	1.16	0.88	0.68	0.52	0.40	0.31	0.24	770
780	20.50	16.79	13.61	10.94	8.72	6.90	5.43	4.24	3.29	2.54	1.96	1.50	1.15	0.88	0.67	0.52	0.40	0.30	0.24	0.18	780
790	16.26	13.21	10.64	8.51	6.75	5.33	4.18	3.26	2.53	1.95	1.50	1.15	0.88	0.67	0.51	0.39	0.30	0.23	0.18	0.14	790
800	12.87	10.39	8.32	6.63	5.24	4.13	3.23	2.51	1.95	1.50	1.15	0.88	0.68	0.52	0.40	0.30	0.23	0.18	0.14	0.11	800
810	10.17	8.17	6.52	5.17	4.08	3.21	2.50	1.95	1.51	1.16	0.89	0.68	0.52	0.40	0.31	0.23	0.18	0.14	0.11	0.08	810
820	8.04	6.43	5.12	4.05	3.19	2.50	1.95	1.51	1.17	0.90	0.69	0.53	0.40	0.31	0.24	0.18	0.14	0.11	0.08	0.06	820
830	6.36	5.07	4.03	3.18	2.50	1.96	1.52	1.18	0.91	0.70	0.54	0.41	0.32	0.24	0.18	0.14	0.11	0.08	0.06	0.05	830
840	5.04	4.01	3.18	2.50	1.96	1.54	1.20	0.93	0.71	0.55	0.42	0.32	0.25	0.19	0.14	0.11	0.08	0.07	0.05	0.04	840
850	4.01	3.18	2.51	1.98	1.55	1.21	0.94	0.73	0.56	0.43	0.33	0.25	0.19	0.15	0.11	0.09	0.07	0.05	0.04	0.03	850
860	3.19	2.53	1.99	1.57	1.23	0.96	0.74	0.58	0.44	0.34	0.26	0.20	0.15	0.12	0.09	0.07	0.05	0.04	0.03	0.02	860
870	2.55	2.01	1.59	1.25	0.97	0.76	0.59	0.46	0.35	0.27	0.21	0.16	0.12	0.09	0.07	0.05	0.04	0.03	0.02	0.02	870
880	2.04	1.61	1.27	0.99	0.78	0.61	0.47	0.36	0.28	0.21	0.16	0.13	0.10	0.07	0.06	0.04	0.03	0.03	0.02	0.02	880
890	1.64	1.29	1.02	0.80	0.62	0.48	0.38	0.29	0.22	0.17	0.13	0.10	0.08	0.06	0.04	0.03	0.03	0.02	0.02	0.01	890
900	1.32	1.04	0.82	0.64	0.50	0.39	0.30	0.23	0.18	0.14	0.10	0.08	0.06	0.05	0.04	0.03	0.02	0.02	0.01	0.01	900
910	1.06	0.84	0.66	0.52	0.40	0.31	0.24	0.19	0.14	0.11	0.08	0.06	0.05	0.04	0.03	0.02	0.02	0.01	0.01	0.01	910
920	0.86	0.68	0.53	0.42	0.32	0.25	0.20	0.15	0.12	0.09	0.07	0.05	0.04	0.03	0.02	0.02	0.01	0.01	0.01	0.01	920
930	0.70	0.55	0.43	0.34	0.26	0.20	0.16	0.12	0.09	0.07	0.06	0.04	0.03	0.02	0.02	0.01	0.01	0.01	0.01	0.01	930
940	0.57	0.45	0.35	0.28	0.21	0.17	0.13	0.10	0.08	0.06	0.04	0.03	0.03	0.02	0.02	0.01	0.01	0.01	0.01		940
950	0.47	0.37	0.29	0.22	0.17	0.14	0.11	0.08	0.06	0.05	0.04	0.03	0.02	0.02	0.01	0.01	0.01	0.01			950
960	0.38	0.30	0.24	0.18	0.14	0.11	0.09	0.07	0.05	0.04	0.03	0.02	0.02	0.01	0.01	0.01	0.01				960
970	0.31	0.25	0.19	0.15	0.12	0.09	0.07	0.05	0.04	0.03	0.02	0.02	0.01	0.01	0.01	0.01					970
980	0.26	0.20	0.16	0.12	0.10	0.08	0.06	0.04	0.03	0.03	0.02	0.02	0.01	0.01	0.01	0.01					980
990	0.21	0.17	0.13	0.10	0.08	0.06	0.05	0.04	0.03	0.02	0.02	0.01	0.01	0.01	0.01						990
1000	0.18	0.14	0.11	0.09	0.07	0.05	0.04	0.03	0.02	0.02	0.01	0.01	0.01	0.01							1000
1010	0.15	0.12	0.09	0.07	0.06	0.04	0.03	0.03	0.02	0.01	0.01	0.01	0.01	0.01							1010
1020	0.12	0.10	0.08	0.06	0.05	0.04	0.03	0.02	0.02	0.01	0.01	0.01	0.01								1020

TABLE IV CONTINUED

TEMP C	LOG$_{10}$ OXYGEN FUGACITY)																			TEMP C
	-20.0	-20.2	-20.4	-20.6	-20.8	-21.0	-21.2	-21.4	-21.6	-21.8	-22.0	-22.2	-22.4	-22.6	-22.8	-23.0	-23.2	-23.4	-23.6	-23.8	
1030	0.10	0.08	0.06	0.05	0.04	0.03	0.02	0.02	0.01	0.01	0.01	0.01									1030
1040	0.09	0.07	0.05	0.04	0.03	0.02	0.02	0.01	0.01	0.01	0.01	0.01									1040
1050	0.07	0.06	0.04	0.03	0.03	0.02	0.02	0.01	0.01	0.01	0.01										1050
1060	0.06	0.05	0.04	0.03	0.02	0.02	0.01	0.01	0.01	0.01											1060
1070	0.05	0.04	0.03	0.02	0.02	0.01	0.01	0.01	0.01	0.01											1070
1080	0.04	0.03	0.03	0.02	0.02	0.01	0.01	0.01	0.01												1080
1090	0.04	0.03	0.02	0.02	0.01	0.01	0.01	0.01													1090
1100	0.03	0.02	0.02	0.02	0.01	0.01	0.01	0.01													1100
1110	0.03	0.02	0.02	0.01	0.01	0.01	0.01														1110
1120	0.02	0.02	0.01	0.01	0.01	0.01	0.01														1120
1130	0.02	0.02	0.01	0.01	0.01	0.01															1130
1140	0.02	0.01	0.01	0.01	0.01																1140
1150	0.01	0.01	0.01	0.01	0.01																1150
1160	0.01	0.01	0.01	0.01																	1160
1170	0.01	0.01	0.01	0.01																	1170
1180	0.01	0.01	0.01																		1180
1190	0.01	0.01	0.01																		1190
1200	0.01	0.01																			1200
1210	0.01																				1210
1220	0.01																				1220
1230																					1230
1240																					1240

TABLE IV CONTINUED

TEMP C	LOG(OXYGEN FUGACITY)										TEMP C
	-24.0	-24.2	-24.4	-24.6	-24.8	-25.0	-25.2	-25.4	-25.6	-25.8	
500	99.72	99.65	99.56	99.44	99.29	99.10	98.86	98.56	98.16	97.66	500
510	99.51	99.38	99.21	99.01	98.74	98.40	97.97	97.41	96.70	95.78	510
520	99.14	98.92	98.63	98.26	97.79	97.18	96.41	95.41	94.11	92.39	520
530	98.52	98.13	97.62	96.98	96.15	95.09	93.71	91.91	89.47	85.92	530
540	97.48	96.80	95.93	94.81	93.37	91.51	89.03	85.58	*****	*****	540
550	95.75	94.60	93.11	91.20	88.71	85.35	80.45	*****	*****	*****	550
560	92.93	91.00	88.50	85.23	80.71	73.82	*****	*****	24.84	17.32	560
570	88.41	85.22	81.00	75.05	*****	*****	31.52	20.66	15.05	11.77	570
580	81.35	76.02	60.44	*****	*****	25.81	17.77	13.28	10.48	8.52	580
590	70.40	61.21	48.00	32.89	21.94	15.61	11.84	9.38	7.60	6.24	590
600	53.94	40.62	27.84	19.15	13.92	10.65	8.43	6.81	5.55	4.54	600
610	34.81	24.17	17.02	12.55	9.64	7.62	6.12	4.96	4.03	3.27	610
620	21.40	15.35	11.41	8.78	6.91	5.52	4.45	3.59	2.90	2.34	620
630	13.99	10.47	8.04	6.31	5.01	4.01	3.22	2.59	2.08	1.67	630
640	9.66	7.42	5.79	4.58	3.64	2.91	2.33	1.86	1.49	1.19	640
650	6.88	5.35	4.20	3.33	2.64	2.10	1.68	1.34	1.07	0.85	650
660	4.98	3.89	3.05	2.42	1.92	1.52	1.21	0.96	0.76	0.61	660
670	3.62	2.83	2.23	1.76	1.39	1.10	0.87	0.69	0.55	0.44	670
680	2.65	2.07	1.63	1.28	1.01	0.80	0.63	0.50	0.40	0.32	680
690	1.94	1.52	1.19	0.94	0.74	0.58	0.46	0.36	0.29	0.23	690
700	1.43	1.11	0.87	0.69	0.54	0.43	0.34	0.27	0.21	0.17	700
710	1.05	0.82	0.64	0.51	0.40	0.31	0.25	0.20	0.15	0.12	710
720	0.78	0.61	0.48	0.37	0.29	0.23	0.18	0.14	0.11	0.09	720
730	0.58	0.45	0.35	0.28	0.22	0.17	0.14	0.11	0.08	0.07	730
740	0.43	0.34	0.26	0.21	0.16	0.13	0.10	0.08	0.06	0.05	740
750	0.33	0.25	0.20	0.16	0.12	0.10	0.08	0.06	0.05	0.04	750
760	0.25	0.19	0.15	0.12	0.09	0.07	0.06	0.05	0.04	0.03	760
770	0.19	0.14	0.11	0.09	0.07	0.05	0.04	0.03	0.03	0.02	770
780	0.14	0.11	0.09	0.07	0.05	0.04	0.03	0.03	0.02	0.02	780
790	0.11	0.08	0.07	0.05	0.04	0.03	0.03	0.02	0.02	0.01	790
800	0.08	0.06	0.05	0.04	0.03	0.02	0.02	0.02	0.01	0.01	800
810	0.06	0.05	0.04	0.03	0.02	0.02	0.02	0.01	0.01	0.01	810
820	0.05	0.04	0.03	0.02	0.02	0.01	0.01	0.01	0.01	0.01	820
830	0.04	0.03	0.02	0.02	0.01	0.01	0.01	0.01	0.01		830
840	0.03	0.02	0.02	0.01	0.01	0.01	0.01	0.01			840
850	0.02	0.02	0.01	0.01	0.01	0.01	0.01				850
860	0.02	0.01	0.01	0.01	0.01	0.01					860
870	0.02	0.01	0.01	0.01	0.01						870
880	0.01	0.01	0.01	0.01							880
890	0.01	0.01	0.01								890
900	0.01	0.01									900
910	0.01										910
920											920
930											930
940											940
950											950

Uncertainties in the calculated values cannot be evaluated directly because uncertainties for thermodynamic quantities are not presented in the JANAF (1971) tables. However, 2σ errors are quoted by Robie and Waldbaum (1968) for ΔG°_f at 298 K as ± 30, 40, 20 and 90 cal for CO, CO_2, H_2O, and CH_4 respectively. Taking 100 calories as an average uncertainty (2σ) in ΔG°_{reac} for reactions (1), (2) and (3), uncertainties in f_{O_2} were calculated indirectly by examining the error in $\%CO_2$. Evaluation of all permutations of an 100 calorie error among reactions (1), (2), and (3) shows that final f_{O_2} will be in error by less than 0.1 log atm unit if H_2-CO_2 mixing is restricted from 99.5 to 0.50 volume percent CO_2.

Figure 2 summarizes the differences between the approximate values for volume percent CO_2 obtained using the equations of Dienes et al. (1974) and the values obtained by the present study. The contour lines represent vol. % CO_2 (present study) - vol. % CO_2 (Dienes et al., 1974); the stipled area represents conditions yielding graphite precipitation. Two observations quickly appear: first, both methods of calculation yeild identical results over the majority of the range considered; second, at the lower temperatures and oxygen fugacities where methane is most stable, the discrepancy between the two methods becomes significant. For example, at log f_{O_2} = -23.0, T = 650°C, the approximate equations yeild 36.40 vol % CO_2 while the correct formulation yields 29.45 vol % CO_2. The difference between the values is significantly greater than the error introduced (2σ = 2.3 vol. % CO_2) by the uncertainties in the

FIGURE 2

Initial volume $\%CO_2$ (present study) - initial volume $\%CO_2$ Dienes et al., 1974). Discrepancies become significant (>1%) only at reducing conditions. Much of the area contoured at -10 or less was stated by Dienes et al., (1974) to be outside the range of their equations' accuracy.

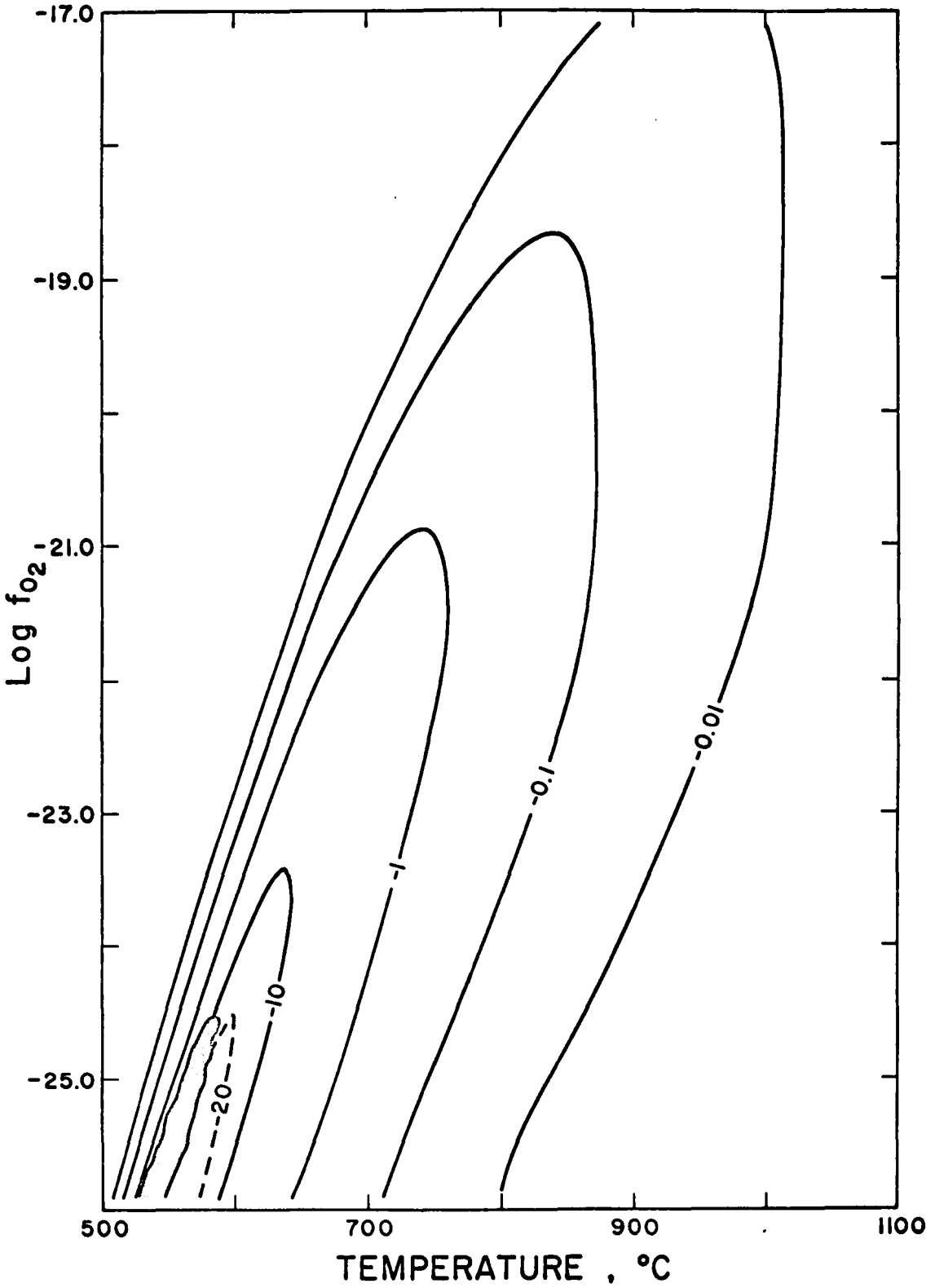
-17.0
-19.0
-21.0
-23.0
-25.0
Log f_{O_2}
500
700
900
1100
TEMPERATURE , °C
-10
-1
-0.1
-0.01
-2
-20

thermodynamic data.

In addition to methane several other C-O-H gases, which are stable under reducing conditions, were investigated as possibly being present in significant quantities at equilibrium. Specifically, formaldehyde (CH_2O), ethylene (C_2H_4), ethylene oxide (C_2H_4O) and ethane (C_2H_6) were considered. However, calculations using available thermochemical data, mainly JANAF (1971), show all these gases to be present at levels less than 0.1 ppm for equilibrium over broad ranges of temperatures and oxygen fugacities. This may be compared with methane, which barely begins to affect the calculations at the 100 ppm level. Thus there appears to be justification in considering the system to be limited to the species H_2, H_2O, CO, CO_2, O_2 and CH_4.

It should be pointed out that the practical use of these tables may be limited by experimental considerations. Huebner (1975) has reported difficulty in attaining equilibrium in H_2-CO_2 gas mixtures at temperatures below 1000°C and has also commented on the effects of flow rate and hot spot versus sample position on f_{O_2} values achieved at equilibrium. Furthermore, error in oxygen fugacity can be introduced because of errors in the mixing of the gases. The effect on the equilibrium oxygen fugacity of a 1% error (absolute) in the volume of CO_2 can be determined from Figure 3. The contours indicate the amount of error in f_{O_2} (in log atm units) and bound a broad, central region over which the effect of the mixing error will be small (< 0.1 log atm units). Restriction of experiments to conditions represented by this central region will minimize uncertainties in f_{O_2}.

FIGURE 3

Contoured error in log (f_{O_2}) assuming a 1% error (absolute) in the volume of CO_2 mixed with H_2. Error introduced due to uncertainties in the thermodynamic data base have not been included.

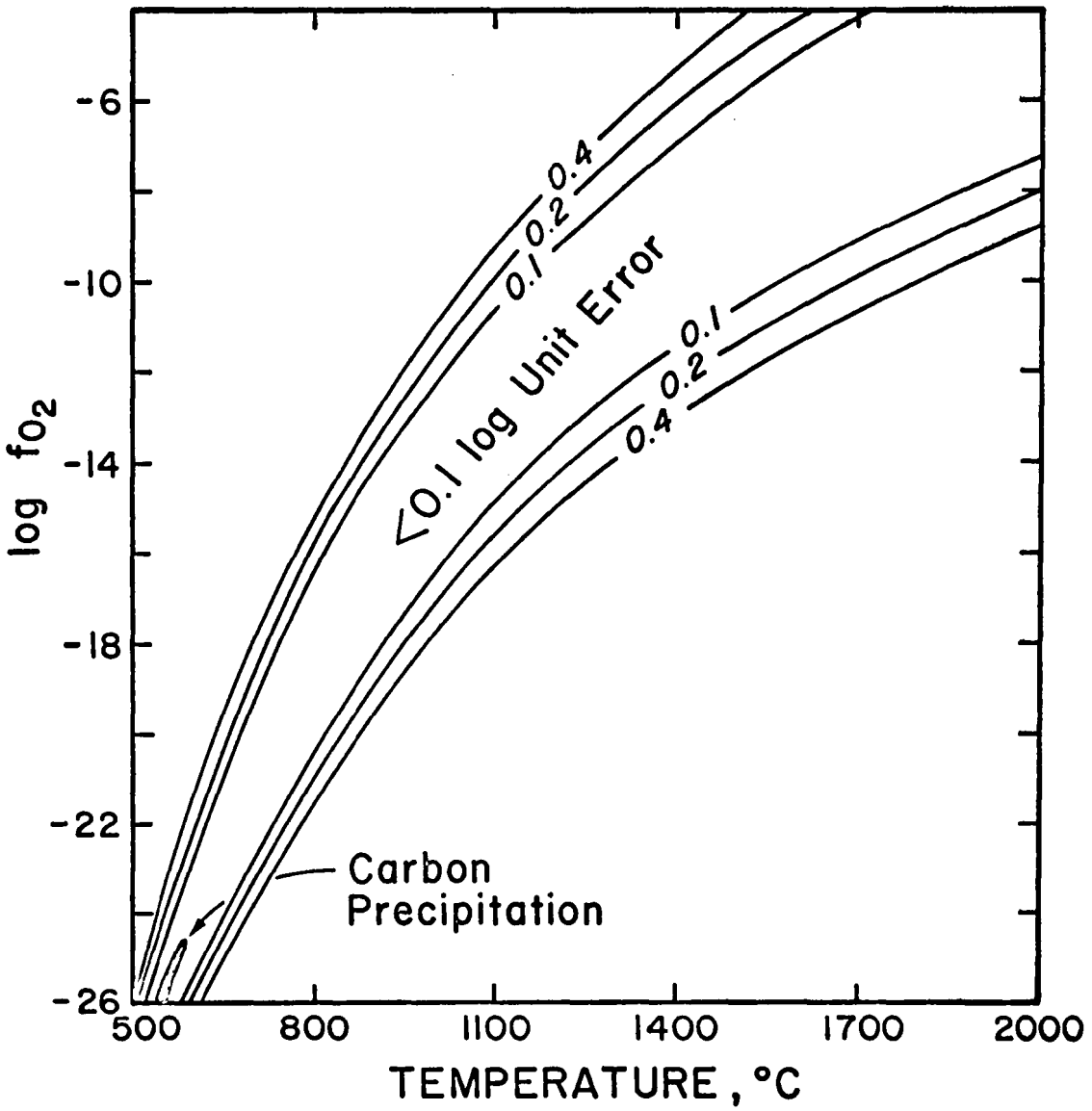
-6
-10
-14
-18
-22
-26
log f_{O_2}
500
800
1100
1400
1700
2000
TEMPERATURE, °C
0.4
0.2
0.1
<0.1 log Unit Error
0.1
0.2
0.4
Carbon
Precipitation

PART II

AN INVESTIGATION OF THE ZOISITE CLINOZOISITE INVERSION

INTRODUCTION

Although coexisting zoisite and clinozoisite have been known for many years (Rodgers, 1924; Orlov, 1925), little attention has been given to the assemblage. Only a handful of workers (Myer, 1966; Ackermand and Raase, 1973; Raith, 1976) have even studied the association in detail. In addition, the relationship of such coexisting pairs to the polymorphism between zoisite and clinozoisite has not been clearly determined. Attempts by Strens (1965) and Holdaway (1972) to systematize such phase relationships using P - T - X schematics present contradictions to available field data. To date the literature contains no reversed, experimental studies of either the zoisite-clinozoisite transition or coexisting zoisite-clinozoisite pairs.

A detailed investigation of this transition will contribute to our understanding of phase relations of the epidote group. This major group of rock-forming silicates has received surprisingly little attention from petrologists and mineralogists. In addition it will help delineate the petrogenesis of rocks containing zoisite-clinozoisite pairs. Holdaway (1972) suggested that coexisting zoisite and clinozoisite might prove to be a useful geothermometer, an idea that is substantiated by this investigation. The present study represents an effort to summarize available field observations and to outline equilibrium phase relations for the zoisite-clinozoisite transition.

Zoisite and clinozoisite can be described approximately by the formula Ca_2^{VII} or $^{VIII}Al_{3-x}^{VI}M_x^{VI}[Si_2O_7][SiO_4]O(OH)$, where M is usually

Fe^{3+} and less commonly Mn^{3+}. The iron-bearing menbers of the epidote group are the only ones to be considered in this study. Substitution of Fe^{3+} ranges from x = 0.0 to 0.6 for zoisite and x = 0.0 to 0.33 for clinozoisite (for x > 0.33 the monoclinic phase is an epidote[3]). These minerals are characteristic of low- to medium-grade metamorphic rocks (greenschist to amphibolite facies) and are most commonly found in calc-silicates but also occur in some mica schists and metabasites (Winkler, 1976; Deer et al., 1962). The optical similarities of the two minerals, especially at low iron concentrations, make their distinction difficult, hence the terms are often used interchangeably by petrographers (e.g. Winkler, 1976, p. 70 ff.). Field observations suggest that low-Fe clinozoisite tends to be found in lower grade rocks (greenschist and albite-epidote amphibolite facies) while low-Fe zoisite is more common in higher grades (albite-epidote amphibolite and amphibolite facies) (Harpum, 1954; Strens, 1963; Ackermand and Raase, 1973). However, it is clear that high iron contents usually favor a true epidote over either zoisite or clinozoisite.

Structurally, both zoisite and clinozoisite are based on infinite chains of edge-sharing octahedra (Dollase, 1968). These chains, which

---

[3] The distinction between clinozoisite and epidote is arbitrarily placed at the change in optic sign from B^+ to B^-. Hörmann and Raith (1971) showed that this change occurs at approximately 5.6 weight percent Fe_2O_3, or at 11% of the hypothetical pistacite molecule ($Ca_2Fe_3Si_3O_{12}(OH)$); Ps 11 = $Ca_2Al_{2.67}Fe_{0.33}Si_3O_{12}(OH)$. The monoclinic solid solution extends to approximately Ps 46 (Strens, 1963).

parallel the Y crystallographic axis, are linked by $[SiO_4]^{4-}$ and $[Si_2O_7]^{6-}$ groups into sheets paralleling (100). These sheets are joined together by seven- or eight-coordinated calcium and $[Si_2O_7]^{6-}$ tetrahedral groups. The structures are distinguished by the type of edge-sharing octahedral chains. Clinozoisite has 2 distinct chains, one without branching octahedra and one with branching octahedra on either side (cf. the topologically identical chain in olivine). Zoisite has only one type of octahedral chain which has branching octahedra on one side only. Studies of both zoisite (Ghose and Tsang, 1971) and clinozoisite (Dollase, 1973) have shown that all Fe^{3+} substitutes into the octahedral M3 (or A13) site, which is the octahedron branching from the edge-sharing octahedral chain. This is not true of high-iron epidotes where Fe^{3+} occupies both the M1 and M3 sites (Dollase, 1973). Dollase (1968) has also noted that the limited compositional range of zoisite as compared to the clinozoisite-epidote series is probably related to the structural distortions introduced into a zoisite-type structure by substituting larger Fe^{3+} ions ($r = 0.645$ Å) for Al^{3+} ($r = 0.530$ Å) in the M3 octahedral site.

FIELD EVIDENCE RELATED TO THE ZOISITE-CLINOZOISITE TRANSITION

A first step in understanding the zoisite-clinozoisite transition is the determination of the limits of Fe^{3+} solubility in the two phases. Compositional ranges for both the orthorhombic (zoisite) and monoclinic (clinozoisite-epidote) members of the epidote group have been studied by Eitel (1919) and Kepezhinskas and Khlestov (1967) (see figures 4a and 4b respectively). On the basis of 53 zoisite and 120 clinozoisite-epidote analyses, Eitel found (1) that iron content is important but not decisive in determining whether the phase will be orthorhombic or monoclinic and (2) that the marked region of compositional overlap strongly suggested a polymorphic relation between zoisite and clinozoisite. The results of Kepezhinskas and Khlestov (1967) are based on compositions of 470 zoisites, epidotes and allanites (orthites). Their results, although based on an independent data set, are strikingly similar to Eitel's. Both studies show zoisite compositions almost reaching Ps 20, $Ca_2Al_{2.4}Fe_{0.6}Si_3O_{12}(OH)$. This is considerably higher than generally realized (Deer et al., 1962) quote Ps 10 as a practical limit). Again, the same conclusion as to the existence of a zoisite-clinozoisite (or zoisite-epidote) polymorphic relationship is reached.

The existence of a polymorphic relation between zoisite and either clinozoisite or epidote senso stricto should be evidenced by naturally occurring pairs. Such assemblages have been reported, with varying degrees of reliability, by Weinschenk (1903), Rodgers (1924), Orlov (1925), Foye (1926), Harpum (1954), Hall (1959), Hansen (ms), Banno (1964),

FIGURE 4

Frequency of occurrence versus composition for orthorhombic (zoisite) and monoclinic (clinozoisite-epidote) epidote group minerals. (a) From Eitel (1919). (b) Modified after Kepezhinskas and Khlestov (1967).

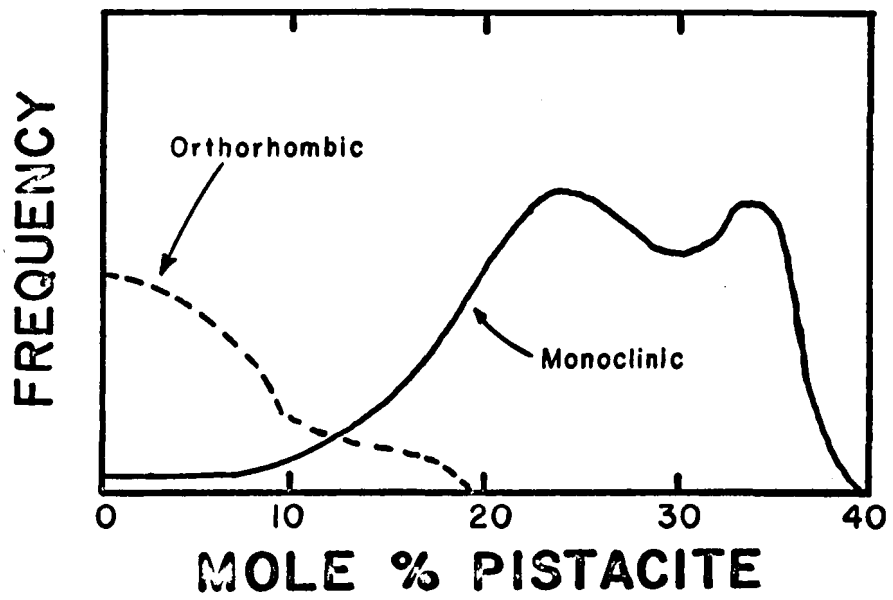
FREQUENCY
Orthorhombic
Monoclinic
0
10
20
30
40
MOLE % PISTACITE

(a)

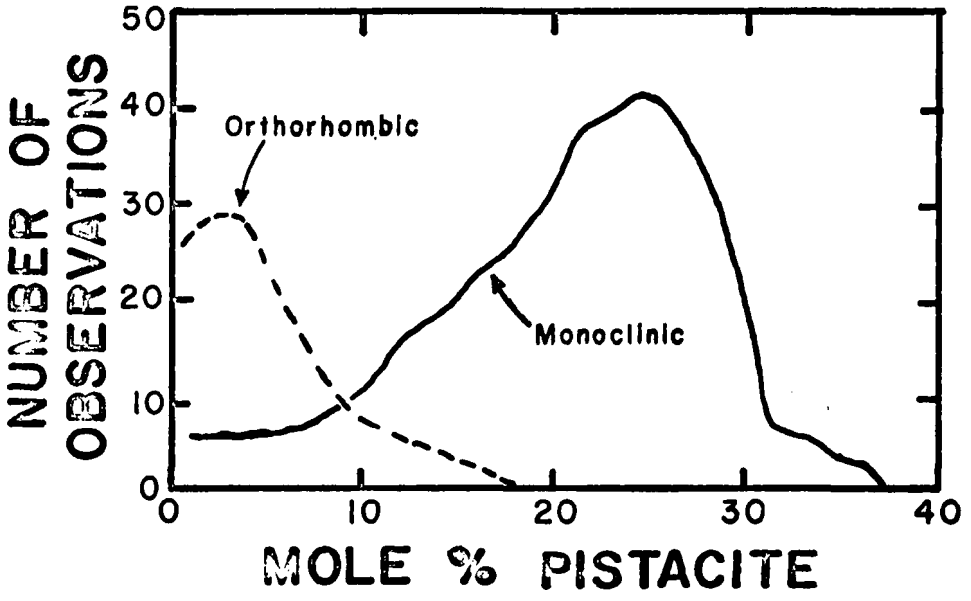
NUMBER OF OBSERVATIONS
50
40
30
20
10
0
Orthorhombic
Monoclinic
0
10
20
30
40
MOLE % PISTACITE

(b)

Strens (1965), Myer (1966), Ackermand and Raase (1973), Hietanen (1974) and Raith (1976). Diverse opinions have been expressed concerning the significance of these assemblages. Harpum (1954), arguing from field observations in Tanganyika, feels that the various members of the epidote group lack overlapping stability fields and therefore such pairs are nonequilibrium assemblages. Myer (1966), Ackermand and Raase (1973) and Raith (1976) describe coexisting zoisite-clinozoisite (or epidote) assemblages that they assert are definitely in equilibrium. Strens (1965) states that zoisite can coexist with epidote but not with clinozoisite, and he cites evidence of apparently nonequilibrium zoisite overgrowths on clinozoisite.

Examination of the possible phase relations for the transition and a comparison with the naturally occurring zoisite-clinozoisite pairs are useful for resolving the various proposed relations. Based on Eitel's (1919) data, Ehlers (1953) hypothesized that the zoisite-clinozoisite relationship has the form of a transition loop, typical for reconstructive transformations in minerals exhibiting solid solution. This is illustrated in figure 5b where zoisite is arbitrarily shown as the high temperature phase. Figure 5a shows the same transition drawn to represent a simple polymorphic transformation between monoclinic and orthorhombic phases. It is clear that the presence or absence of a regular compositional gap between coexisting zoisite-clinozoisite pairs can differentiate between these two possibilities. Although only four well-documented studies of stably coexisting zoisite-clinozoisite (or epidote) assemblages could be found (Table V), they are in agreement with

FIGURE 5

Two possible forms of the zoisite-clinozoisite transition. (a) Simple polymorphic transformation. (b) Solid solution transition loop. Zoisite has arbitrarily been drawn as the high temperature phase.

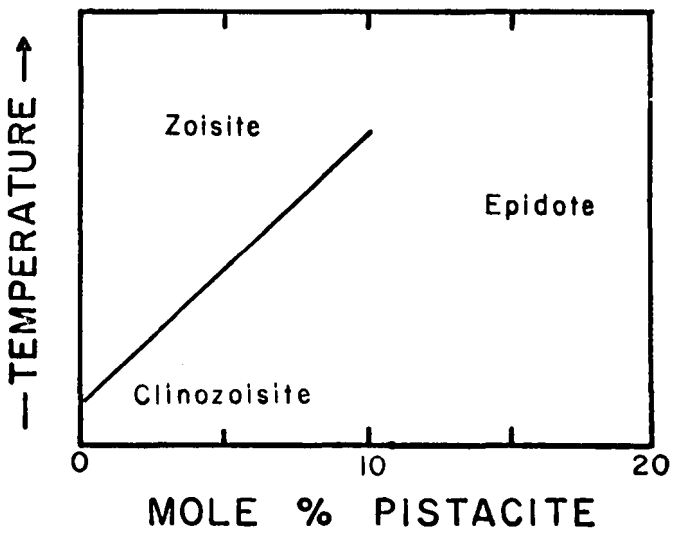
TEMPERATURE
Zoisite
Epidote
Clinozoisite
0
10
20
MOLE % PISTACITE

(a)

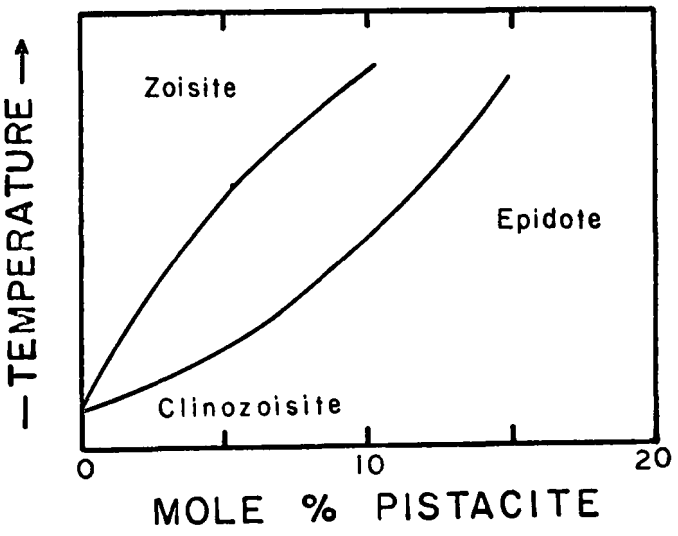
TEMPERATURE
Zoisite
Epidote
Clinozoisite
0
10
20
MOLE % PISTACITE

(b)

TABLE V

WELL DOCUMENTED EXAMPLES OF COEXISTING ZOISITE AND CLINOZOISITE (OR EPIDOTE)

Author	Description	
Strens (1965)	Epidote-zoisite-almandine-chlorite rock (quartz free) from Mendocino County, California, Well crystallized epidote occurs between blades of zoisite. Thin section examination revealed no signs of disequilibrium.	Microprobe analysis yielded zoisite of Ps 2.6 and epidote of Ps 16.8. Grains are said to be homogeneous.
Myer (1966)	Layered calc-silicates from Trollheimen, Norway show apparently stable epidote-ferrian zoisite assemblage. Metamorphism to lower amphibolite facies.	Optical and x-ray examination indicate an epidote of Ps 12. Zoisite is referred to only as being ferrian (i.e. α -zoisite of old notation).
Ackermand and Raase (1973)	Clinozoisite- and zoisite-bearing biotite schists (lower amphibolite facies) from the Tauern Window, Austria. Zoisite and clinozoisite grains are in contact; textures suggest equilibrium growth of both. Maximum T estimated at from 550°C to 600°C.	Microprobe analyses at boundaries of touching grains give: Zoisite: Ps 4.1, Ps 3.2 Clinozoisite: Ps 10.4, Ps 8.6
Raith (1976)	Progressively metamorphosed basic volcanics from Tauern Window, Austria contain zoisite-epidote assemblages in greenschists (upper greenschist facies), garnet amphibolites and eclogites. No mention is made of grain contact. P, T estimates are 5kb minimum at 420° to 560°C.	Optical examination indicates epidotes have fairly constant composition (Ps 8) while zoisites change from Ps 1 to Ps 6 with increasing metamorphic grade.

the existence of a compositional gap between the phases, with the monoclinic phase always having the higher iron content. Field evidence also indicates that the zoisite in such pairs increases in iron content with increasing metamorphic grade (Raith, 1976). The change in the clinozoisite (or epidote) composition with metamorphic grade is not well understood at this time. Raith (1976) describes a constant iron content while Ackermand and Raase (1973) describe pairs where iron content increases with rising iron content in the zoisite. Strens' (1965) pair seems anomalous. Myer (1966), besides noting coexisting zoisite-epidote in the Trollheimen, Norway calc-silicates, points out that other rocks in the area demonstrate the role of bulk composition in controlling whether zoisite (low-iron bulk composition), epidote (high-iron bulk compositions) or a zoisite-epidote pair will crystallize.

The sum of the evidence from natural occurrences leads to the following conclusions:

1. Coexisting zoisite-clinozoisite (or zoisite-epidote) pairs display a compositional gap consistent with the observation that transformations in minerals exhibiting solid solution are of the transition loop type (Ehlers, 1953).

2. At pressure, temperature and oxygen fugacity conditions consistent with stable zoisite-clinozoisite pairs, increasing iron (Fe^{3+}) in the bulk composition produces the sequence zoisite → zoisite + clinozoisite (or epidote) → clinozoisite (or epidote) (Myer, 1966).

3. Naturally occurring clinozoisites appear to extend to the iron-free end-member $Ca_2Al_3Si_3O_{12}(OH)$ (Eitel, 1919; Kepezhinskas and Khlestov,

1967). Hence the zoisite-clinozoisite transition loop must begin at the iron-free composition and extend to the more iron-rich compositions. The seeming contradiction of this with Raith's (1976) observation of a nearly constant clinozoisite composition of Ps 8 in coexisting pairs can not be resolved on the basis of presently available data.

4. Increasing metamorphic grade causes an iron increase in the zoisites of the coexisting pairs (Raith, 1976). With the added restriction that zoisite is the iron-poor phase in any pair, this leads to the conclusion that zoisite is the high-temperature phase (pressure should not be particularly important since molar volumes for zoisite and clinozoisite are very similar. See Holdaway, p. 331f). Since many of the coexisting pairs reported occur in lower amphibolite grade rocks, the clinozoisite to zoisite transformation for the iron-free composition must therefore occur at still lower grade.

5. A phase diagram consistent with these basic observations would be topologically similar to figure 5b.

An approximate model for the clinozoisite-zoisite inversion as supplied by figure 5b can be used to explain apparently nonequilibrium occurrences of clinozoisite overgrown by zoisite. Rodgers (1924), Orlov (1925) and Strens (1965) all note such occurrences, Strens observing that the zoisite was epitactically related to the clinozoisite core (Y and Z coincident based on optical examination). Using figure 5b as a guide, such overgrowths can be viewed as indicative of a complete transition from clinozoisite stability to zoisite stability. The clinozoisite, having failed to completely react away, is now rimmed by the stable

product, zoisite. Such a situation might be due to either prograde metamorphism or a change in bulk composition during growth (to less iron-rich composition), or both. Hence such an occurrence can be viewed as further evidence for a clinozoisite-zoisite polymorphic relation of the transition loop type, contrary to statements by Strens (1965).

Previous Experimental Work

Few experimental investigations are available on the monoclinic to orthohombic transformation in the epidote group minerals. Ehlers' (1953) work has already been mentioned, and his suggestion of the solid-solution transition loop provides a reasonable fit to the field evidence. Strens (1965) proposed a T-X diagram based on a combination of experimental observations and naturally occurring two-phase assemblages. In his phase diagram Strens proposes a solvus in the monoclinic epidote field, a feature recently substantiated by field work (Raith, 1976). However, at the low iron compositions Strens allows neither for the existence of stable iron-free clinozoisite nor for a transition loop between zoisite and clinozoisite.

Pistorius, Kennedy and Sourirajan (1962) studied the relations between anorthite, zoisite and lawsonite at high temperatures and pressures using a "simple squeezer" device. Their synthesis diagram, constructed using the zeolite scolecite ($CaAl_2Si_3O_{10} \cdot 3H_2O$) as the starting material, shows zoisite to be the high-temperature and high-pressure phase in the clinozoisite to zoisite transition. However, their transition was at 750°C and 21 kbar, moving to higher pressures as the temperature dropped. This would indicate that zoisite could not exist stably in the crust, contradicting field evidence. The authors made no attempt to demonstrate reversibility for their proposed univarient reaction, and attempts to duplicate the results using different starting materials were unsuccessful (Boettcher, 1970).

Holdaway (1972) attempted to determine the P-T configuration of the

clinozoisite to zoisite transformation for iron-free compositions by comparing experimental zoisite stability limits (Newton, 1965, 1966) with thermodynamically derived limits for clinozoisite. After having determined experimental equilibria involving epidote (Ps 33) and clinozoisite (Ps 10), Holdaway used a one site-two site mixing model to derive molar entropies at 627°C as a function of composition for epidotes and clinozoisites. The extrapolated molar entropy for clinozoisite (Ps 0) was 183.3 $\pm$ 4.0 cal. K^{-1}. This was lower than the molar entropy for zoisite (Ps 0) of 189.0 $\pm$ 2.0 cal. K^{-1}, which Holdaway calculated from equilibria experimentally determined by Boettcher (1970) and Newton (1965, 1966), and is therefore supportive of zoisite being the high temperature phase. Holdaway finally concluded that:

1. The zoisite-clinozoisite (Ps 0) equilibrium has very little pressure dependence, the calculated slope being +1300 bars K^{-1}.

2. At elevated pressures (> 3 kbar) the clinozoisite-zoisite (Ps 0) inversion becomes a stable reaction and occurs at 635 $\pm$ 75°C.

3. The addition of ferric iron produces a divariant equilibrium which raises the transition temperature (i.e. restricts the stability field of zoisite).

A temperature of 560°C or greater seems excessively high for the lower stability of zoisite, a fact which Holdaway himself recognized. Both Holdaway (1972) and Ackermand and Raase (1973) point out that field evidence strongly suggests stable zoisite at temperatures below 550°C. It appears therefore that the uncertainties in the available thermodynamic data prevent anything more accurate than a rough approximation to the position of the clinozoisite to zoisite transformation.

Experimental Methods

All experiments were performed using standard cold-seal hydrothermal techniques with a series of horizontally mounted René 41 bombs. Experimental pressures ranging from 5 to 6.5 kbar were measured with a factory-calibrated Heise Bourden tube gauge and are believed to be accurate to within 50 bars. Pressure variations during any run were less than 50 bars unless otherwise noted.

Temperatures were measured with external chromel-alumel thermocouples calibrated against the melting points of NaCl, CsCl and LiCl. Filler rods were used both in the calibration and in the experimental runs. Temperature variations over the course of any run were less than $\pm$ 3°C and the overall uncertainty in the run temperatures is $\pm$ 6°C.

Platinum capsules were used for all runs except 105-77 and 106-77 where gold capsules were used. Pt capsules were chosen because they were not brittle and would allow H_2 diffusion for "bomb wall" buffering. Oxygen fugacities are presumed to have been buffered by the Ni and NiO of the René 41 bomb wall for runs in Pt capsules. Oxygen fugacities for runs in Au capsules are unknown.

Qualitative examination of run products (phase identification and abundance estimation) was performed using optical and powder x-ray techniques. Lattice constant refinements were performed using BaF_2 (a = 6.1978(20) Å) or NBS-SI (a = 5.43088 Å) as internal standards. Data for such refinements were collected on a Picker horizontal powder diffractometer with graphite monochrometer using 4 scans (2 oscillations) at 1/4° per minute over the range 2θ = 10° to 60°. At lower 2θ's line position

was taken as midpoint at 2/3 height (CuKα); when $\alpha_1 - \alpha_2$ splitting became noticeable, line position at peak top (CuKα_1 or α_2 as appropriate) was employed. Between 15 and 21 lines were used for each zoisite or clinozoisite lattice constant refinement. Calculations were carried out using the LCLSQ 4 program of Burnham (1962) as modified by Finger, using space group Pnma for zoisite and $P2_1/m$ for clinozoisite.

Microprobe analyses of synthetic zoisites and clinozoisites were performed on an ARL SEMQ. Synthetic anorthite glass was used as the standard for Ca, Al and Si, and the Marjalahti olivine with 8.97 weight percent iron was used as the standard for Fe. Matrix corrections were performed using the ZAF correction procedure of Springer (1976). For the epidote minerals all iron was presumed to be ferric.

A limited number of the larger single crystals (> 100 μm in length) were separated out for x-ray determination of their symmetry. Zero - level Weissenberg photographs were found to be the most useful; exposure times were shortened by oscillating over a 20° range. The phases can be most easily distinguished if X* oscillates between 21° and 41° from parallelism with the x-ray beam.

Starting materials for synthesis runs consisted of stoichiometric mixtures of synthetic anorthite, silica glass and certified reagent $CaCO_3$ and Fe_2O_3. Anorthite was crystallized from gel at 700°C and 3 kbar for 3 to 5 days and examined by powder x-ray diffractometry to insure crystallinity. After drying at 120°C for at least 3 hours, the reactants were weighed, mixed and vigorously hand ground under acetone. This is referred to as an anorthite mix.

Starting compositions were prepared in 5 mole percent intervals of the epidote molecule, $Ca_2Al_2FeSi_3O_{12}(OH)$, from Ep 0 to Ep 55 (Ps 0 to approximately Ps 18.3). Each synthesis run contained 25 to 30 mg of an anorthite mix plus enough distilled water to keep the mole fraction of CO_2 in the final run fluid below 0.05. Synthesis runs are numbered 11-76 through 72-77, 80-77, 81-77, 105-77 and 106-77.

Reversibility runs were performed using the products from individual synthesis runs. These starting materials contained at least 90% epidote (zoisite and/or clinozoisite) and usually as much as 95%. The compositional homogeneity of the starting material was estimated by optical and electron probe examination.

Results

The results of both synthesis and reversal runs are shown in Table VI. Except for runs at pressures below 5.5 kbar the synthesis yield of zoisite and/or clinozoisite using an anorthite starting mixture was excellent, almost always exceeding 90% and quite often 95%. It was also observed that as the pressure and/or temperature of synthesis were increased, the resulting crystals increased in size. At the optimum conditions of 650°C and 6500 bars the average zoisite crystal was ∿40 μm long and the average clinozoisite was ∿10 μm long. However, in any run there were always a few larger (>100 μm) crystals, especially in synthesis runs crystallizing zoisites. Zoisite crystals from run 11-76 were from 500 μm to 1500 μm in length. Both zoisites and clinozoisites tended to grow as bladed crystals elongated along Y and flattened on the (100) plane.

Along with the epidote minerals synthesized in these runs, other phases were present at low levels (usually <2%). These included unreacted silica glass, calcite, garnet, anorthite, quartz, magnetite and rarely hematite. Of these only garnet and magnetite were ubiquitous. Magnetite tended to crystallize as tiny ($\leq$2 μm) needles adhering to the surface of other grains, but magnetite grains were also observed. Their presence could often only be detected by the effect of a strong magnet on epidote or garnet grains. Garnet was present in almost every synthesis run in amounts often exceeding 2%. The optical properties ($1.734 \leq n \leq 1.740$) and unit cell parameters ($11.851\text{Å} \leq a \leq 11.856\text{Å}$, see Table VII) of the synthetic garnets are extremely close to those of pure grossular (n = 1.734 and a = 11.851Å; Winchell, 1958).

TABLE VI

SUMMARY OF EXPERIMENTAL RUNS

RUN NUMBER	STARTING MATERIAL	BULK COMPOSITION	TEMP. (°C)	PRESSURE (bars)	RUN TIME (days)	RUN PRODUCTS Zo	Clz	Gt	An	Cc	Qz	Gl	Mt	H
11-76	Anorth. mix	Ep 5	651	see note	14	o		vm	vm				vm	
12-76	Anorth. mix	Ep 5	650	6490	31	o		m				vm	vm	
18-76	Anorth. mix	Ep 20	650	6490	31	o		m				t	t	
20-76	Anorth. mix	Ep 25	649	6500	15	o		m				m	t	
21-76	Anorth. mix	Ep 25	650	5810	15	mj		m	m	t			m	
22-76	Anorth. mix	Ep 25	649	6500	15	mj	m	m				t	t	
23-76	Anorth. mix	Ep 25	649	5810	15	m	mj	m			m		vm	
24-76	Anorth. mix	Ep 30	651	6510	33	mj	m	m			t		vm	
25-76	Anorth. mix	Ep 35	651	6510	33	mj	mj	m					vm	
26-76	Anorth. mix	Ep 40	651	6505	21		o	vm				t	t	
27-76	Anorth. mix	Ep 45	651	6505	21	t	o	vm				t	t	
28-76	Anorth. mix	Ep 40	552	6500	21		o	vm		vm			t	
29-76	Anorth. mix	Ep 45	552	6500	21		o	vm		vm			t	
30-76	Anorth. mix	Ep 50	650	6510	20	mj	mj	m					t	t
31-76	Anorth. mix	Ep 55	650	6510	20		o	m					vm	t
32-76	Anorth. mix	Ep 25	549	5800	21		o	m		m				t
33-76	Anorth. mix	Ep 40	549	5800	21		o			m	vm		t	
34-76	Anorth. mix	Ep 25	552	6500	17		o			vm			t	
35-76	Anorth. mix	Fp 5	552	6500	17	o		vm		vm			t	
36-76	Anorth. mix	Ep 40	650	6500	14		o	vm		vm	vm		vm	
37-76	Anorth. mix	Ep 25	650	6500	14		mj		mj	m			t	t
38-76	Anorth. mix	Fp 45	651	6510	8		mj	mj	m		m		vm	
39-76	Anorth. mix	Ep 50	651	6510	8		mj	m		m		t	t	
42-77	Anorth. mix	Ep 0	502	6500	24	o		m						
43-77	Anorth. mix	Ep 5	502	6500	24	mj	mj	vm				vm		

Explanation of Symbols

An	Anorthite	Gl	Glass	Mt	Magnetite
Cc	calcite	Gt	Garnet	Qz	Quartz
Clz	Clinozoisite	H	Hematite	Zo	Zoisite

o	greater than 90%	vm	less than 2%
mj	greater than 33%	t	trace
m	less than 33%		

Notes

Run 11-76: total pressure loss
Run 25-76: xtls. typically Clz rimmed by zoisite
Run 30-76: Clz and Zo are distinct
Run 37-76: Clz, An and Cc are actually in approx. equal amounts

TABLE VI CONTINUED

RUN NUMBER	STARTING MATERIAL	BULK COMPOSITION	TEMP. (°C)	PRESSURE (bars)	RUN TIME (days)	RUN PRODUCTS Zo	Clz	Gt	An	Cc	Qz	Gl	Mt	H
44-77	Anorth. mix	Ep 10	500	6500	29	mj	mj	vs	vs	vs		vs		
45-77	Anorth. mix	Ep 15	500	6500	29	vs	o	vs	vs	vs				vs
46-77	Anorth. mix	Ep 25	550	6500	23		o	vs			vs		t	
47-77	Anorth. mix	Ep 20	550	6500	23	mj	mj	vs		s		vs	t	
48-77	Anorth. mix	Ep 15	549	see note	16	mj	mj	vs				t	t	
49-77	Anorth. mix	Ep 10	549	see note	16	mj	s	vs		t		t	t	
50-77	Anorth. mix	Ep 40	601	6500	16		o			vs	vs	vs	t	
51-77	Anorth. mix	Ep 35	601	6500	16		o	vs		t		t	vs	
52-77	Anorth. mix	Ep 30	600	6500	16		o	vs		t			t	
53-77	Anorth. mix	Ep 25	600	6500	16		o	vs		t	vs		vs	
57-77	Anorth. mix	Ep 20	600	6500	32	mj	mj	vs		t	vs		t	
58-77	Anorth. mix	Ep 15	600	6500	32	o	vs	vs		t	t		t	
59-77	Anorth. mix	Ep 10	650	5800	32	o		vs			vs		t	
60-77	Anorth. mix	Ep 15	650	5800	32	o		vs	t	t	vs		t	
61-77	Anorth. mix	Ep 20	650	5800	32	o		s	s					
62-77	Anorth. mix	Ep 30	650	5800	32	mj	s	s	s	vs				
63-77	Anorth. mix	Ep 5	651	5005	32			mj	mj	s				
64-77	Anorth. mix	Ep 10	651	5005	32			mj	mj				vs	
65-77	Anorth. mix	Ep 15	648	5000	32			mj	mj	vs			vs	
66-77	Anorth. mix	Ep 20	648	5000	32			mj	mj				vs	
67-77	Anorth. mix	Ep 25	650	5000	32			mj	mj				vs	
68-77	Anorth. mix	Ep 30	650	5000	32			mj	mj				vs	
71-77	Anorth. mix	Ep 0	404	6495	15				o	s				
72-77	Anorth. mix	Ep 0	475	6500	15	o			vs	vs				
73-77	42-77	(Ep 0)	404	6495	15	o		vs	vs	vs				

Notes

Run 47-77: Clz by far predominates

Runs 48-,49-77: pressure started at 6500b, ended at 5600b

Run 66-77: An and Gt in approx. equal amounts

Run 73-77: a composition in braces indicates original bulk composition of starting material; true composition may be iron-poor.

TABLE VI CONTINUED

RUN NUMBER	STARTING MATERIAL	BULK COMPOSITION	TEMP. (°C)	PRESSURE (bars)	RUN TIME (days)	RUN PRODUCTS Zo	Clz	Gt	An	Cc	Qz	Gl	Mt	H
74-77	42-77	(Ep 0)	457	6500	15	o		vm	vm	vm				
75-77	20-76	(Ep 25)	560	6500	15	o		m		vm			t	
76-77	22-76	(Ep 25)	560	6500	15	o		m					t	
80-77	Anorth. mix	Ep 10	551	6503	15	m	mj	vm	m	vm				
81-77	Anorth. mix	Ep 15	551	6503	15	m	o	m	vm				vm	
84-77	35-76	(Ep 5)	451	see note	13	o			vm	vm				
85-77	45-77	(Ep 15)	603	6500	14	m	mj	vm		vm			t	
86-77	51-77	(Ep 35)	721	see note	14			mj	mj	vm			vm	
87-77	52-77	(Ep 30)	681	6500	14	m	mj	m		vm			vm	vm
89-77	25-76	(Ep 35)	603	6500	15	mj	m	m					t	t
90-77	24-76	(Ep 30)	603	6500	15	o		m				t	t	
91-77	23-76	(Ep 25)	602	5800	15	m	mj	m		vm			vm	
92-77	62-77	(Ep 30)	602	5800	15	mj		m				m	t	
93-77	75-77	(Ep 25)	417	6500	14	o		m		t		m	t	
94-77	57-77	(Ep 20)	417	6500	14	mj	mj	vm				vm	t	
95-77	50-77	(Ep 40)	407	6510	14		o	t		vm		t	t	
96-77	49-77	(Ep 10)	407	6510	14	o	m	vm		vm			t	t
99-77	57-77	(Ep 20)	654	6500	14	o		m				m	vm	
100-77	27-76	(Ep 45)	654	6500	14	mj	mj	m		vm			t	vm
101-77	26-76	(Ep 40)	705	see note	14	o		m	m	vm			vm	
102-77	31-76	(Ep 55)	705	see note	14	m		mj	mj			vm	vm	
103-77	28-76	(Ep 40)	602	6500	14		o	m				vm	vm	
104-77	30-76	(Ep 50)	602	6500	14	mj	mj	m				vm	vm	
105-77	Anorth. mix	Ep 35	653	6500	8	vm	o	m					vm	
106-77	Anorth. mix	Ep 35	653	6500	8	vm	o	vm					vm	

Notes

Run 84-77: pressure started at 6500b,ended at 5550b
Run 86-77: pressure started at 6500b, ended at 5050b
Run 94-77: Zo and Clz in approx. equal amounts
Runs 101-, 102-77: pressure started at 6500b, ended at 6350b
Run 104-77: Zo, Clz and Gt are actually in approx. equal amounts
Runs 105-, 106-77: seed xtls from run 11-76 added

TABLE VII

REFINED LATTICE CONSTANTS

PHASE	RUN NUMBER	BULK COMPOSITION	NO. REFL.	a	b	c	β	Vol
Clinozoiste	33-76	Ep 40	19	8.875(1)[1]	5.599(1)	10.156(3)	115.49(1)	455.6(2)
	34-76	Ep 25	18	8.864(3)	5.583(2)	10.138(3)	115.49(1)	452.9(5)
	36-76	Ep 40	21	8.872(2)	5.597(2)	10.143(4)	115.45(2)	454.9(3)
	38-76	Ep 45	21	8.874(2)	5.596(1)	10.152(3)	115.48(1)	455.1(2)
	39-76	Ep 50	21	8.863(3)	5.603(2)	10.131(4)	115.41(2)	454.5(5)
	106-77	Ep 35	16	8.870(3)	5.600(2)	10.144(4)	115.45(3)	455.0(4)
Zoisite	99-77	(Ep 20)	18	16.195(2)	5.548(1)	10.033(2)	-	901.5(2)
	101-77	(Ep 40)	15	16.194(2)	5.551(1)	10.037(2)	-	902.3(3)
Garnet	39-76	Ep 50	1	11.851[a]				
	86-77	(Ep 35)	9	11.852(2)				
	99-77	(Ep 20)	1	11.851[a]				
	101-77	(Ep 40)	5	11.856(2)				
	102-77	(Ep 55)	9	11.855(2)				

[1] Numbers in parenthases are e.s.d.'s output by cell edge refinement progras

[a] Only the intense (420) reflection was clearly distinguished from the Zo/Clz peaks

Optical examination of the synthesized epidote minerals plus the presence of iron oxides in the synthesis products raised questions concerning the compositions of the phases. Microprobe examination of many of the larger ($\sim$75 μm long) zoisites and clinozoisites was carried out for the direct determination of phase composition. The microprobe data, summarized in figure 6, reveal a marked iron deficiency and compositional inhomogeneity in these larger crystals. Because of the possibility that these larger crystals were not representative samples of the total run, average compositions for entire runs were estimated from refined lattice constants using data obtained through powder x-ray diffractometry. The high-iron runs 33-76, 34-76, 36-76, 38-76, and 39-76 were used because an iron deficiency would be most easily detected in them. Results are shown in Table VII. The final unit cell volumes, when compared against determinative curves of volume versus composition (figure 7), show that for all of these runs the crystals are, on the average, iron deficient.

Such an iron deficiency implies the loss of iron to other phases, to the Pt capsule or to the formation of iron oxides. Data pertinent to the composition of the garnets have already been presented and indicate that this phase has little if any iron. Also, the runs contain only very minor to trace amounts of iron oxides as magnetite or rarely hematite. These phases do not appear to be abundant enough to account for all the observed iron loss. Microprobe examination of several Pt run capsules showed that these had absorbed iron. Table VIII summarizes data showing that the immediate inner layer of an average capsule contains about 3.6 weight percent iron. Even a thin layer ($\sim$10 μm) of such an iron concentration

FIGURE 6

Microprobe composition versus bulk starting composition for selected larger zoisite or clinozoisite crystals. Crystals were taken from runs 11-76, 12-76, 18-76, 24-76, 25-76, 26-76, 27-76, 30-76 and 48-77. Symbols designate zoisite (X), clinozoisite (.) or uncertain epidote phase (+).

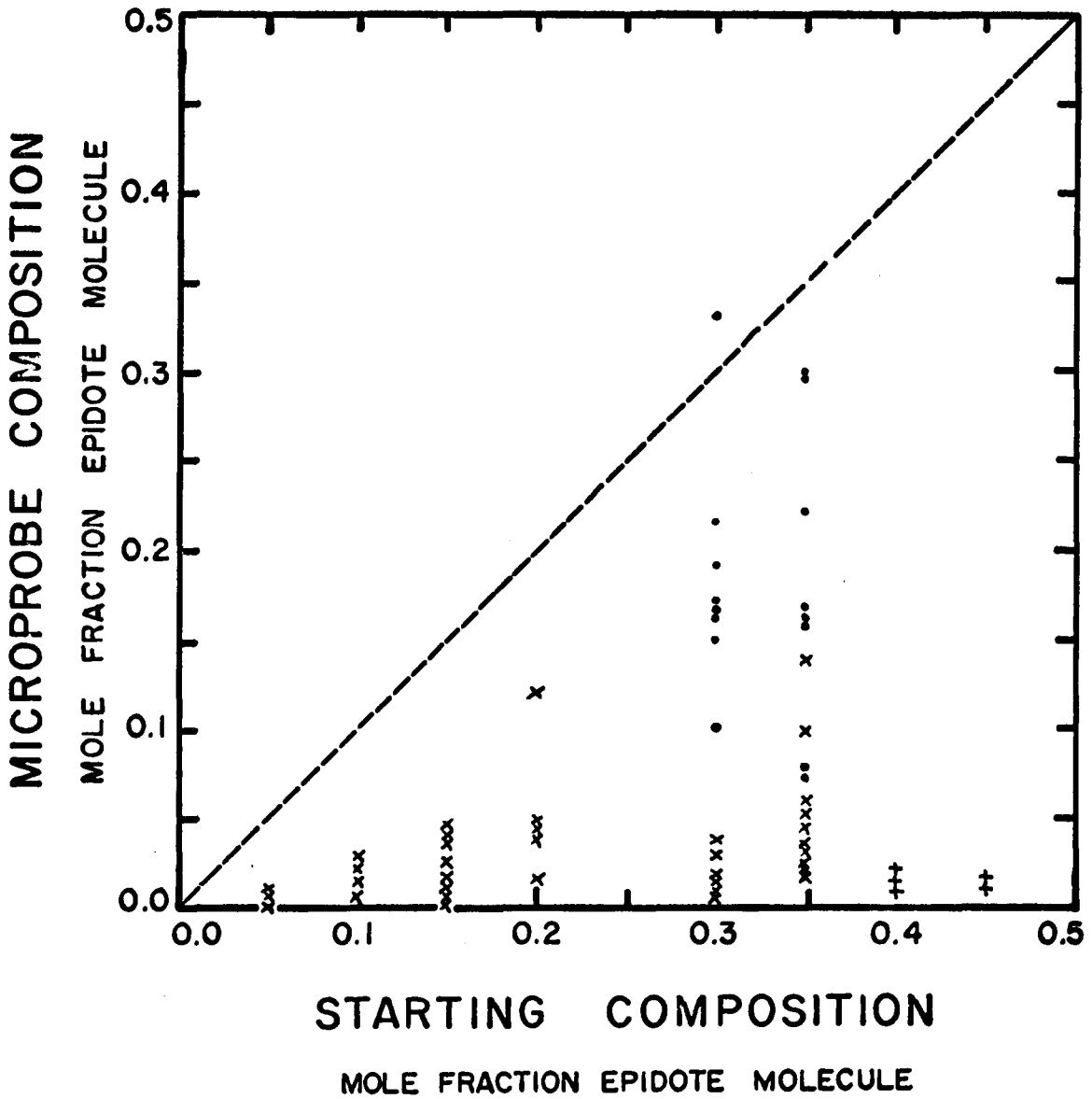
MICROPROBE COMPOSITION
MOLE FRACTION EPIDOTE MOLECULE
0.0
0.1
0.2
0.3
0.4
0.5
STARTING COMPOSITION
MOLE FRACTION EPIDOTE MOLECULE

FIGURE 7

Unit cell volume (clinozoisite phase) versus starting composition for a number of synthesis runs. Bars represent the estimated standard deviation. The lines are the determinative curves of Myer (1965) and Kepezhinskas (1969). Synthetic clinozoisites appear to be iron-deficient.

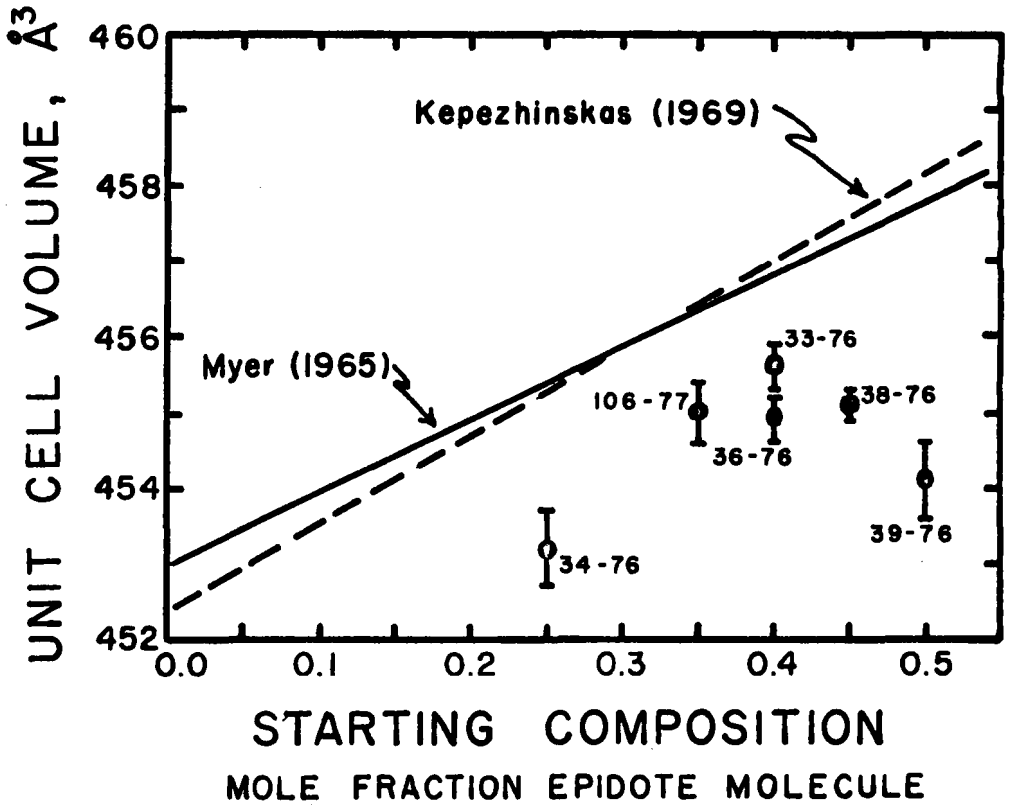
UNIT CELL VOLUME, Å3
460
458
456
454
452
0.0
0.1
0.2
0.3
0.4
0.5
Kepezhinskas (1969)
Myer (1965)
33-76
106-77
36-76
38-76
39-76
34-76
STARTING COMPOSITION
MOLE FRACTION EPIDOTE MOLECULE

TABLE VIII

IRON ABSORPTION BY PLATINIUM CAPSULES AT INNER SURFACE

RUN NUMBER	BULK COMPOSITION	WEIGHT[1,2] % Fe	ATOMIC FRACTION Fe
61-77	Ep 20	4.17	0.132
61-77	Ep 20	4.54	0.143
62-77	Ep 30	5.83	0.178
66-77	Ep 20	3.43	0.110
66-77	Ep 20	3.86	0.123
66-77	Ep 20	2.51	0.083
67-77	Ep 25	5.09	0.158
67-77	Ep 25	3.60	0.115
68-77	Ep 30	4.64	0.145
68-77	Ep 30	4.36	0.137
Unused Capsule[3]		0.56	0.019

[1] As determined by microprobe analysis using metallic iron as the Fe standard.

[2] Capsules were merely hammered flat in order to preserve the surface layer. Local surface irregularities will introduce moderate errors into the matrix corrections procedure.

[3] Unused capsules are pure platinium. Hence the indicated iron content reflects compositional uncertainty due to the lack of a polished surface.

in the capsule wall would be adequate to account for the discrepancy. Similar phenomena are reported by Liou (1973) confirming present observations and pointing out the danger of using Pt capusles with iron-bearing run materials, even at low temperatures or moderate to high oxygen fugacities. It would therefore appear wise to use very small, crimped silver liners inside the Pt capsules (as in Eugster and Wones, 1962) in future experiments to prevent iron loss from the starting materials. Note that the clinozoisites of run 106-77 apparently have an iron deficiency (figure 7) even though the run used an Au capsule. Using a truly inert sample capsule will not guarantee on-composition crystallization.

The presence of hematite plus magnetite in a number of the synthesis runs was alarming because it indicated that oxygen fugacity in the runs was higher than the hypothesized Ni-NiO oxygen buffer of the bomb wall. This high oxygen fugacity may be related to the absorption of iron by the Pt capsules. The iron-platinum alloy might have a lower permeability to H_2 diffusion that would prevent an effective buffering of the capsule fluid by the René 41 bomb.

Reversibility runs that used the zoisite and/or clinozoisite synthesized from anorthite mix starting materials were made in order to delineate the T-X regions of zoisite and clinozoisite stability at 6500 bars. The results of the reversibility runs are listed in Table VI. Several important observations can be made:

1. Clinozoisite neither nucleated in any run starting with just a zoisite phase nor increased in abundance in a run starting with mixed zoisite and clinozoisite crystals.

2. Zoisite markedly increased in abundance over the amount present in a zoisite-clinozoisite starting mixture over the temperature range 407°C (run 96-77) to 681°C (run 89-77) at 6500 bars. In one run (101-77) zoisite nucleated from an originally pure clinozoisite starting mixture. Because of the observations and the knowledge that the crystals were generally much less iron-rich than the original bulk composition, the reversibility runs give no information about either the width or the position of the zoisite to clinozoisite transition loop.

One conclusion can be reached from the reversibility experiments: the clinozoisite to zoisite transition for the pure end-member composition must occur below 407°C at 6500 bars pressure. Evidence for this low temperature comes from run 96-77 in which an original zoisite-clinozoisite mixture shows a distinct growth of the zoisite phase at 407°C. Any increase in zoisite in such a mixture, no matter what the composition, implies that the temperature of the run is <u>above</u> the lower temperature limit for the proposed zoisite-clinozoisite transition loop (temperature T_1, figure 8).

After studying a number of unusual crystals synthesized in run 25-76, an entirely new approach was devised to determine the positioning and width of the clinozoisite to zoisite transition loop. One such crystal, 25-76-1, is shown in figure 9. It illustrates the relationship typically exhibited by the crystals of clinozoisite (anomalous blue interference color) completely rimmed by zoisite (anomalous yellow-gray interference color). Further examination of this crystal and others using single crystal x-ray diffraction techniques revealed that the zoisite is epitactically related to the clinozoisite. Figure 10 shows a zero-level

FIGURE 8

T - X schematic for proposed zoisite-clinozoisite transition loop. T_1 marks the lower temperature limit of zoisite stability, and of the transition loop itself, at 6500 bars. Zoisite can increase in zoisite-clinozoisite mixtures only at run temperatures above T_1.

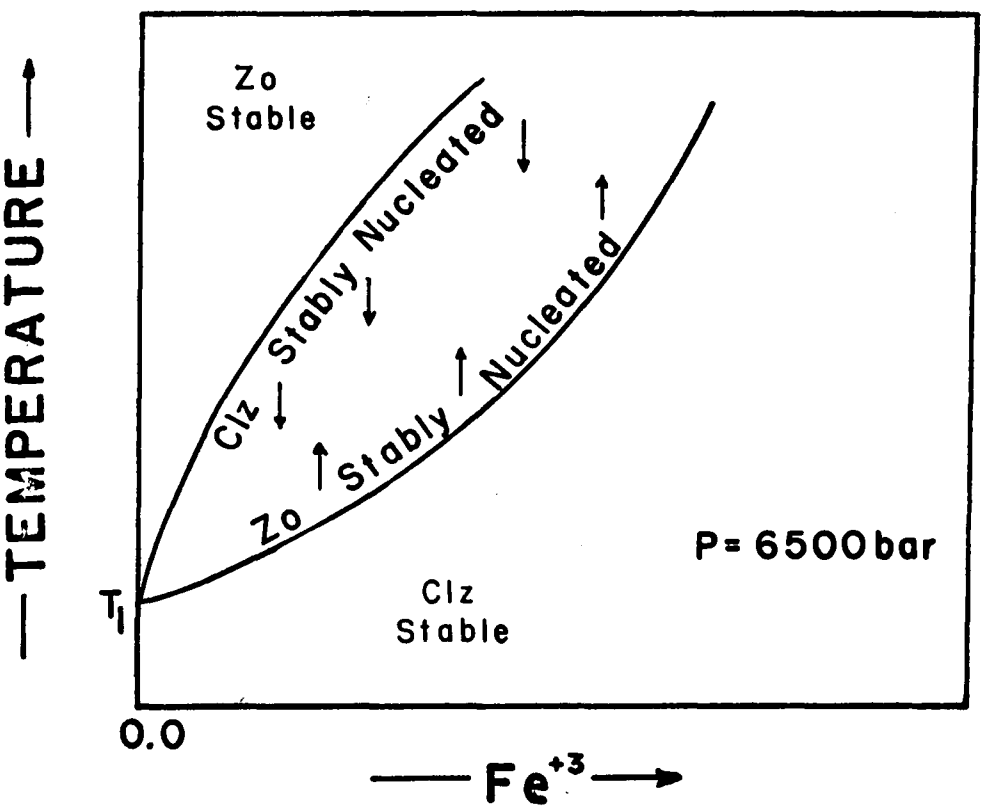
Zo
Stable
Clz Stably Nucleated
Zo Stably Nucleated
P= 6500 bar
Clz
Stable
T1
0.0
TEMPERATURE
Fe+3

Figure 9

Crystal 25-76-1. The crystal is 260 μm long and 35 μm wide (20 μm thickness is into photograph). (a) View down X* in cross-polarized light. Clinozoisite is the anomalous blue core; zoisite is the anomalous yellow-gray rim. Actual colors are slightly deeper. (b) View in plane-polarized light from opposite side of crystal.

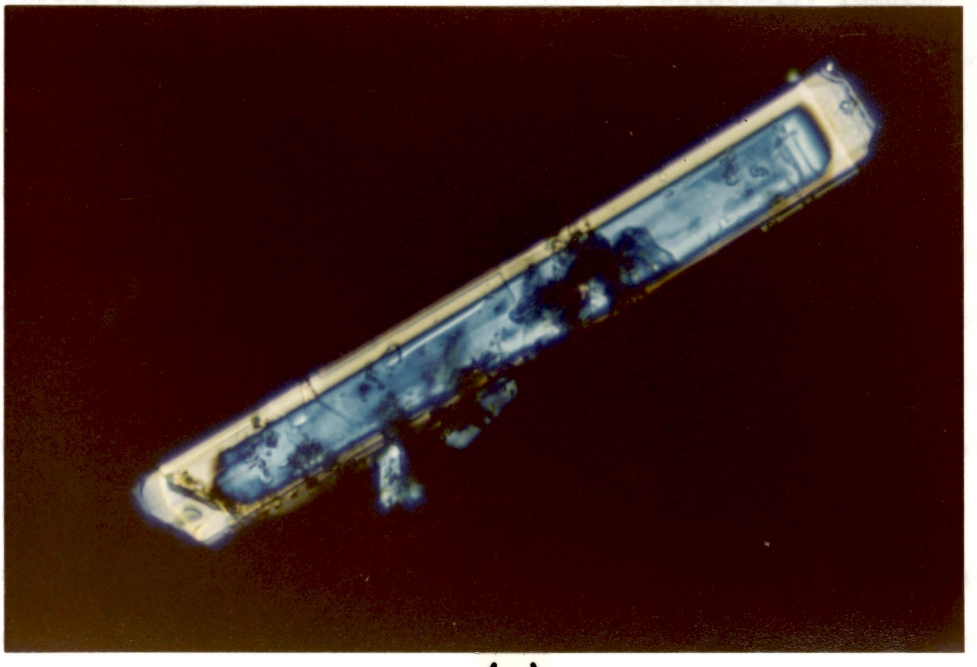

(a)

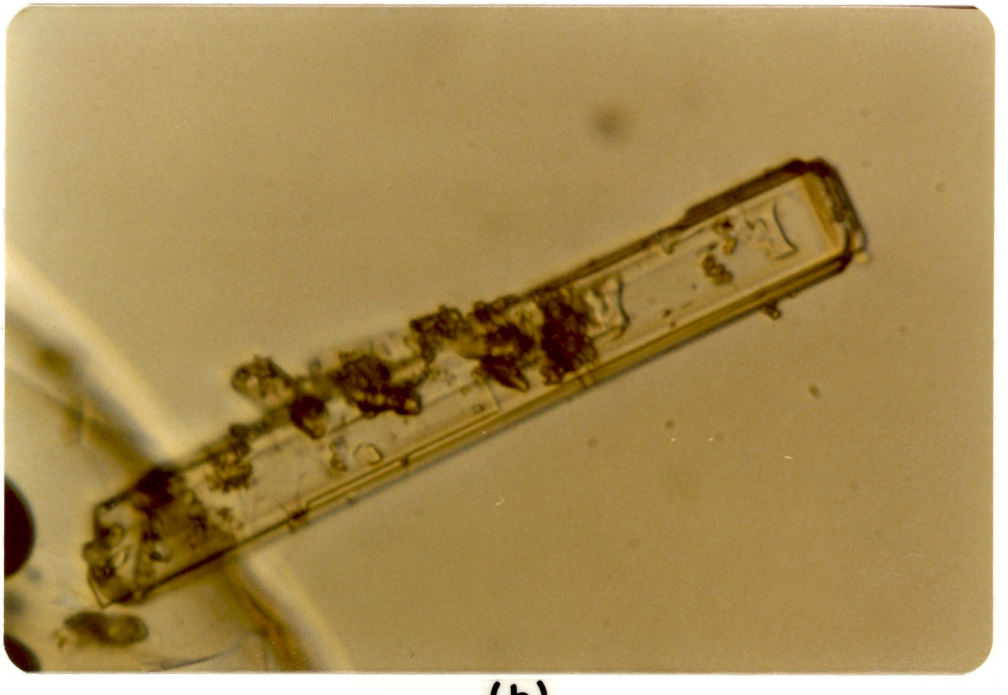

(b)

Weissenberg photograph (limited oscillation) essentially identical to the one taken for cyrstal 25-76-1. Both core (clinozoisite) and rim (zoisite) must have Y in common since the (h0ℓ) reflections for both phases are simultaneously aligned. Also it can be seen that the (001)* reciprocal planes for the zoisite and clinozoisite are parallel; hence they have a common Z axis. Systematic absences for both the zoisite and the clinozoisite are consistent with their accepted space group symmetries of Pnma and $P2_1/m$ respectively. In addition, lattice constants measured from such zero-level photographs agree well with published values of Dollase (1968). The extreme diffuseness of the reflections is apparently due to the combined contributions of unusual crystal shape (25-76-2 is 370 x 40 x 14 μm), structural imperfections, and slight misalignment.

These synthetic crystals are identical to natural overgrowths described by Strens (1965, p. 472). In both cases the two phases have their Y and Z crystallographic axes in common. Such crystals, it will be argued, are indicative of stability for the overgrowth phase. The zoisite which rims the clinozoisite core has a lower free energy than a clinozoisite of identical composition. If this were not true, clinozoisite would certainly have continued to grow, thereby eliminating the added free-energy of the clinozoisite-zoisite interface. Because of this relationship, electron microprobe examination of crystals showing zoisite-on-clinozoisite epitactic overgrowths (or vice versa) should provide data useful for bracketing the position of the transition loop at constant temperature and pressure.

Four such crystals were selected for electron microprobe study based

FIGURE 10

Portion of (h0ℓ) Weissenberg photograph of crystal 25-76-2. This crystal is similar to 25-76-1, figure 9. The overlays identify the reflections belonging to zoisite and two clinozoisite twins (twin law is (100) mirror; reflections are indexed for only one twin). The zoisite overgrowth of the crystal is epitactically related to the clinozoisite core (both have Y and Z in common).

ZOISITE
CLINOZOISITE

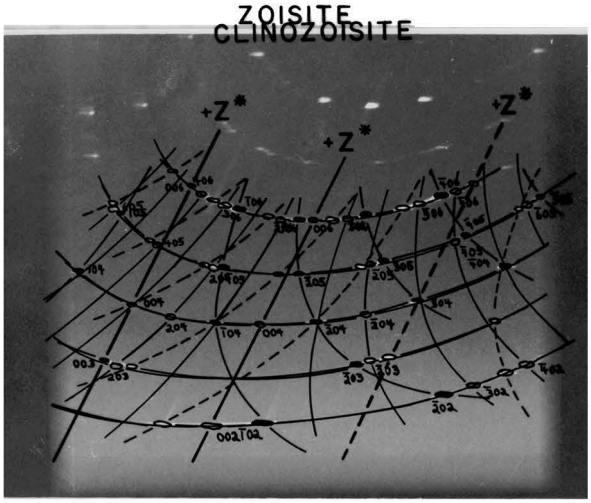

ZOISITE

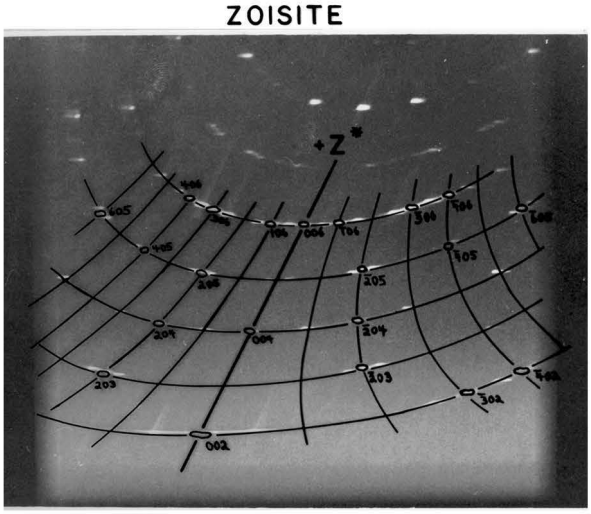

CLINOZOISITE

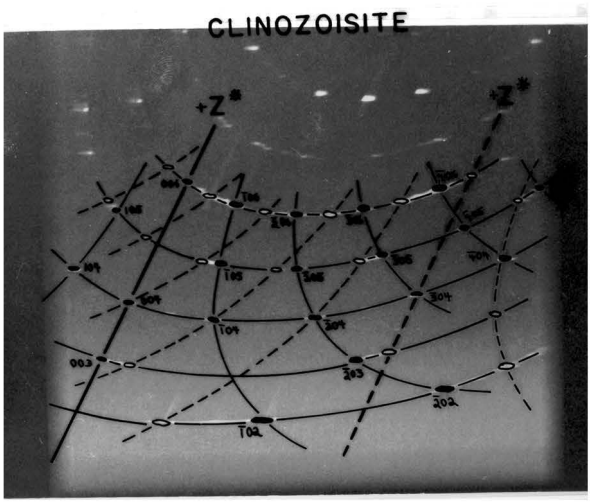

on the preceding observations. All four were grown at 650°C and 6500 bars pressure. Crystals 25-76-1 and 25-76-2 were chosen as representative of zoisite rimming clinozoisite, and 105-77-1 and 106-77-1 were chosen for clinozoisite rimming zoisite. These latter two crystals were specially grown using iron-free zoisites from run 11-76 as seeds in an anorthite mix of composition Ep 35 (Ps 11.7). Crystal 105-77-1 (figure 11) is typical of most crystals with overgrowths prepared in runs 105-77 and 106-77. As seen in the photograph, the clinozoisite overgrowths (again having an anomalous blue interference color) tended to be restricted to the (010) faces of the seed crystals. This is in contrast to crystals from run 25-76 where the zoisite tended to completely encase the clinozoisite core. Once again the epitactic relationship between zoisite and clinozoisite was established using zero-level Weissenberg photographs. (figure 12).

These single crystals were mounted in epoxy with X* vertical (as photographed) and were carefully polished until they were approximately halved. They were then examined with an electron microprobe, and the resulting x-ray intensities were converted to oxide weight percentages. Figures 13 and 14 show the positions of microprobe analysis on each crystal. The number beside each point gives the composition in terms of mole percent pistacite. All four crystals show a definite compositional gap between zoisite and clinozoisite, the gap being extreme for crystals 105- and 106-77-1. The originally iron-free zoisite of 105-77-1 grew more iron rich (Ps 3.2) while being epitactically overgrown by clinozoisite. The composition of the clinozoisite rim near the contact with the

FIGURE 11

Crystal 105-77-1. The crystal is 220 μm long and 100 μm wide (20 μm thickness is into photograph). (a) View down X* in cross-polarized light. Clinozoisite is the anomalous blue rim to the right; zoisite is the white to gray portion. Bright colors at lower left of crystal are due to glue. (b) View in plane-polarized light.

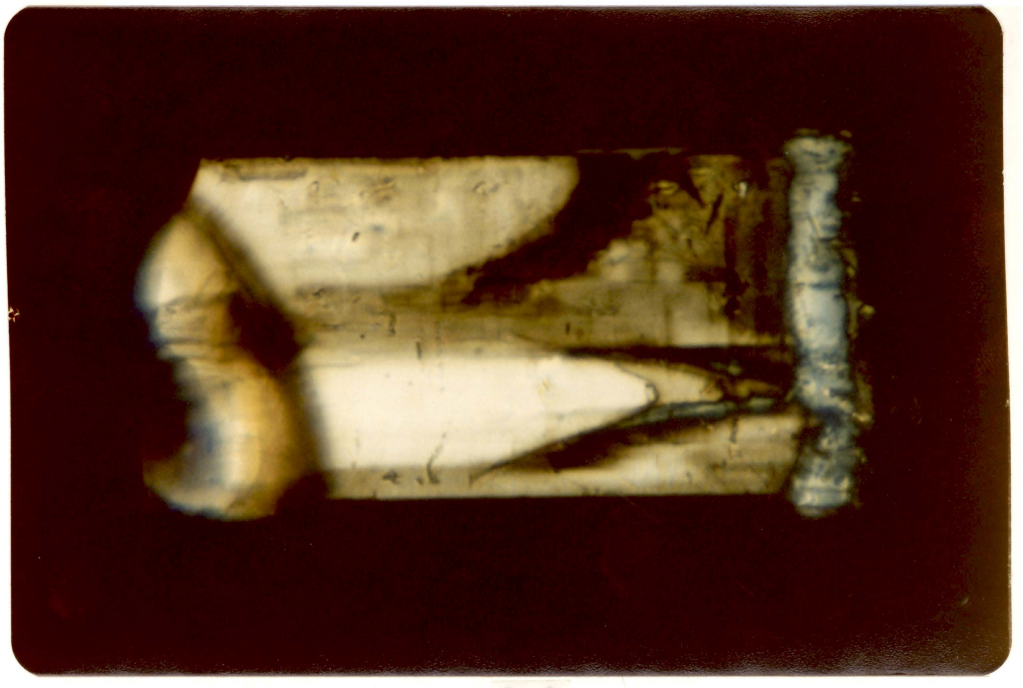

(a)

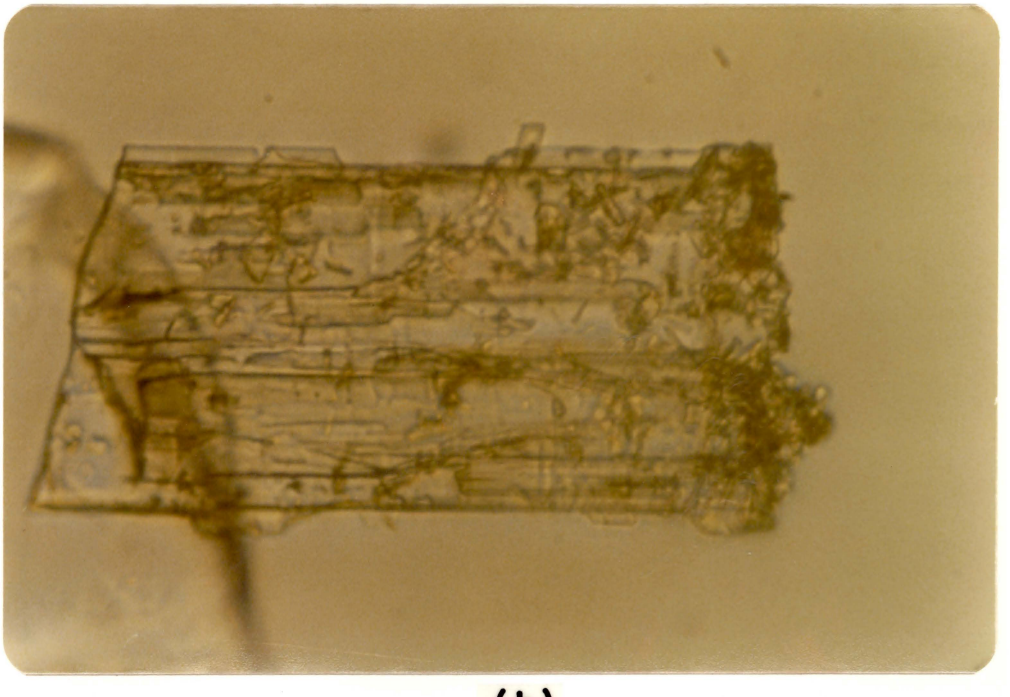

(b)

FIGURE 12

Portion of (h0ℓ) Weissenberg photograph of crystal 105-77-1 (see figure 11). The overlays identify the reflections belonging to zoisite and two clinozoiste twins (twin law is (100) mirror; reflections are indexed for only one twin). Clinozoisite is epitactically related to zoisite seed crystal (Y and Z in common). The extra reflections are due to CuKβ and WLα radiations. (h0ℓ) Weissenberg for 106-77-1 is essentially identical.

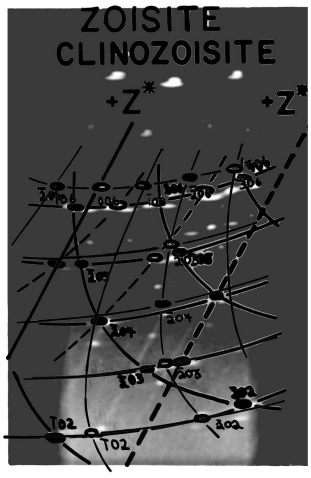
ZOISITE
CLINOZOISITE
+Z*
+Z*

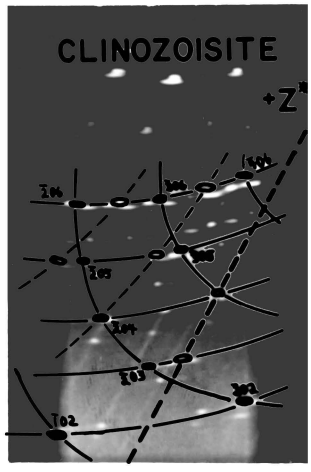
CLINOZOISITE
+Z*

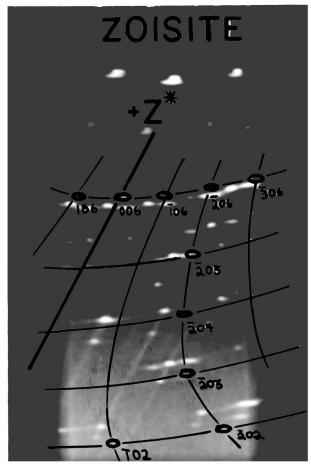
ZOISITE
+Z*

FIGURE 13

Locations of electron microprobe analyses on crystals 25-76-1 and 25-76-2. Numbers next to locating points give composition in mole percent pistacite. (a) Crystal 25-76-1, 260 μm long by 35 μm wide. (b) Crystal 25-76-2, 370 μm long by 40 μm wide. Both crystals were mounted for probing with X* vertical (as shown).

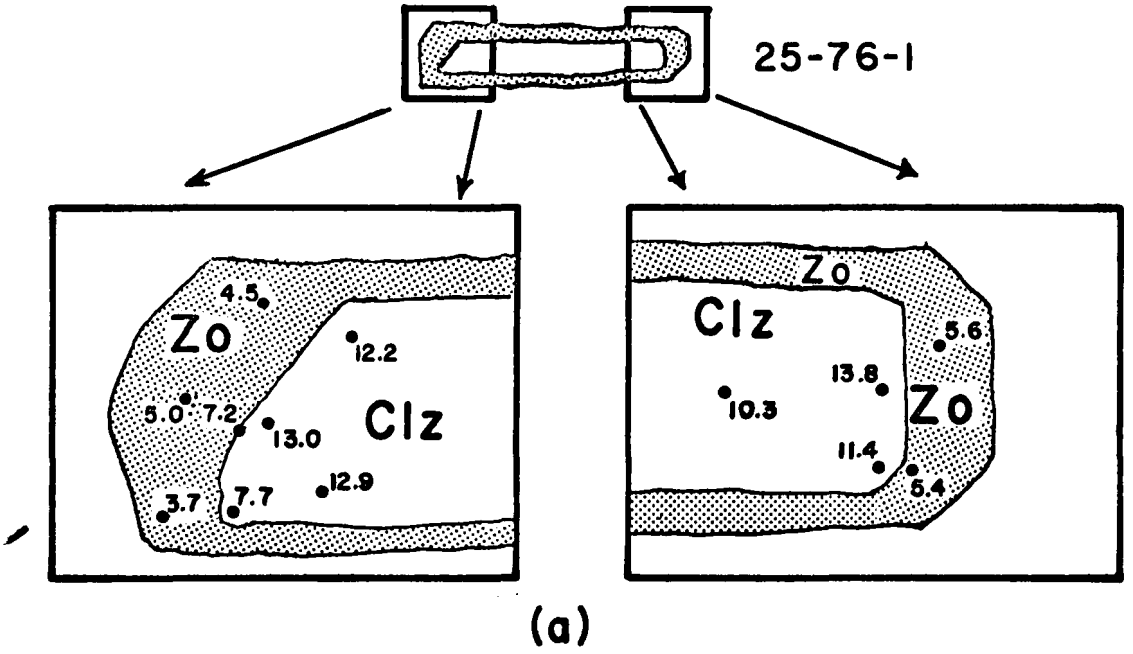
25-76-1
Zo
Clz
4.5
12.2
5.0
7.2
13.0
12.9
3.7
7.7
Zo
5.6
13.8
10.3
11.4
5.4

(a)

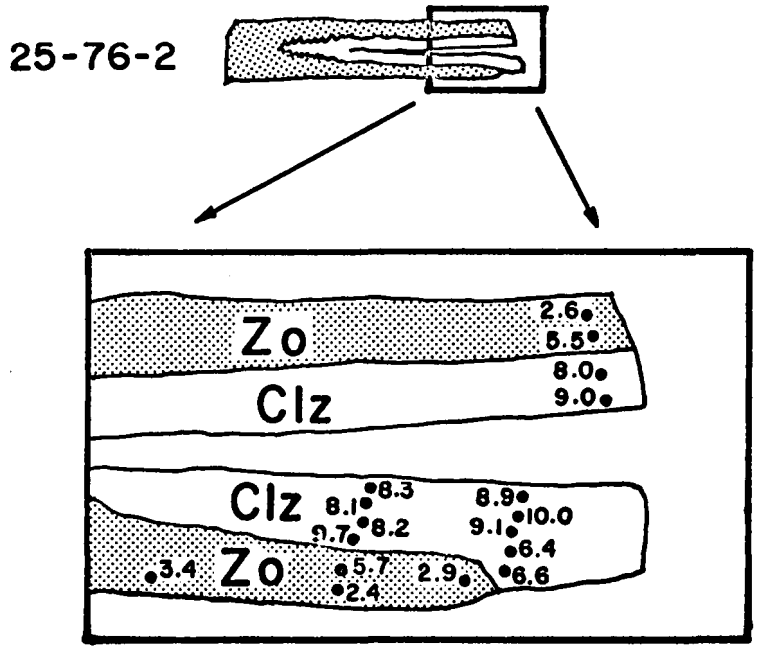
25-76-2
Zo
Clz
2.6
5.5
8.0
9.0
Clz
8.1
8.3
8.9
10.0
9.1
8.2
9.7
6.4
3.4
Zo
5.7
2.9
6.6
2.4

(b)

FIGURE 14

Locations of electron microprobe analyses on crystals 106-77-1 and 105-77-1. Numbers next to locating points give composition in mole percent pistacite. (a) Crystal 106-77-1, 260 μm long by 155 μm wide. (b) Crystal 105-77-1, 220 μm long by 110 μm wide. Both crystals were mounted for probing with X* vertical (as shown).

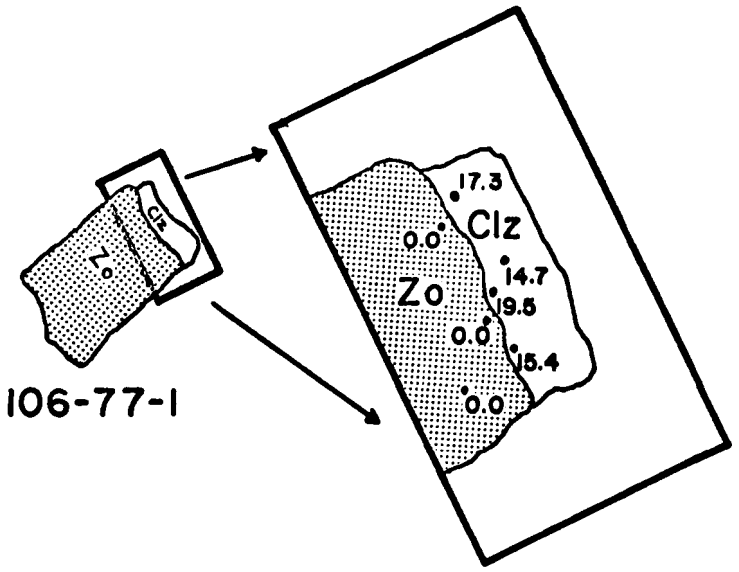
106-77-1
Clz
Zo
17.3
0.0
14.7
19.5
0.0
15.4
0.0

(a)

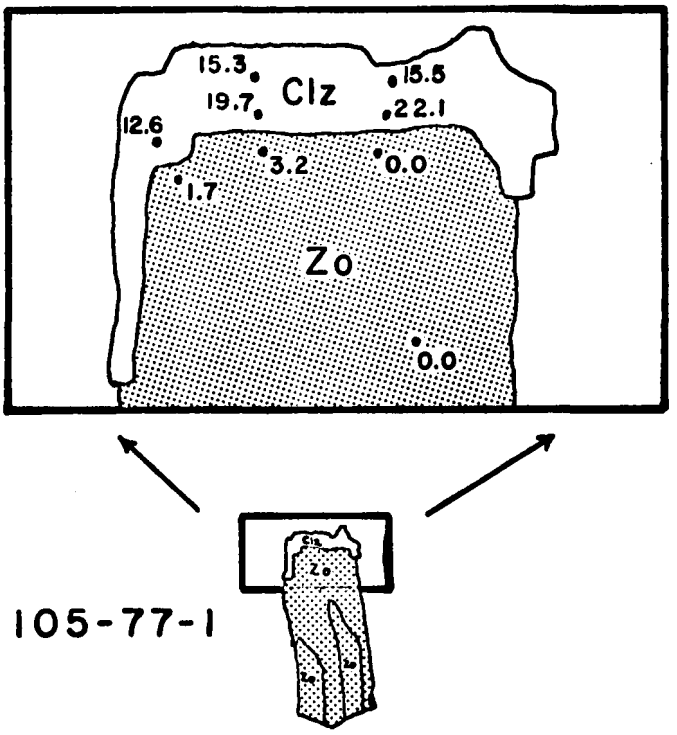
15.3
19.7
Clz
15.5
22.1
12.6
3.2
0.0
1.7
Zo
0.0
105-77-1

(b)

zoisite core for this crystal varies from Ps 22.1 to Ps 12.6 (figure 14b). As the clinozoisite rim continued to grow it became less iron-rich. Based on these observations the following conclusions can be reached:

(1) microprobe analyses on crystals from run 25-76 indicate that zoisite has a lower free energy than clinozoisite for compositions $\leq$ Ps 5.6 at 650°C and 6500 bars.

(2) Similar analyses on crystals 105-77-1 and 106-77-1 indicate that at compositions $\geq$ Ps 12.6 clinozoisite has a lower free energy than zoisite, again at 650°C and 6500 bars.

DISCUSSION

A clearer understanding of the experimental results can be obtained by consideration of free energy versus composition plots. Such a plot, which is consistent with all observations made thus far, is shown in figure 15a (see Gordon, 1968 for an introduction to G-X plots). For iron-poor compositions zoisite has the lower free energy and hence is the stable phase, while at iron-rich compositions clinozoisite has the lower free energy and is therefore stable. The line segment NM, which is tangent to the two free energy curves, defines the region of coexisting zoisite and clinozoisite. The minimum free energy assemblage for bulk compositions between x_1 and x_3 consists of a mixture of zoisite crystals of composition x_1 and clinozoisite crystals of composition x_3. The cross-over in free energy occurs at a composition of x_2.

Under ideal equilibrium conditions figure 15a could be used to make important statements about possible zoisite and clinozoisite compositions. For instance, under equilibrium conditions at 650°C and 6500 bars no zoisite can have a composition more iron-rich than x_1, and no clinozoisite can have a composition less iron-rich than x_3. However, caution must be employed before applying such equilibrium constraints to crystals synthesized from relatively high free energy starting materials in relatively short time spans. Consider the epitactically overgrown crystals previously described. It should not be assumed that the outermost layer of the zoisite/clinozoisite core is in thermodynamic equilibrium with the immediately adjacent layer of the clinozoisite/zoisite overgrowth. To do so

FIGURE 15

Free energy - composition (G-X) schematics for zoisite and clinozoisite solid solutions. (a) Possible G-X relations for zoisite and clinozoisite at 650°C and 6500 bars. Coexisting zoisite and clinozoisite have compositions x_1 and x_3 respectively, as determined by the line segment NM tangent to both curves. At some composition x_2 the phases have identical free energies. (b) Compositional changes for crystal 105-77-1 as seen in terms of free energy. The arrows represent the changing composition for both phases.

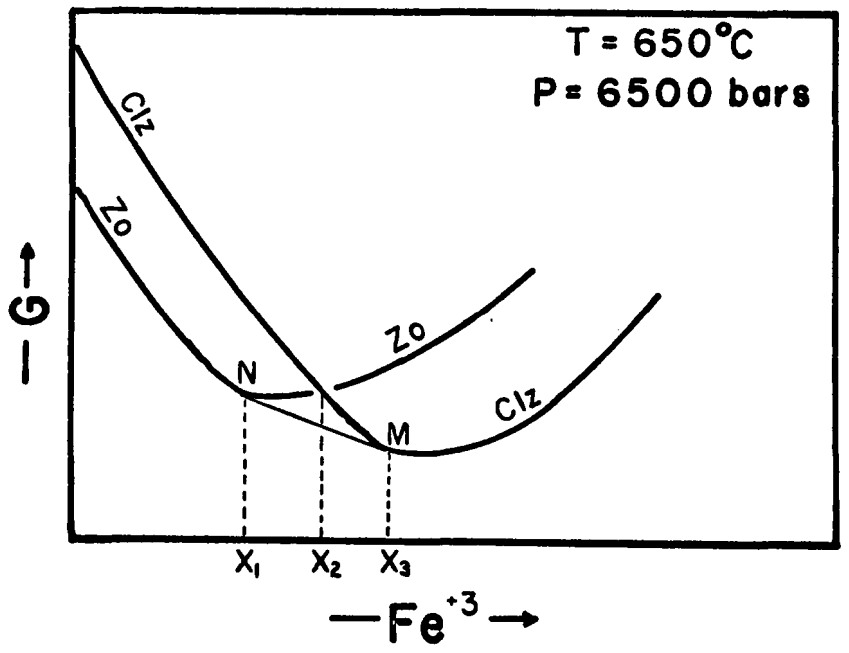
T = 650°C
P = 6500 bars
Clz
Zo
Zo
N
M
Clz
X1
X2
X3
G
—Fe+3→

(a)

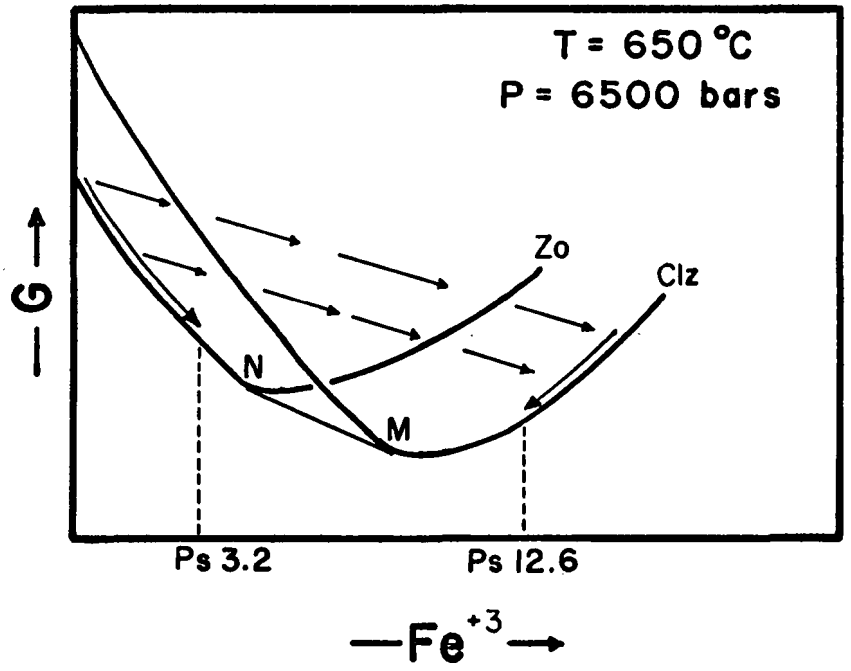
T = 650 °C
P = 6500 bars
Zo
Clz
N
M
Ps 3.2
Ps 12.6
G
—Fe+3→

(b)

would be to accept at least four different "equilibrium" compositional gaps between zoisite and clinozoisite, since microprobe data shows that each crystal has different compositions at the contact points of the two phases. Instead, a correct statement is that the composition of the overgrowth phase places a bracket on x_2, the crossover point composition. In other words, data collected in this study for crystals synthesized at 650°C and 6500 bars show that Ps 5.6 $\leq x_2 \leq$ Ps 12.6. It must not be assumed that the overgrowth, whether zoisite or clinozoiste, will initially have a composition corresponding to either x_1 or x_3.

In the midst of these negative warnings one positive observation can be made based on crystal 105-77-1. For this crystal it was noted that the initially iron-free zoisite seed became more iron-rich, while the initially very iron-rich clinozoisite overgrowth was zoned outward to lower iron compositions. When such compositional trends are placed on a G-X plot (figure 15b), they illustrate the precise situation to be expected if the two phases were moving toward an equilibrium condition. Hence it is felt that the zoisite and clinozoisite compositions of Ps 3.2 and Ps 12.6 respectively obtained from crystal 105-77-1 should be viewed as bracketing the transition loop proper and not just the free energy crossover point.

Figure 16 summarizes the experimental constraints that have been deduced for the zoisite-clinozoisite transition loop at 6500 bars. The exact width and positioning of the equilibrium transition loop are unknown. The dashed (hypothetical) transition loop shown is consistent with the experimental results and with what data are available on naturally

FIGURE 16

Possible transition loop for the zoisite - clinozoisite transformation. Compositional brackets at 650°C are derived from electron microprobe analyses of crystal 105-77-1. Naturally coexisting pairs were used as guides in estimating the loop's width. The insert shows how this simple transition loop might be modified to accommodate tentative suggestions of zoisite unmixing based on field observations of Ackermand and Raase (1973) and Raith (1976).

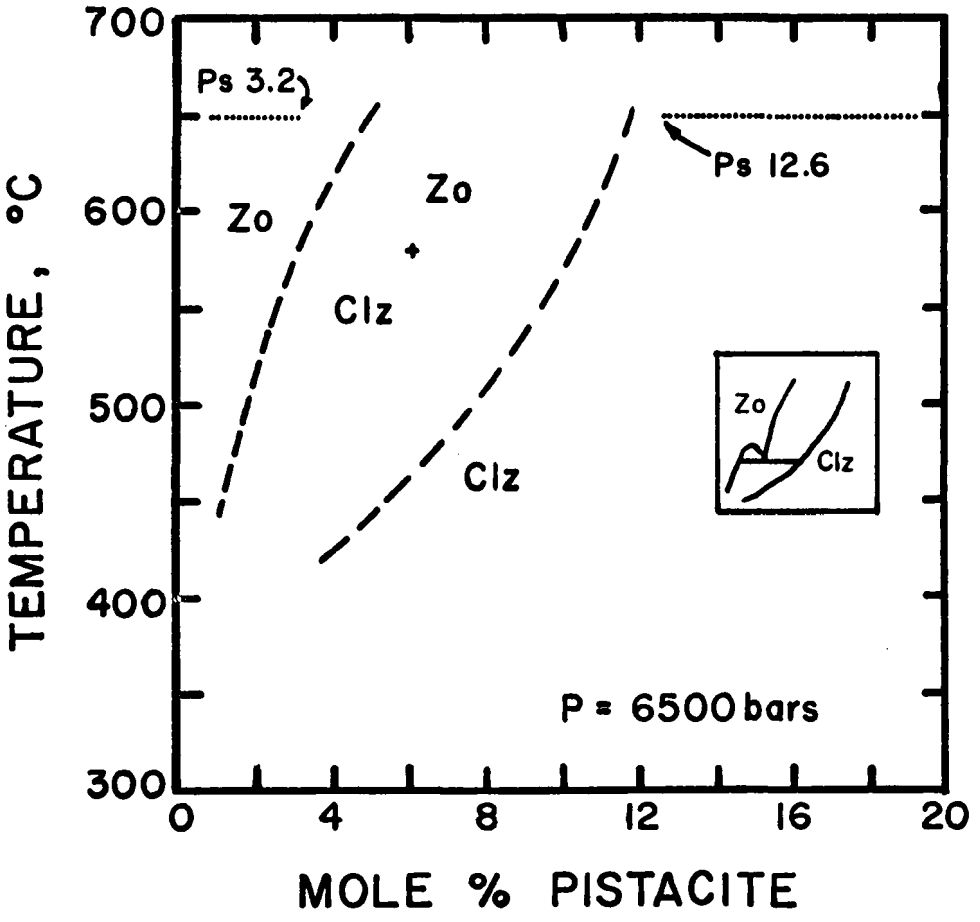
700
600
500
400
300
0
4
8
12
16
20
TEMPERATURE, °C
MOLE % PISTACITE
Ps 3.2
Ps 12.6
Zo
Zo
Clz
Clz
Zo
Clz
P = 6500 bars

occurring zoisite-clinozoisite pairs. The temperature at which the loop closes for Ps 0 is unknown but is constrained to be below 407°C. This temperature is in agreement with field evidence for low temperature (< 560°C) zoisite stability (Holdaway, 1972; Ackermand and Raase, 1973). The loop as drawn should prove to be a valuable starting point for future experimental studies. The inset on figure 16 represents the as yet very tentative suggestion from the field evidence of Ackermand and Raase (1973) and Raith (1976) of a low temperature solvus in the zoisite field.

Experimental work to date has been largely restricted to pressures of 6500 bars. Extrapolation to other pressures should have little effect on the shape and position of the transition loop. As pointed out by Holdaway (1972), the tiny difference in molar volume between iron-free zoisite and clinozoisite means that their univarient equilibrium should have little pressure dependence. He calculated a dP/dT of +1300 bar K^{-1} for the reaction Clz→Zo at 900K using the molar volume data of Pistorius (1961) and molar entropy data derived from experimentally bracketed equilibria. A graphical compilation of more recent volume data for zoisite and clinozoisite (figure 17) shows that zoisite is the denser phase and that dP/dT should actually be negative for Clz Zo. These data indicate a ΔV of approximately -0.6cc. Holdaway calculated molar entropies of 183 calorie K^{-1} and 189 calorie K^{-1} for clinozoisite and zoisite respectively at 900K. No new entropy data for iron-free clinozoisite could be found in the literature, but two new values for zoisite at 900K have been published (188 calorie K^{-1} (Perkins et al., 1977); and 191 calorie K^{-1}

FIGURE 17

Graphical summary of zoisite and clinozoisite molar volumes. Data were taken from the following sources: open symbols, Dollase (1968); solid symbols, Myer (1966); half-open symbols, Hörmann and Raith (1971). The lines are extensions of published determinative curves.

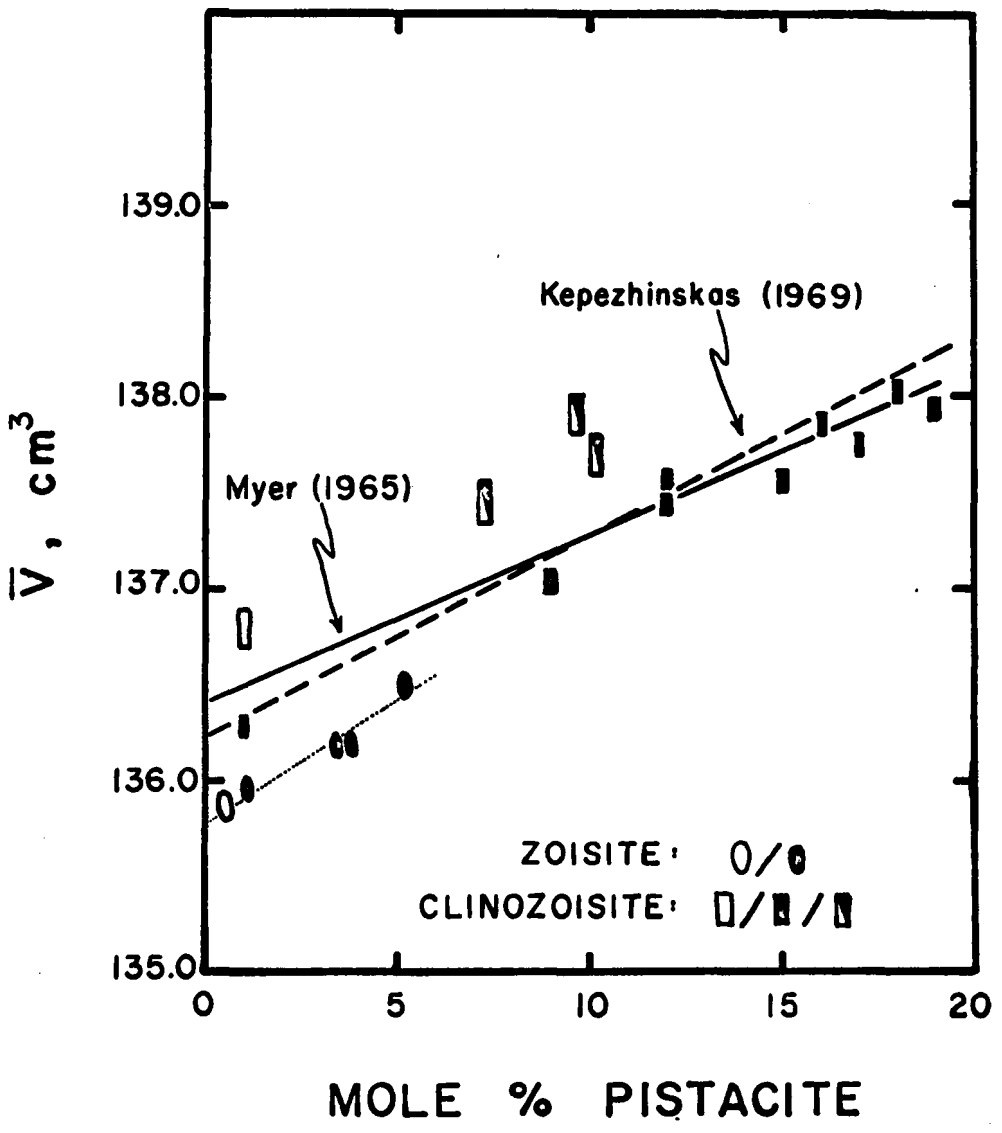
139.0
138.0
137.0
136.0
135.0
0
5
10
15
20
$\bar{V}$, cm^3
Kepezhinskas (1969)
Myer (1965)
ZOISITE: 0/0
CLINOZOISITE: □/■/■
MOLE % PISTACITE

(Kiselva, 1974)). Using the lower value, ΔS = 5 calorie K^{-1}, the calculated slope becomes -349 bar K^{-1} at 900K. Although lower than Holdaway's, this value still indicates an essentially pressure insensitive equilibrium for the Fe-free end-members. Figure 17 shows ΔV remaining essentially constant for increasingly iron-rich compositions, indicating that the positioning of the whole transition loop also changes very slowly with pressure. This observation, besides justifying the extrapolation of present data to lower pressures, suggests that future experimental work should take advantage of the increased reactivity accompanying higher pressures.

CONCLUSIONS

Obviously a substantial amount of work remains to be done before the details of the clinozoisite to zoisite transition loop are fully known. A logical first step is the reversible determination of the iron-free equilibrium zoisite $\rightleftharpoons$ clinozoisite. The major obstacle which has prevented experimental study of this reaction has been the inability to obtain iron-free clinozoisite starting material. A fruitful approach to this problem might be to use low-iron clinozoisites (either natural or synthetic) as nuclei for growing synthetic, iron-free clinozoisite. Such a nucleation process, repetitively performed at low temperatures ($\sim$400°C) and high pressures ($>$ 5kbar), could conceivably yield substantial amounts of relatively pure clinozoisite.

The major task awaiting future investigators is the determination of the width and positioning of the transition loop for iron-bearing compositions. But the difficulties of synthesizing homogenous, on-composition starting batches of either zoisite or clinozoisite will probably prohibit the use of traditional experimental methods. Methods that concentrate on single crystals, such as the one used in this study, offer a promise of success not only for epidotes, but also for any phase presenting compositional control difficulties. Such techniques focus attention on compositional changes in the outermost layers of crystals carefully selected and characterized before experimentation begins. Such compositional changes reflect the tendencies of these crystals to come to equilibrium with their surroundings, i.e. the rest of the starting

material. The equilibration may take the form of recrystallization or overgrowths. This approach should be contrasted with the standard technique for locating solvi or transition loops, which is the promotion and examination of unmixing in initially homogenous crystals. This latter method is clearly impractical for phases which fail to show homogenization on a geological time scale (e.g. garnet and epidote).

The general use of epitactic overgrowths for the determination of solvi or transition loops, as an extension of the approach employed in this study, appears to have only limited usefulness. It is certainly a valid technique for bracketing the free energy crossover of the coexisting phases. But locating the beginning of the transition loop may prove difficult if the "overgrowth" phase has difficulty nucleating, allowing the "core" phase to reach compositions within the loop. Needless to say, subsolidus transitions between phases lacking possible epitactic relationships could not be investigated with this method.

A more fruitful approach for bracketing a subsolidus solvus or transition loop would be to supply seed crystals for both phases in the same run, thereby eliminating nucleation problems. Seed crystals of selected compositions could then be allowed to equilibrate at conditions of interest, the overgrowths bracketing compositions of coexistence from either the outside or the inside of the loop or solvus. The major drawback to this approach may prove to be the general difficulty in achieving the necessary overgrowths in reasonable times. Overgrowths can be more speedily developed by adding stoichiometric mixtures of "high free energy" oxide materials. The danger in this approach lies in obtaining

overgrowths which extend compositionally into the solvus or transition loop because of a local equilibrium condition in which the seed crystal of one phase was effectively isolated in the oxides from the other phase's seed crystal nuclei. Future experimental studies with epidote group minerals, or any other minerals for which the method seems fruitful, will be faced with working out the best balance between these different approaches. Self-consistency in the results will prove to be a key guide in judging reliability.

REFERENCES

Ackermand, D. and P. Raase (1973) Coexisting zoisite and clinozoisite in biotite schists from the Hohe Tauern, Austria. Contr. Mineral. Petrol. 42, 333-341.

Banno, S. (1964) Petrologic studies on Sanbagawa crystalline schists in the Bessi-Ino district, Central Sikoku, Japan. J. Fac. Sci. Univ. Tokyo, sec. II, 15, 203-319.

Boettcher, A. L. (1970) The system $CaO-Al_2O_3-SiO_2-H_2O$ at high pressures and temperatures. J. Petrol. 11, 337-379.

Burnhan, C. W. (1962) Lattice constant refinement. Carnegie Instit. Wash. Yearbook 61, 132-135.

Coughlin, J. P. (1954) Contributions to the data on theoretical metallurgy XII. Heats and free energies of formation of inorganic oxides. U.S. Bureau of Mines Bull. 542.

Deer, W. A., R. A. Howie and J. Zussman (1962) Epidote group, in Rock Forming Minerals: I, Ortho- and Ring-Silicates. New York: John Wiley and Sons. p. 183-210.

Denbigh, K. (1971) The Principles of Chemical Equilibrium. Cambridge: Cambridge University Press. 494 p.

Dienes, P., R. H. Nafziger, G. C. Ulmer and E. Woermann (1974) Temperature-Oxygen Fugacity Tables for Selected Gas Mixtures in the System C-H-O at One Atmosphere Total Pressure. Bull. #88 of the Earth and Mineral Sciences Experiment Station, The Pennsylvania State University. 129 p.

Dollase, W. A. (1968) Refinement and comparison of the structures of zoisite and clinozoisite. Amer. Mineral. 53, 1882-1898.

_____ (1973) Mössbauer spectra and iron distribution in the epidote minerals. Zeit. für Krist. 138, 41-63.

Ehlers, E. G. (1953) An investigation of the stability relations of the Al - Fe members of the epidote group. J. Geol. 61, 231-251.

Eitel, W. (1919) Die Grenzen der Mischkristallbildung in der Mineralien der Epidotgruppe. Neues Jahrb., Beilage-Band 42, 173-271.

Elliot, J. F. and M. Gleiser (1960) Thermochemistry for Steelmaking, Vol. I. Mass.: Addison-Wesley.

Eugster, H. P. and D. R. Wones (1962) Stability relations of the ferruginous biotite, annite. J. Petrol. 3, 82-125.

Foye, W. G. (1926) The occurrence of thulite at Haddam, Connecticut. Amer. Mineral. 11, 210-213.

Ghose, S. and T. Tsang (1971) Ordering of V^{2+}, Mn^{2+} and Fe^{3+} ions in zoisite, $Ca_2Al_3Si_3O_{12}(OH)$. Science 171, 374-376.

Gordon, P. (1968) Principles of Phase Diagrams in Materials Systems. New York: McGraw-Hill. 232p.

Hall, L. M. (1959) The geology of the St. Johnsbury quadrangle, Vermont and New Hampshire. Vermont Geol. Survey Bull., no. 13, 105p.

Hansen, E. C., ms. (1963) Strain facies of the metamorphic rocks in Trollheimen, Norway: Ph.D. thesis, Yale Univ.

Harpum, J. R. (1954) Formation of epidote in Tanganyika. Bull. Geol. Soc. Amer. 65, 1075 - 1092.

Hietanen, A. (1974) Amphibole pairs, epidote minerals, chlorite, and plagioclase in metamorphic rocks, Northern Sierra Nevada, California, Amer. Mineral. 59, 22-40.

Holdaway, M. J. (1972) Thermal stability of Al - Fe epidote as a function of f_{O_2} and Fe content. Contr. Mineral. Petrol. 37, 307-340.

Hörmann, P. K. and M. Raith (1971) Optische Daten, Gitterkonstanten, Dichte, und magnetische Suszeptibilitat von Al - Fe (III) Epidoten. Neues Jahrb. Min. Abhdl., 116, 41-60.

Huebner, J. S. (1971) Buffering techniques for hydrostatic systems at elevated pressures, in Research Techniques for High Pressure and High Temperature, G. C. Ulmer, ed. New York: Springer-Verlag. pp. 123-177.

_____ (1975) Oxygen fugacity values of furnace gas mixtures. Amer. Mineral. 60, 815-823.

JANAF (1971) Thermochemical Tables: Second edition, U.S. Dept. Commerce (D. R. Stull and H. Prophet, Project Directors), NSRDS-NBS 37.

Kepezhinskas, K. B. (1969) Determination of the composition of minerals of the epidote group from their physical properties. Dokl. Acad. Sci. U.S.S.R., Earth Sci. Sect. 185, 104-106.

_____ and V. V. Khlestov (1967) Compositional relations in minerals of the epidote group. Dokl. Acad. Sci. U.S.S.R., Earth Sci. Sect. 175, 130-132.

Kiseleva, I. A., N. D. Topor and E. D. Andreyenko (1974) Thermodynamic parameters of minerals of the epidote group. Geochem. Internat. 11, 389-398.

Liou, J. G. (1973) Synthesis and stability relations of epidote, $Ca_2Al_2FeSi_3O_{12}(OH)$. J. Petrol. 14, 381-413.

Myer, G. H. (1965) X-ray determinative curve for epidote. Amer. Jour Sci. 263, 78-86.

_____(1966) New data on zoisite and epidote. Amer. Jour. Sci. 264, 364-385.

Nafziger, R. H., G. C. Ulmer and E. Woermann (1971) Gaseous buffering for the control of oxygen fugacity at one atmosphere in Research Techniques for High Pressure and High Temperatures, G. C. Ulmer, ed. New York: Springer-Verlag. pp. 9-41.

Newton, R. C. (1965) The thermal stability of zoisite. Jour. Geol. 73, 431-441.

_____(1966) Some calc-silicate equilibrium relations. Amer. Jour. Sci. 264, 204-222.

Orlov, A. (1925) On members poor in iron of the zoisite-epidote group. Mém. Soc. Roy. Sci. Bohême. no. 19, 42p.

Osborn, E. F. and A. Muan (1963) Physical chemistry of steelplant refractories, in Electric Furnace Steelmaking Vol. II. Theory and Fundamentals. E. C. Sims, ed. New York: Interscience.

Perkins, D., E. J. Essene, E. F. Westrum, Jr. and V. J. Wall (1977) Application of new thermodynamic data to grossular phase relations. Contrib. Mineral. Petrol. 64, 137-147.

Pistorius, C. W. F. T. (1961) Synthesis and lattice constants of pure zoisite and clinozoisite. Jour. Geol. 69, 604-609.

_____, G. C. Kennedy and S. Sourirajan (1962) Some relations between the phases anorthite, zoisite and lawsonite at high temperatures and pressures. Amer. Jour. Sci. 260, 44-56.

Raith, M. (1976) The Al - Fe (III) epidote miscibility gap in a metamorphic profile through the Penninic series of the Tauern Window, Austria. Contrib. Mineral. Petrol. 57, 99-117.

Rodgers, A. F. (1924) Clinozoisite from lower California, Amer. Mineral. 9, 221-224.

Springer, G. (1976) Correction procedures in electron-probe analysis-in M.A.C. Short Course Notes in Microprobe Techniques, D. G. W. Smith, ed. Edmonton: Mineralogical Association of Canada. p. 45-62.

Strens, R. G. J. (1963) Some relations between members of the epidote group. Nature 198, 80-81.

_____ (1965) Stability and relations of the Al - Fe epidotes. Mineral. Mag. 35, 464-475.

Wagman, D. D., J. E. Kilpatrick, W. J. Taylor, K. S. Pitzer and F. D. Rossini (1945) Heats, free energies, and equilibrium constants of some reactions involving O_2, H_2, H_2O, C, CO, CO_2, and CH_4. U. S. National Bureau of Stds. Research Paper RP1634. J. Research Nat. Bur. Std. 34, 143-160.

Weeg, G. P. and G. B. Reed (1966) Introduction to Numerical Analysis. Mass.: Ginn and Company. 184p.

Weinschenk, E. (1903) Die Kontaktmetamorphische Schieferhülle und ihre Bedeutung für die Lehre vom allgemeinen Metamorphisms. Abhandl. Bayer. Akad. Wiss. Math.-Physik. Kl. 22, Abt. 2, 261-340.

Wicks, C. E. and F. E. Block (1963) Thermodynamic properties of 65 elements, their oxides, halides, carbides and nitrides. U. S. Bureau of Mines Bull. 605.

Winchell, H. (1958) The composition and physical properties of garnet. Amer. Mineral. 43, 595-600.

Winkler, H. G. F. (1976) Petrogenesis of Metamorphic Rocks. New York: Springer-Verlag. 334p.

APPENDIX

SOURCE LISTING OF THE PROGRAM USED TO GENERATE THE INITIAL VOLUME % CO_2 TABLES

```
C*************************************************************************
C
C                              GAS  TABLE  PROGRAM
C
C          THIS PROGRAM CALCULATES TABLES LISTING THE INITIAL PERCENTAGE
C          CO2 IN AN H2O - CO2 GAS MIXTURE YIELDING THE SPECIFIED TEM-
C          PERATURE - OXYGEN FUGACITY PAIR
C
C
C               THE FIRST 20 INPUT CARDS CONTROL OUTPUT FORMAT.  AFTER
C          THE MARKER CARD ('1') COME THE CONTROL CARDS WITH FORMAT (2F5.0,
C          F10.3).  THE FIRST TWO NUMBERS ARE THE STARTING AND STOPPING
C          TEMPERATURES (DEGREES CELSIUS), AND THE THIRD NUMBER IS THE
C          STARTING LOG(OXYGEN FUGACITY).  THE PROGRAM AUTOMATICALLY TAB-
C          ULATES VALUES AT 10 DEGREE CELSIUS AND 0.2 LOG ATM UNIT INTER-
C          VALS.  ONE SUCH CARD COVERS A 2.0 LOG ATM UNIT RANGE IN OXYGEN
C          FUGACITY.  THE PROGRAM WILL TERMINATE AFTER PROCESSING THE LAST
C          CONTROL CARD.
C
C
C*************************************************************************
C
C
      REAL  C(2),CO2(2,10),DG(4),FMT(8),FRMT(20,8),KK(4),LGF(10),P(2,5)
      DATA  R,TT/1.98726E-3,273.18/
      DO 9  LL=1,20
      READ(5,8)  (FRMT(LL,J),J=1,8)
    8 FORMAT(8A4)
    9 CONTINUE
   99 CONTINUE
      READ(5,999)  LXYZ
  999 FORMAT(I1)
```

```
      JK=60
   10 CONTINUE
      READ(5,20,END=400)  T1,T2,LGF(1)
   20 FORMAT(2F5.0,F10.3)
      IF (T1.LT.0.000)  GO TO 99
      IF (JK+15.LE.60)  GO TO 25
      WRITE(6,22)
   22 FORMAT('1'////4X,'TEMP  C',22X,'LOG( OXYGEN FUGACITY )',23X,'TEMP
     1 C'/)
      JK=0
   25 DO 28  J=2,10
   28 LGF(J)=LGF(J-1)-0.200
      IF (JK.GT.0)  WRITE(6,29)
   29 FORMAT(////)
      WRITE(6,30)  (LGF(J),J=1,10)
   30 FORMAT(14X,10(F5.1,1X)/)
      JK=JK+7
      T=T1
C
C                              ENTER  CALCULATIONAL  LOOP
C
   75 CONTINUE
      IF(T2.LT.T)  GO TO 10
   77 DG(1)=62.11033-2.144446E-2*T+4.720325E-7*T**2-4.557429E-12*T**3-7.
     1343018E-15*T**4
      DG(2)=94.25770+7.321946E-4*T-3.416474E-7*T**2+4.785862E-11*T**3
      DG(3)=55.02525-1.121221E-2*T-2.080041E-6*T**2+7.648489E-10*T**3-1.
     1123283E-13*T**4
      DG(4)=-35.67445+5.344917E-2*T+9.900155E-6*T**2-6.474264E-9*T**3+2.
     1077475E-12*T**4-2.697849E-16*T**5
      DO 80  J=1,4
   80 KK(J)=EXP(-DG(J)/(R*(T+TT)))
```

```
      DO 250 J=1,10
      P1=10.0000**LGF(J)
      P2=SQRT(P1)
C
C                              ITERATIVE  LOOP  FOLLOWS
C
      I=0
      C(2)=0.000
      DO 150  K=1,70
      P(2,4)=(P2-C(2)*(P2+KK(3)/3.00))/(P2+KK(3))
      CC=KK(1)*(1.00-P1)/(KK(1)+P2)
      AA=P2*(1.00-P1)/(P2+KK(3))
      BB=(P2+KK(3)/3.00)*(1.00-P1)/(P2+KK(3))
      DD=P2*(1.00-P1)/(3.00*(KK(1)+P2))
      P(2,3)=(CC-2.00*P1)/(AA+2.00*P1-C(2)*(DD+BB+1.33333*P1))
      IF (K.EQ.1)  BO=100.0/(1.00+P(2,3))
      P(2,2)=(KK(1)+C(2)*P(2,3)*P2/3.00)/(KK(1)+P2)
      CX=2.00+P(2,2)+P(2,3)*(2.00-P(2,4)-1.33333*C(2))
      PH2O=P(2,3)*2.00*(P(2,4)+C(2)/3.00)/CX
      PCO2=2.00*(1.00-P(2,2))/CX
      PCO=2.00*(P(2,2)-P(2,3)*C(2)/3.00)/CX
      PH2=2.00*P(2,3)*(1.00-P(2,4)-C(2))/CX
      PCH4=(KK(4)*PCO*PH2**3)/PH2O
      P(2,1)=PCH4*(6.0+3.0*P(2,2)+P(2,3)*(6.0-3.0*P(2,4)))/(P(2,3)*(2.0+
     14.00*PCH4))
      P(2,5)=P(2,1)-C(2)
      IF (ABS(P(2,5)).LT.0.00001)  GO TO 170
      IF (I.EQ.1)  GO TO 97
      IF (P(2,5).GE.0.000) GO TO 130
      I=1
   97 CONTINUE
      FP=(P(2,5)-P(1,5))/(C(2)-C(1))
```

```
      C(1)=C(2)
      C(2)=C(1)-P(2,5)/FP
      DO 100  L=1,5
      CC=ABS(P(1,L)-P(2,L))
      DD=0.0001*ABS(P(1,L))
      IF (CC.GT.DD)  GO TO 130
  100 CONTINUE
      GO TO 170
  130 DO 140  L=1,5
  140 P(1,L)=P(2,L)
      IF (I.EQ.0)  C(1)=C(2)
      IF (I.EQ.0)  C(2)=C(2)+0.007
  150 CONTINUE
C
C                              NO CONVERGENCE, SET CO2 TO -99.99
C
      CO2(1,J)=1.0000
      CO2(2,J)=-99.99
      GO TO 249
C
C                              PARAMETERS  CONVERGE,  RECORD THEM
C
  170 CO2(1,J)=0.00
      IF (P1.LT.1.01*PCO2*KK(2))  GO TO 180
      CO2(2,J)=100.00/(1.00+P(2,3))
      GO TO 249
  180 CO2(2,J)=1000.00
  249 CONTINUE
  250 CONTINUE
      II=IFIX(T)
      IF (JK.LT.60)  GO TO 270
      WRITE(6,22)
```

```
      WRITE(6,30)  (LGF(J),J=1,10)
      JK=7
  270 CONTINUE
      IF (CO2(2,1).GE.99.995)  GO TO 280
      IF (CO2(2,10).GE.0.005)  GO TO 290
      DO 273  J=1,10
      IF (CO2(2,J).LT.0.0050)  GO TO 275
  273 CONTINUE
  275 DO 277  LL=1,8
  277 FMT(LL)=FRMT(J,LL)
      J=J-1
      IF (J.LE.0.AND.LXYZ.EQ.1)  GO TO 360
      IF (J)  278,278,279
  278 WRITE(6,FMT)  II,II
      GO TO 350
  279 WRITE(6,FMT)  II,(CO2(2,K),K=1,J),II
      GO TO 350
  280 DO 283  J=1,10
      IF (CO2(2,J).LT.99.995)  GO TO 285
  283 CONTINUE
      J=11
  285 L1=J+9
      DO 287  LL=1,8
  287 FMT(LL)=FRMT(L1,LL)
      IF (J.GT.10.AND.LXYZ.EQ.1)  GO TO 360
      IF (J-10)  289,289,288
  288 WRITE(6,FMT)  II,II
      GO TO 350
  289 WRITE(6,FMT)  II,(CO2(2,K),K=J,10),II
      GO TO 350
  290 WRITE(6,291)  II,(CO2(2,J),J=1,10),II
  291 FORMAT(5X,I4,5X,10(F5.2,1X),5X,I4)
```

```
  350 JK=JK+1
  360 T=T+10.0
      GO TO 75
  400 WRITE(6,22)
      STOP
      END

          ******  INPUT  DATA  ******
(5X,I4,70X,I4)
(5X,I4,5X,F5.2,60X,I4)
(5X,I4,5X,2(F5.2,1X),53X,I4)
(5X,I4,5X,3(F5.2,1X),47X,I4)
(5X,I4,5X,4(F5.2,1X),41X,I4)
(5X,I4,5X,5(F5.2,1X),35X,I4)
(5X,I4,5X,6(F5.2,1X),29X,I4)
(5X,I4,5X,7(F5.2,1X),23X,I4)
(5X,I4,5X,8(F5.2,1X),17X,I4)
(5X,I4,5X,9(F5.2,1X),11X,I4)
(5X,I4,11X,9(F5.2,1X),5X,I4)
(5X,I4,17X,8(F5.2,1X),5X,I4)
(5X,I4,23X,7(F5.2,1X),5X,I4)
(5X,I4,29X,6(F5.2,1X),5X,I4)
(5X,I4,35X,5(F5.2,1X),5X,I4)
(5X,I4,41X,4(F5.2,1X),5X,I4)
(5X,I4,47X,3(F5.2,1X),5X,I4)
(5X,I4,53X,2(F5.2,1X),5X,I4)
(5X,I4,59X,F5.2,6X,I4)
(5X,I4,70X,I4)
1
880. 2000.  -4.00
880. 2000.  -6.00
720. 2000.  -8.00
```

```
720. 2000. -10.00
600. 2000. -12.00
600. 2000. -14.00
500. 1680. -16.00
500. 1680. -18.00
500. 1240. -20.00
500. 1240. -22.00
500.  950. -24.00
```

The vita has been removed from the scanned document

CALCULATION OF TEMPERATURE - OXYGEN FUGACITY TABLES FOR H_2 - CO_2 GAS MIXTURES AT ONE ATMOSPHERE TOTAL PRESSURE

and

AN INVESTIGATION OF THE ZOISITE - CLINOZOISITE TRANSITION

by

Arthur R. Prunier, Jr.

(ABSTRACT)

Part I: Calculation of Temperature - Oxygen Fugacity Tables for H_2 - CO_2 Gas Mixtures at One Atmosphere Total Pressure.

The initial CO_2 volumes yielding selected oxygen fugacities at specified temperatures have been computed for H_2 - CO_2 gas mixtures at one atmosphere total pressure. The calculations are based on the thermochemical data of the JANAF (1971) Tables for the species CO_2-H_2-H_2O-CO-O_2-CH_4 and are carried out using the Newton-Raphson method of successive approximation. The new tables replace older ones (Dienes, Nafziger, Ulmer and Woermann, 1974) in which the effects of CH_4 on the system were treated only in an approximate manner.

Part II: An Investigation of the Zoisite - Clinozoisite Transition

Available data on natural coexisting zoisite - clinozoisite ($Ca_2Al_{3-x}Fe_x[Si_2O_7][SiO_4]O(OH)$ with $x \leq 0.33$) assemblages imply that the two phases are related by a solid solution transition loop, with

zoisite being the low-iron, high-temperature, high-pressure phase. Reversibility experiments at 6500 bars constrain the iron-free equilibrium clinozoisite zoisite to lie below 407°C. Electron microprobe and single crystal x-ray diffraction studies of epitactically related zoisite-clinozoisite crystals grown from seeded mixtures of anorthite, calcite, hematite and silica glass at 6500 bars and 650°C are shown to bracket the transition loop between Pistacite 3.2 ($Ca_2Al_{2.90}Fe_{0.10}Si_3O_{12}(OH)$) and Pistacite 12.6 ($Ca_2Al_{2.62}Fe_{0.38}Si_3O_{12}(OH)$). Experimental techniques used in this investigation, which focus on detalied analysis of single crystals, offer promise as a means for determining equilibrium phase relations of epidotes and other frequently zoned mineral groups.